1.0

1.1

1.25   1.4   1.6

2.8   2.5
3.2   2.2
3.6
4.0   2.0

1.8

MICROCOPY RESOLUTION TEST CHART

Aerodynamic Characteristics of Three Helicopter Rotor Airfoil Sections at Reynolds Numbers from Model Scale to Full Scale at Mach Numbers from 0.35 to 0.90

(6) Aerodynamic Characteristics of Three Helicopter Rotor Airfoil Sections at Reynolds Numbers From Model Scale to Full Scale at Mach Numbers From $\emptyset$.35 to 0.90.

(10) Kevin W. Noonan ▇▇ Gene J. Bingham

Structures Laboratory, AVRADCOM Research and Technology Laboratories
Langley Research Center
Hampton, Virginia

(14) NASA-1-131

(11) Sep 80   (12) 85

NASA

National Aeronautics
and Space Administration

Scientific and Technical
Information Branch

1980

(16) 1L161101 AH45

SUMMARY

An investigation has been conducted in the Langley 6- by 28-Inch Transonic Tunnel to determine the two-dimensional aerodynamic characteristics of three helicopter rotor airfoils at Reynolds numbers from typical model scale to full scale at Mach numbers from about 0.35 to 0.90. The model-scale Reynolds numbers ranged from about 0.7×10^6 to 1.5×10^6 and the full-scale Reynolds numbers ranged from about 3.0×10^6 to 6.6×10^6. The airfoils tested were the NACA 0012 ($0°$ Tab), the SC 1095-R8, and the SC 1095. Both the SC 1095 and the SC 1095-R8 airfoils had trailing-edge tabs.

The results of this investigation indicate that Reynolds number effects can be significant on the maximum normal-force coefficient and all drag-related parameters; namely, drag at zero normal force, maximum normal-force—drag ratio, and drag-divergence Mach number. In general, the increments in these parameters at a given Mach number owing to the model-scale to full-scale Reynolds number change are different for each of the airfoils.

INTRODUCTION

The development of new rotors generally includes predictions of the full-scale rotor performance based on extrapolation of small-scale-model rotor wind-tunnel results and based on rotor-performance analysis programs using two-dimensional airfoil data at full-scale Reynolds numbers. Both prediction methods have inherent difficulties. The extrapolation of model-scale data requires a knowledge of how to increment the airfoil-section data for Reynolds number effects, and data for this purpose are seldom available. Rotor-performance analysis programs are already quite sophisticated, but they require a detailed knowledge of the rotor flow field. Improvements of these analysis programs can best be accomplished by correlation studies which require airfoil-section data at both model-scale and full-scale Reynolds numbers.

In order to provide data for evaluating extrapolation methods and for rotor-performance correlation studies, the two-dimensional aerodynamic characteristics of three helicopter rotor airfoils have been determined at Mach numbers from 0.35 to 0.90 and at Reynolds numbers from model scale to full scale. The model-scale Reynolds numbers ranged from about 0.7×10^6 to 1.5×10^6, and the full-scale Reynolds numbers ranged from about 3.0×10^6 to 6.6×10^6. The airfoils investigated were the NACA 0012 ($0°$ Tab), the SC 1095-R8, and the SC 1095. All three airfoils have a tab, which is a flat platelike extension to the normal trailing edge of an airfoil, that is usually used to reduce the airfoil pitching-moment coefficient. These airfoils were chosen because some data on model rotors and full-scale rotors utilizing these airfoils were available (refs. 1 and 2) or were expected to become available.

SYMBOLS

The units used for the physical quantities in this paper are given in both the International Systems of Units (SI) and U.S. Customary Units. The measurements and calculations were made in U.S. Customary Units.

c airfoil chord, cm (in.)

c_d section profile-drag coefficient, $\displaystyle\sum_{Wake} c_d' \frac{\Delta h}{c}$

c_d' point-drag coefficient,

$$2\left(\frac{p}{p_\infty}\right)^{6/7}\left[\frac{(p_t/p)^{2/7}-1}{(p_{t,\infty}/p_\infty)^{2/7}-1}\right]^{1/2}\left\{\left(\frac{p_t}{p_{t,\infty}}\right)^{1/7}-\left[\frac{(p_t/p_\infty)^{2/7}-1}{(p_{t,\infty}/p_\infty)^{2/7}-1}\right]^{1/2}\right\}$$

$c_{d_{M_{dd}}}$ section profile-drag coefficient at drag-divergence Mach number

c_m section pitching-moment coefficient about quarter-chord,

$$\sum_{U.S.}\left[c_p\left(0.25-\frac{x}{c}\right)\left(\frac{\Delta x}{c}\right)+c_p\left(\frac{z}{c}\right)\left(\frac{\Delta z}{c}\right)\right]+\sum_{L.S.}\left[c_p\left(0.25-\frac{x}{c}\right)\left(\frac{\Delta x}{c}\right)\right.$$
$$\left.+c_p\left(\frac{z}{c}\right)\left(\frac{\Delta z}{c}\right)\right]$$

c_n section normal-force coefficient, $\displaystyle\sum_{U.S.} c_p\left(\frac{\Delta x}{c}\right)+\sum_{L.S.} c_p\left(\frac{\Delta x}{c}\right)$

c_p static-pressure coefficient, $\dfrac{p_l-p_\infty}{q_\infty}$

h height of wake-survey probe tubes from given reference plane, cm (in.)

M Mach number

M_{dd} Mach number for drag divergence, $dc_d/dM = 0.1$

p static pressure, Pa (psi)

2

q   dynamic pressure, $\frac{1}{2}\rho v^2$, Pa (psi)

R   Reynolds number based on airfoil chord and free-stream conditions

t   airfoil thickness, cm (in.)

v   velocity, m/sec (ft/sec)

x   airfoil abscissa, cm (in.)

z   airfoil ordinate, cm (in.)

z_c ordinate of airfoil mean line, cm (in.)

α angle of attack, angle between airfoil chord line and airstream direction, deg

α_c angle of attack corrected for lift-interference effects, deg

ρ density, kg/m^3 $(slugs/ft^3)$

Subscripts:

l local

max   maximum

o   zero normal force

sep   separation

t   total

∞ free stream

Abbreviations:

L.S.   lower surface

U.S.   upper surface

APPARATUS AND METHODS

Airfoils

The airfoil profiles are shown in figure 1 and the thickness distributions and mean lines are shown in figure 2. The SC 1095-R8 airfoil was derived from the SC 1095 airfoil by the addition of a drooped nose; the mean line of the resultant airfoil forward of about 20-percent chord is drooped relative to that

of the SC 1095 airfoil, and the thickness of the SC 1095-R8 airfoil forward of about 15-percent chord is greater than that of the SC 1095 airfoil. Both airfoils have a trailing-edge tab which is about 3-percent chord in length and is deflected upwards about 3°. The maximum thickness of the SC 1095 airfoil as tested is 9.1-percent chord and is located at the 25-percent-chord station; the maximum thickness of the SC 1095-R8 airfoil as tested is 9.0-percent chord and is also located at the 25-percent-chord station. The maximum camber of the SC 1095 airfoil is 0.8-percent chord; the SC 1095-R8 airfoil has the same positive camber as the SC 1095, but it has a maximum mean-line ordinate of -1.6-percent chord. The addition of the 0° Tab to the NACA 0012 airfoil results in a reduction of the maximum thickness from 12-percent chord to 11.7-percent chord. The design coordinates for these airfoils are given in tables I to III.

The airfoils were machined from heat-treated stainless-steel blocks and had spans of 15.27 cm (6.010 in.) and chords of about 7.87 cm (3.1 in.). The models had about 22 orifices located in one chordwise row on each surface; the orifice rows were positioned 12.6-percent span on either side of midspan (tables IV to VI). Slots were milled in the airfoil surface and tubes were placed in the slots and then covered with epoxy. The final airfoil contour had a surface finish of 0.813 µm (0.000032 in.). The orifices were then drilled from the opposite sides of the model so there were no surface irregularities near the orifice row. The orifices had a diameter of 0.0508 cm (0.020 in.) and were drilled perpendicular to the local-surface contour.

Wind Tunnel

Tunnel description.- The Langley 6- by 28-Inch Transonic Tunnel (ref. 3) is a blowdown wind tunnel with a slotted floor and ceiling and is generally operated at stagnation pressures from about 207 kPa (30 psia) to 621 kPa (90 psia) and at Mach numbers from 0.35 to 0.90. The selection of the 0.05-open-slot geometry is described in detail in reference 4. Mach number is controlled by hydraulically actuated choker doors located downstream of the test section. The airfoil model spans the 15.27-cm (6.010-in.) width of the tunnel (fig. 3) and is rigidly attached by mounting tangs to two circular end plates which are driven by a hydraulic actuator to position the airfoil at the desired angle of attack. A test run usually consists of an angle-of-attack sweep at a constant Mach number and Reynolds number.

Two-dimensionality of flow.- The results of a previous investigation of rotorcraft airfoils in the Langley 6- by 28-Inch Transonic Tunnel (ref. 5) have shown that the indicated maximum normal-force coefficient is reduced by tunnel-wall boundary-layer influences. This reduction is characteristic of two-dimensional wind tunnels without proper sidewall boundary-layer control and occurs because the tunnel-wall boundary layer is thicker than that of the airfoil; therefore, initial separation begins at the tunnel wall. Efforts are under way to correct this difficulty, but the solution was not available for the investigation described in this paper.

Although it is not possible to determine precisely the affected Mach number range or the loss in maximum normal-force coefficient of the airfoils reported herein, a comparison of the NACA 0012 data measured in this facility

4

with 0.125 open slots (ref. 5) with unpublished data from two other facilities has been useful in indicating the magnitude of these losses. The maximum normal-force coefficients measured in the Langley Low-Turbulence Pressure Tunnel and the United Technologies Research Center 8 foot tunnel at similar Reynolds numbers and at a Mach number of 0.36 are higher than that from the Langley 6- by 28-Inch Transonic Tunnel by about 0.15. The difference between the data from the Langley 6- by 28-Inch Transonic Tunnel and the United Technologies data decreased to 0.10 at a Mach number of about 0.55. Incremental values for other airfoils may vary slightly because of specific configuration influences.

An investigation conducted in the Office National d'Etudes et de Recherches Aérospatiales (ONERA) R1 Ch wind tunnel (ref. 6) has shown that the tunnel side-wall boundary layer can affect the normal-force coefficients at all angles of attack (that is, with either attached or separated boundary layers). In this investigation, the sidewall boundary-layer thickness was varied by applying sidewall suction upstream of the model while the Mach number and Reynolds number were held constant. Generally an increase in sidewall boundary-layer thickness resulted in a decrease in the normal-force coefficient at a given angle of attack; the trend reversed at Mach numbers greater than 0.85 with a supercritical airfoil.

Apparatus

Wake-survey probe.- A traversing wake-survey probe is cantilevered from one tunnel sidewall to measure the profile drag of the airfoils. The probe vertical sweep rate, which was selected after experimental determination of acceptable lag time in the pressure measurements, was about 2.54 cm/sec (1.00 in/sec).

The probe was located 3.69 chords (based on the 7.87-cm (3.10-in.) chord model) downstream of the airfoil trailing edge and has a maximum vertical travel of about ±27.9 cm (±11.0 in.) from the tunnel center line (fig. 3). Data are acquired with four total-pressure tubes, which are made of stainless-steel tubing, with a 1.53-mm outside diameter and a 1.02-mm inside diameter (0.060 in. by 0.040 in.); the tubes are spaced 0.953 cm (0.375 in.) apart laterally as shown in figure 4.

Instrumentation.- All measurements made during the test program were obtained with the use of a high-speed, computer-controlled digital data acquisition system and were recorded by a high-speed tape-recording unit (ref. 3). All free-stream conditions were determined from stagnation and static pressures. All airfoil surface pressures and all wake pressures were measured with precision capacitive potentiometer pressure transducers. The electrical outputs from each of these transducers were connected to individual autoranging signal conditioners which have seven available ranges. The output signals from the four signal conditioners measuring the wake pressures were filtered with 20-Hz low-pass filters before input to the data acquisition system; the range of frequencies to be passed was experimentally determined during a previous investigation. The geometric angle of attack was determined from the output of a digital shaft encoder attached to a pinion engaging a rack on one model support end plate.

5

Tests and Methods

All of the testing was conducted with smooth model surfaces. Tests were made at stagnation pressures from 121 kPa (17.5 psia) to 138 kPa (20 psia) to obtain Reynolds numbers typical of model-scale rotors at Mach numbers from about 0.35 to 0.90. This range of stagnation pressures was below that normally run in the Langley 6- by 28-inch Transonic Tunnel, and a tunnel calibration at these pressures indicated that a new calibration should be used to reduce these data. An additional new calibration was used to reduce data at stagnation pressures from 165 kPa (24 psia) to 193 kPa (28 psia). This range of stagnation pressures was used to obtain data at Reynolds numbers between model scale and full scale. The full-scale Reynolds number data were obtained by testing at stagnation pressures from 531 kPa (77 psia) to 621 kPa (90 psia) at the lowest and highest test Mach numbers, respectively. Geometric angles of attack ranged from -4° to 18° at increments of 2° at the lower test Mach numbers; this range was decreased at the higher test Mach numbers.

Section normal-force and pitching-moment coefficients were calculated from the airfoil surface pressures by a trapezoidal integration of the pressure coefficients. The pressure coefficient at the most rearward orifice on each surface was applied from that station to the airfoil trailing edge in the integration because the small model size did not allow installation of orifices in the airfoil tab. Each of the pressure coefficients represents the average of five measurements obtained in a 1.0-second interval. A form of the equation described in reference 7 was used to calculate the point-drag coefficients from the measured wake pressures, and a trapezoidal integration of the point-drag coefficients was used to calculate the drag coefficient. The static pressures used in the wake drag calculation were measured with tunnel sidewall orifices located at the same longitudinal tunnel station as the tips of the tubes on the wake-survey probe. All of the drag coefficients presented in this paper represent the mean of the measurements made with three total-pressure tubes on the wake-survey probe in one sweep through a wake. The corrections for lift interference, which have been applied to the angles of attack, were obtained from references 4 and 8. The basic equations for the correction (see ref. 8) are

$$\alpha_c = \alpha + \Delta\alpha$$

where

$$\Delta\alpha = \frac{-c_n}{8}\left(\frac{c}{36.195}\right)\left(\frac{1}{k+1}\right)\left(\frac{180}{\pi}\right)$$

$$k = \frac{a}{h} K$$

and a is the slot spacing and h is the semiheight of the tunnel. The slotted-wall boundary-condition coefficient k for the present tunnel configuration is 0.4211K. A value of 3.5 was selected for the slotted-wall perform-

6

ance coefficient K, based on the data and discussion presented in reference 4. This substitution results in a correction given by the equation

$$\Delta\alpha = -c_n c(0.0800)$$

where c is in centimeters, α is in degrees, and the constant is in degrees per centimeter.

PRESENTATION OF RESULTS

The results of the investigation have been reduced to coefficient form and are presented in the following table:

Results	Airfoil	Figure
c_n against α_c; c_m and c_d against c_n	NACA 0012 (0° Tab) SC 1095-R8 SC 1095	5 6 7
$c_{n,max}$ against M	NACA 0012 (0° Tab) SC 1095-R8 SC 1095	8
$c_{d,o}$ against M	NACA 0012 (0° Tab) SC 1095-R8 SC 1095	9
$(c_n/c_d)_{max}$ against M	NACA 0012 (0° Tab) SC 1095-R8 SC 1095	10
c_n against M_{dd}	NACA 0012 (0° Tab) SC 1095-R8 SC 1095	11
$c_{d_{M_{dd}}}$ against c_n	NACA 0012 (0° Tab) SC 1095-R8 SC 1095	12
C_p against x/c	NACA 0012 (0° Tab) SC 1095-R8 SC 1095	13, 16, 20 14, 17 15, 18
$(\alpha_c)_{sep}$ and $(x/c)_{sep}$ against M	SC 1095-R8	19
C_p against M	SC 1095-R8 SC 1095	21
c_d against M	SC 1095-R8	22

DISCUSSION

Normal Force

Maximum normal-force coefficient.- The maximum normal-force coeffi-
cients of the NACA 0012 (0° Tab), the SC 1095-R8, and the SC 1095 airfoils have
been determined from the normal-force curves presented in figures 5(a), 6(a),
and 7(a), respectively, and are plotted as a function of Mach number in fig-
ure 8. Figure 8 shows that the effect of Reynolds number on $c_{n,max}$ is differ-
ent for the three airfoils. The maximum normal-force coefficient increases with
increasing Reynolds number for the range of Mach numbers presented for both the
NACA 0012 (0° Tab) and the SC 1095-R8 airfoils but not for the SC 1095 airfoil.
Increases in Reynolds number result in little change or a small reduction in
$c_{n,max}$ for the SC 1095 airfoil. In addition, the increment in $c_{n,max}$ result-
ing from the same increment in Reynolds number $\Delta c_n/\Delta R$ is not the same for the
NACA 0012 (0° Tab) and the SC 1095-R8 airfoils. These results are not sur-
prising since the flow field on these airfoils at $c_{n,max}$ generally includes
regions of supercritical flow, and it has been shown that the type and magnitude
of the scale effect on $c_{n,max}$ for the incompressible case do not vary in any
consistent manner (ref. 9). These trends can be explained by the normal-force
curves and the pressure distributions (figs. 13 to 18). The increases in
$c_{n,max}$ of the NACA 0012 (0° Tab) and the SC 1095-R8 airfoils are the result of
either one or both of the following: (1) Increased suction (more negative C_p)
on the upper surface near the leading edge at the same angle of attack (figs. 13
and 14); and (2) a delay of the turbulent boundary-layer separation to a higher
angle of attack at the higher Reynolds number. (See figs. 5(a), 13, 16, 6(a),
14, and 17.) The values of $c_{n,max}$ for the SC 1095 airfoil generally decrease
with increasing Reynolds number because of the occurrence of substantial
boundary-layer separation at a lower angle of attack at the higher Reynolds num-
ber (figs. 7(a) and 15). This trend of $c_{n,max}$ is possibly caused by a forward
movement of a laminar separation bubble with increasing Reynolds number which
would result in a greater length of turbulent boundary layer at the higher
Reynolds number. The presence of a laminar separation bubble may be responsi-
ble for the related tendency of α_c for $c_{n,max}$ to be generally lower at the
higher Reynolds numbers ($M \lesssim 0.54$).

At the full-scale Reynolds numbers the values of $c_{n,max}$ for the
SC 1095-R8 airfoil are higher than those for the SC 1095 airfoil at all Mach
numbers presented, but at the model-scale Reynolds numbers the values of $c_{n,max}$
for the SC 1095-R8 airfoil exceed those for the SC 1095 airfoil only for Mach
numbers up to about 0.40 (fig. 8). This trend at the highest Reynolds number is
the expected result of the increased leading-edge camber and greater thickness
in the leading-edge region of the SC 1095-R8 airfoil. Figure 8 also shows that
the airfoil with the highest values of $c_{n,max}$, the SC 1095-R8, has the greatest
sensitivity to increasing Mach number for $M < 0.55$. The decrease in $c_{n,max}$
of the SC 1095-R8 airfoil is the result of either supercritical flow-induced
separation occurring at a lower angle of attack or a more extensive separation
(separation point farther forward) occurring at the same angle of attack with
increasing Mach number (figs. 17 and 19). Since the SC 1095-R8 airfoil is more
highly loaded in the leading-edge region than the other two airfoils and the
boundary-layer separation reduces the leading-edge suction, the reduction in
$c_{n,max}$ with Mach number is greater for this airfoil.

For the range of Mach numbers presented in figure 8, the stall of both the NACA 0012 (0° Tab) and the SC 1095-R8 airfoils becomes less abrupt as a result of increasing Reynolds number from model scale to full scale (figs. 5(a) and 6(a)). The stall of the SC 1095 airfoil becomes less abrupt with increasing Reynolds number for Mach numbers of about 0.39 and 0.44 but not at the other Mach numbers (fig. 7(a)). The pressure distributions presented in figures 16 to 18 indicate that the stall of these airfoils is of the trailing-edge type by the characteristic loss of pressure recovery (more negative C_p) on the upper surface near the trailing edge.

Slope.- The slopes of the normal-force curves of both cambered airfoils increase slightly with increasing Reynolds number at almost all Mach numbers presented. The slopes of the curves of the NACA 0012 (0° Tab) airfoil are essentially insensitive to Reynolds number changes except at the highest test Mach number. Figure 5(a) shows a large and unusual change in the slope of the normal-force curve of the NACA 0012 (0° Tab) airfoil with increasing Reynolds number at a Mach number of about 0.88. The test runs at this Mach number and a Reynolds number of 2.1×10^6 were made twice and the repeatability of the data was excellent. The pressure distributions presented in figure 20 for an angle of attack of about -2.0° indicate that the shock position on the upper surface moves forward as a result of increasing Reynolds number from 1.5×10^6 to 2.1×10^6 and then moves rearward again at the highest Reynolds number. This forward shift of the shock position results in substantially more down load (negative lift) on the rear of the airfoil at a Reynolds number of 2.1×10^6, thus giving rise to a steeper slope.

The SC 1095-R8 and SC 1095 airfoils both have near-zero normal force at $\alpha_c = 0^\circ$, although they are cambered airfoils. This near-zero normal force is the result of both the camber-line geometry and the trailing-edge tab.

Pitching Moment

The pitching-moment coefficient about the aerodynamic center (c_m at $c_n = 0$) is essentially unchanged by increases in Reynolds number at all Mach numbers presented for these three airfoils (figs. 5(b), 6(b), and 7(b)). These figures also show that the only effect of Reynolds number is to change the "knee" of the curve; that is, increases in Reynolds number generally move the nose-down break to higher normal-force coefficients for all the airfoils at Mach numbers up to about 0.78. This result is expected where the maximum normal-force coefficients increase with increasing Reynolds number. At a Mach number of about 0.88, the trend of the pitching moment of the NACA 0012 (0° Tab) airfoil is substantially different at a Reynolds number of 2.1×10^6 than at the lowest and highest Reynolds numbers. The reason for this difference is the shift of the shock position with Reynolds number mentioned previously. The pitching-moment coefficient about the aerodynamic center (c_m at $c_n = 0$) of the SC 1095-R8 airfoil displays the most sensitivity to increasing Mach number. Analysis of the pressure distributions (figs. 17 and 18) indicates that the SC 1095-R8 airfoil develops supercritical flow on the lower surface at a lower free-stream Mach number than the SC 1095 airfoil, and it is the growth of this supersonic zone with increasing Mach number that causes the greater Mach number sensitivity (fig. 21).

It is interesting to note that the data of figures 6(b) and 7(b) suggest that both of the cambered airfoils were designed for zero pitching-moment coefficient, although some authors have mentioned a pitching-moment level of up to $|0.02|$ as acceptable (ref. 10). The zero pitching-moment level of the SC 1095 and the SC 1095-R8 airfoils is due to the trailing-edge tab. It is also interesting to note that the leading-edge modifications made to the SC 1095 airfoil which resulted in the SC 1095-R8 configuration did not change the pitching-moment coefficient about the aerodynamic center by more than about 0.01 for Mach numbers as high as 0.73 but did increase the values of $c_{n,max}$ significantly.

Drag

Drag at zero normal force.- At a constant Mach number, the effect of increasing Reynolds number from model scale to full scale is to reduce $c_{d,o}$ for both cambered airfoils for all Mach numbers presented and to reduce $c_{d,o}$ for the NACA 0012 (0° Tab) airfoil for Mach numbers up to about 0.65 (fig. 9). The difference in $c_{d,o}$ of the NACA 0012 (0° Tab) airfoil at model-scale and full-scale Reynolds numbers is small at the lowest test Mach number (0.34), and this difference gradually disappears with increasing Mach number. The incremental decrease in $c_{d,o}$ at a given Mach number is generally different for each of the airfoils; the $\Delta c_{d,o}$ for the SC 1095-R8 airfoil is the largest, and that for the NACA 0012 (0° Tab) airfoil, the smallest. These trends are the result of the well-known reduction in laminar and turbulent boundary-layer skin friction with increasing Reynolds number (ref. 11).

The insensitivity of $c_{d,o}$ of the NACA 0012 (0° Tab) airfoil to Reynolds number is consistent with low-speed data of the NACA 0012 airfoil (refs. 9 and 12). The value of $c_{d,o}$ for the NACA 0012 (0° Tab) airfoil at a Mach number of 0.43 and a Reynolds number of 3.9×10^6 is about 0.0005 higher than that measured for the NACA 0012 airfoil in the Langley Low-Turbulence Pressure Tunnel at a Mach number of 0.36 and the same Reynolds number (unpublished data). The difference in drag level may be due to a higher turbulence level in the Langley 6- by 28-Inch Transonic Tunnel at stagnation pressures above about 517 kPa (75 psia). Unpublished NACA 0012 airfoil data measured on two different chord models at the same Mach number and Reynolds number in the Langley 6- by 28-Inch Transonic Tunnel indicate a higher $c_{d,o}$ for the smaller chord model, thus implying a higher turbulence level at the higher stagnation pressure (552 kPa (80 psia)). Therefore the increments in $c_{d,o}$ from model-scale to full-scale Reynolds numbers presented in this paper are believed to be smaller than those which would be measured in free air.

Analysis of the pressure distributions indicates that the increase in $c_{d,o}$ with increasing Mach number for each of the airfoils at both model-scale and full-scale Reynolds numbers is the result of the development of supercritical flow and shock waves.

Maximum normal-force—drag ratio.- The values of $(c_n/c_d)_{max}$ have been determined from the drag data shown in figures 5(c), 6(c), and 7(c) and are presented as a function of Mach number in figure 10. At a constant Mach number, the values of $(c_n/c_d)_{max}$ for all the airfoils increase with an increase in Reynolds number from model scale to full scale for all Mach numbers presented.

10

The increases in this parameter with Reynolds number are the result of both a lower skin-friction drag for a given normal-force coefficient and a delay of turbulent boundary-layer separation to higher normal-force coefficients at the higher Reynolds numbers. The increments in $(c_n/c_d)_{max}$ due to Reynolds number at a given Mach number less than 0.70 are generally quite different for each of the airfoils. The increases in $(c_n/c_d)_{max}$ due to Reynolds number are generally small for all the airfoils at Mach numbers above about 0.70 where supercritical flow effects predominate over the viscous effects. This predominance can be illustrated by showing that the knee of the drag curve is controlled by the development of supercritical flow and not by separation. By drawing a tangent to the drag curve of the NACA 0012 (0° Tab) airfoil at a Mach number of 0.77 and a Reynolds number of 6.5×10^6 (fig. 5(c)), $(c_n/c_d)_{max}$ is shown to occur at a normal-force coefficient of about 0.26. The pressure distribution (fig. 16(j)) corresponding to a higher c_n (0.36) indicates supercritical flow on the upper surface from about 3- to 50-percent chord and no characteristics of separation. (Minor separation could exist aft of 93-percent chord.)

Drag divergence.- The drag coefficients at constant values of c_n were cross plotted to obtain the drag-divergence Mach numbers. The normal-force coefficients corresponding to the drag-divergence Mach numbers at model-scale and full-scale Reynolds numbers are presented in figure 11. The effect of Reynolds number on M_{dd} is greatest for normal-force coefficients above about 0.7 for all the airfoils. The drag divergence at high normal-force coefficients ($c_n > 0.7$) may be controlled more by shock-induced boundary-layer separation than by sonic flow (ref. 13) moving aft of the airfoil crest. An analysis of the pressure distributions for these airfoils at model-scale Reynolds numbers suggests that this is the case. This explanation for drag divergence would be consistent with the generally larger effect of Reynolds number on M_{dd} at the high values of c_n because boundary-layer thickness would be crucial to drag divergence resulting from flow separation. The drag-divergence Mach number at zero normal-force coefficient of the NACA 0012 (0° Tab) and the SC 1095 airfoils is unchanged by the increase in Reynolds number, but that of the SC 1095-R8 airfoil is reduced by about 0.02 because of the increase in Reynolds number. Figure 11 also indicates that the drag-divergence Mach numbers corresponding to all normal-force coefficients between about -0.1 and 0.3 of the SC 1095-R8 airfoil are lower at the full-scale Reynolds numbers than at the model-scale Reynolds numbers. A study of the curves of c_d against M for this range of normal-force coefficients (fig. 22) indicates that the drag coefficients at a Mach number of 0.78 at the full-scale Reynolds numbers would have to be lower for the M_{dd} to be as high as that at the model-scale Reynolds numbers. Although Reynolds number has essentially no effect on M_{dd} of the NACA 0012 (0° Tab) airfoil at normal-force coefficients up to about 0.75, the drag coefficient at M_{dd} is reduced at the full-scale Reynolds number for normal-force coefficients greater than 0.2 (fig. 12). Figure 12 shows that $c_{d_{M_{dd}}}$ decreases

with increasing Reynolds number for almost all normal-force coefficients for both cambered airfoils.

CONCLUSIONS

An investigation has been conducted in the Langley 6- by 28-Inch Transonic Tunnel to determine the two-dimensional aerodynamic characteristics of three helicopter rotor airfoils at Reynolds numbers from model scale to full scale at Mach numbers from about 0.35 to 0.90. The airfoils included in this investigation were the NACA 0012 (0° Tab), the SC 1095-R8, and the SC 1095. Analysis of the test data has resulted in the following conclusions:

1. The maximum normal-force coefficients of the NACA 0012 (0° Tab) and the SC 1095-R8 airfoils increased with increasing Reynolds number at all Mach numbers presented. The maximum normal-force coefficients of the SC 1095 airfoil at full-scale Reynolds numbers were about the same or slightly lower than those at model-scale Reynolds numbers.

2. The pitching-moment coefficients about the aerodynamic center of these three airfoils were essentially unchanged with increases in Reynolds number at all Mach numbers presented.

3. At a constant Mach number, the drag coefficient at zero normal force $c_{d,o}$ of both cambered airfoils decreased with increasing Reynolds number for all test Mach numbers. At a constant Mach number up to about 0.65, the values of $c_{d,o}$ of the NACA 0012 (0° Tab) airfoil decreased with increasing Reynolds number. The difference in $c_{d,o}$ of the NACA 0012 (0° Tab) airfoil at model-scale and full-scale Reynolds numbers was small at a Mach number of 0.34. This difference gradually disappeared as the Mach number increased to 0.65.

4. For all test Mach numbers presented, the maximum normal-force—drag ratios of these three airfoils at the full-scale Reynolds number were higher than those at the model-scale Reynolds number.

5. In general, the effect of Reynolds number on drag-divergence Mach number was greatest for normal-force coefficients above about 0.7 for these three airfoils. The drag-divergence Mach number at zero normal-force coefficient of the NACA 0012 (0° Tab) and the SC 1095 airfoils was insensitive to Reynolds number changes, but that of the SC 1095-R8 airfoil was reduced by about 0.02 because of the change from model-scale to full-scale Reynolds number.

Langley Research Center
National Aeronautics and Space Administration
Hampton, VA 23665
July 3, 1980

REFERENCES

1. Weller, William H.: Experimental Investigation of Effects of Blade Tip Geometry on Loads and Performance for an Articulated Rotor System. NASA TP-1303, 1979.

2. Stroub, Robert H.: Full-Scale Wind Tunnel Test of a Modern Helicopter Main Rotor - Investigation of Tip Mach Number Effects and Comparisons of Four Tip Shapes. Preprint No. 03, Proceedings of the 34th Annual National Forum, American Helicopter Soc., Inc., May 1978.

3. Ladson, Charles L.: Description and Calibration of the Langley 6- by 28-Inch Transonic Tunnel. NASA TN D-8070, 1975.

4. Barnwell, Richard W.: Design and Performance Evaluation of Slotted Walls for Two-Dimensional Wind Tunnels. NASA TM-78648, 1978.

5. Noonan, Kevin W.; and Bingham, Gene J.: Two-Dimensional Aerodynamic Characteristics of Several Rotorcraft Airfoils at Mach Numbers From 0.35 to 0.90. NASA TM X-73990, 1977.

6. Bernard-Guelle, René: Influence of Wind Tunnel Wall Boundary Layers on Two-Dimensional Transonic Tests. NASA TT F-17,255, 1976.

7. Baals, Donald D.; and Mourhess, Mary J.: Numerical Evaluation of the Wake-Survey Equations for Subsonic Flow Including the Effect of Energy Addition. NACA WR L-5, 1945. (Formerly NACA ARR L5H27.)

8. Davis, Don D., Jr.; and Moore, Dewey: Analytical Study of Blockage- and Lift-Interference Corrections for Slotted Tunnels Obtained by the Substitution of an Equivalent Homogeneous Boundary for the Discrete Slots. NACA RM L53E07b, 1953.

9. Loftin, Laurence K., Jr.; and Smith, Hamilton A.: Aerodynamic Characteristics of 15 NACA Airfoil Sections at Seven Reynolds Numbers From 0.7×10^6 to 9.0×10^6. NACA TN 1945, 1949.

10. Wortmann, F. X.; and Drees, Jan M.: Design of Airfoils for Rotors. CAL/AVLABS Symposium Proceedings: Aerodynamics of Rotary Wing and V/STOL Aircraft, Volume I - Rotor/Propeller Aerodynamics, Rotor Noise, June 18-20, 1969.

11. Schlichting, Hermann (J. Kestin, transl.): Boundary-Layer Theory. Sixth ed. McGraw-Hill Book Co., Inc., c.1968.

12. Abbott, Ira H.; Von Doenhoff, Albert E.; and Stivers, Louis S., Jr.: Summary of Airfoil Data. NACA Rep. 824, 1945. (Supersedes NACA WR L-560.)

13. Bingham, Gene J.: An Analytical Evaluation of Airfoil Sections for Helicopter Rotor Applications. NASA TN D-7796, 1975.

TABLE I.- DESIGN COORDINATES FOR

NACA 0012 (0° Tab) AIRFOIL

$$\begin{bmatrix} \text{Stations and ordinates given in percent} \\ \text{airfoil chord} \end{bmatrix}$$

Station	Upper surface	Lower surface
0	0	0
.244	.851	-.851
.488	1.193	-1.193
.977	1.664	-1.664
1.465	2.015	-2.015
2.441	2.553	-2.553
3.418	2.972	-2.972
4.395	3.318	-3.318
5.859	3.748	-3.748
7.324	4.101	-4.101
9.766	4.573	-4.573
11.719	4.871	-4.871
14.648	5.220	-5.220
16.602	5.399	-5.399
19.531	5.603	-5.603
24.414	5.802	-5.802
29.297	5.861	-5.861
34.180	5.809	-5.809
39.063	5.667	-5.667
43.945	5.450	-5.450
48.828	5.170	-5.170
53.711	4.836	-4.836
58.594	4.456	-4.456
63.477	4.036	-4.036
68.359	3.578	-3.578
73.242	3.086	-3.086
78.125	2.562	-2.562
83.008	2.004	-2.004
87.891	1.414	-1.414
92.773	.788	-.788
97.137	.195	-.195
100.000	.195	-.195

14

TABLE II.- DESIGN COORDINATES FOR SC 1095-R8 AIRFOIL

$$\begin{bmatrix} \text{Stations and ordinates given in} \\ \text{percent airfoil chord} \end{bmatrix}$$

Station	Upper surface	Lower surface	Station	Upper surface	Lower surface
0	-1.621	-1.621	12.939	4.748	-3.693
.086	-1.113	-2.129	15.337	4.949	-3.693
.230	-.681	-2.427	17.735	5.103	-3.693
.470	-.182	-2.714	20.132	5.208	-3.693
.710	.201	-2.887	22.530	5.275	-3.693
.950	.518	-3.002	24.928	5.304	-3.693
1.189	.796	-3.088	27.326	5.304	-3.693
1.429	1.055	-3.156	29.724	5.294	-3.683
1.669	1.285	-3.204	34.519	5.208	-3.626
1.909	1.496	-3.251	39.315	5.064	-3.530
2.148	1.707	-3.290	44.111	4.882	-3.395
2.388	1.890	-3.328	48.907	4.642	-3.232
2.628	2.072	-3.357	53.702	4.364	-3.031
2.868	2.235	-3.386	58.498	4.028	-2.801
3.108	2.388	-3.415	63.294	3.654	-2.532
3.347	2.532	-3.443	68.089	3.232	-2.235
3.587	2.657	-3.462	72.885	2.762	-1.909
3.827	2.782	-3.482	77.681	2.264	-1.554
4.307	3.002	-3.520	82.477	1.726	-1.189
4.786	3.194	-3.549	87.272	1.180	-.806
5.266	3.367	-3.578	92.068	.614	-.422
5.745	3.520	-3.597	94.466	.317	-.221
6.225	3.654	-3.606	95.137	.230	-.173
6.704	3.779	-3.626	95.521	.192	-.153
7.664	4.000	-3.654	96.864	.249	-.067
8.623	4.182	-3.664	98.782	.345	.038
9.582	4.335	-3.674	100.000	.403	.086
10.541	4.479	-3.683			

TABLE III.- DESIGN COORDINATES FOR SC 1095 AIRFOIL

[Stations and ordinates given in percent airfoil chord]

Station	Upper surface	Lower surface	Station	Upper surface	Lower surface
0	0	0	16.946	5.152	-3.622
.242	.668	-.533	19.367	5.258	-3.680
.484	.988	-.804	21.788	5.326	-3.709
.726	1.259	-1.036	24.208	5.355	-3.728
.968	1.501	-1.230	26.629	5.355	-3.728
1.210	1.714	-1.385	29.050	5.345	-3.718
1.453	1.908	-1.540	33.892	5.258	-3.660
1.695	2.092	-1.666	38.733	5.113	-3.563
1.937	2.256	-1.772	43.575	4.929	-3.428
2.179	2.411	-1.879	48.417	4.687	-3.263
2.421	2.556	-1.975	53.258	4.406	-3.060
2.663	2.682	-2.063	58.100	4.067	-2.828
2.905	2.808	-2.150	62.942	3.689	-2.556
3.389	3.031	-2.305	67.783	3.263	-2.256
3.873	3.225	-2.450	72.625	2.789	-1.927
4.358	3.399	-2.576	77.467	2.285	-1.569
4.842	3.554	-2.692	82.309	1.743	-1.201
5.326	3.689	-2.789	87.150	1.191	-.813
5.810	3.815	-2.866	91.992	.620	-.426
6.778	4.038	-3.002	94.413	.320	-.223
7.747	4.222	-3.108	95.091	.232	-.174
8.715	4.377	-3.196	95.478	.194	-.155
9.683	4.522	-3.273	96.834	.252	-.068
12.104	4.793	-3.428	98.770	.349	.039
14.525	4.997	-3.544	100.000	.407	.087

TABLE IV.- STATIC-PRESSURE ORIFICE LOCATIONS

FOR NACA 0012 (0° Tab) AIRFOIL

[Locations given in percent airfoil chord]

Upper-surface station	Lower-surface station
0	0
1.10	1.01
2.47	2.50
4.96	5.06
7.25	7.04
9.82	9.76
14.67	14.68
19.54	19.55
24.59	24.62
29.52	29.34
34.15	34.28
39.02	38.95
43.90	43.96
48.84	48.80
53.74	53.70
58.52	58.48
63.52	63.50
68.32	68.40
73.17	73.23
77.98	78.19
83.01	83.11
88.00	87.95
92.92	92.83

TABLE V.- STATIC-PRESSURE ORIFICE LOCATIONS

FOR SC 1095-R8 AIRFOIL

[Locations given in percent airfoil chord]

Upper-surface station	Lower-surface station
0	0
1.12	1.31
2.06	-----
3.24	3.69
5.70	6.11
7.90	8.52
10.40	12.85
15.24	-----
20.10	20.03
24.88	24.84
29.67	29.62
34.46	34.41
39.29	39.20
44.09	44.00
48.88	48.81
53.67	53.60
58.50	58.39
63.28	63.22
68.07	68.02
72.87	72.80
77.66	77.59
82.49	82.37
87.28	87.19

TABLE VI.- STATIC-PRESSURE ORIFICE LOCATIONS

FOR SC 1095 AIRFOIL

[Locations given in percent airfoil chord]

Upper-surface station	Lower-surface station
0	0
1.05	1.20
2.40	2.33
4.66	4.63
7.10	7.05
9.56	9.56
14.34	14.51
19.33	19.34
24.21	24.16
29.07	29.05
33.89	33.87
38.77	38.72
43.59	43.58
48.46	48.41
53.30	53.25
58.16	58.08
63.00	62.98
67.85	67.71
72.68	72.66
77.50	77.53
82.29	82.37
87.25	87.19
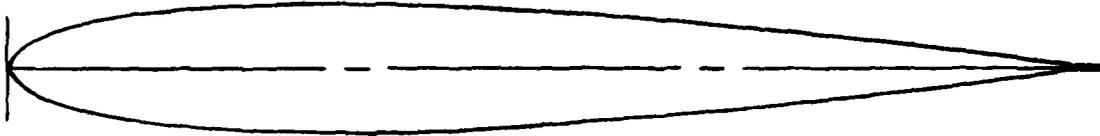
NACA 0012 (0° Tab)
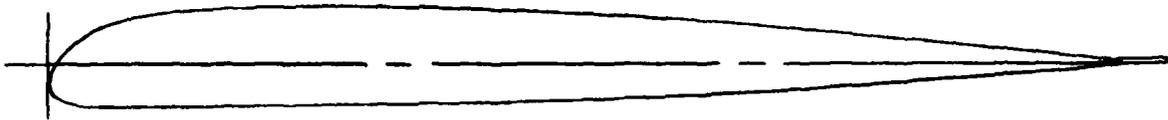
SC 1095-R8
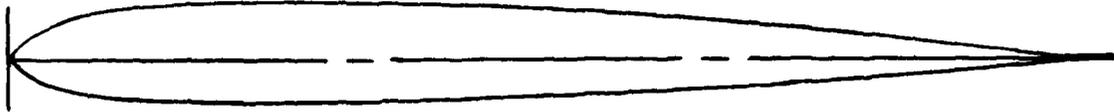
SC 1095

Figure 1.- Airfoil profiles.
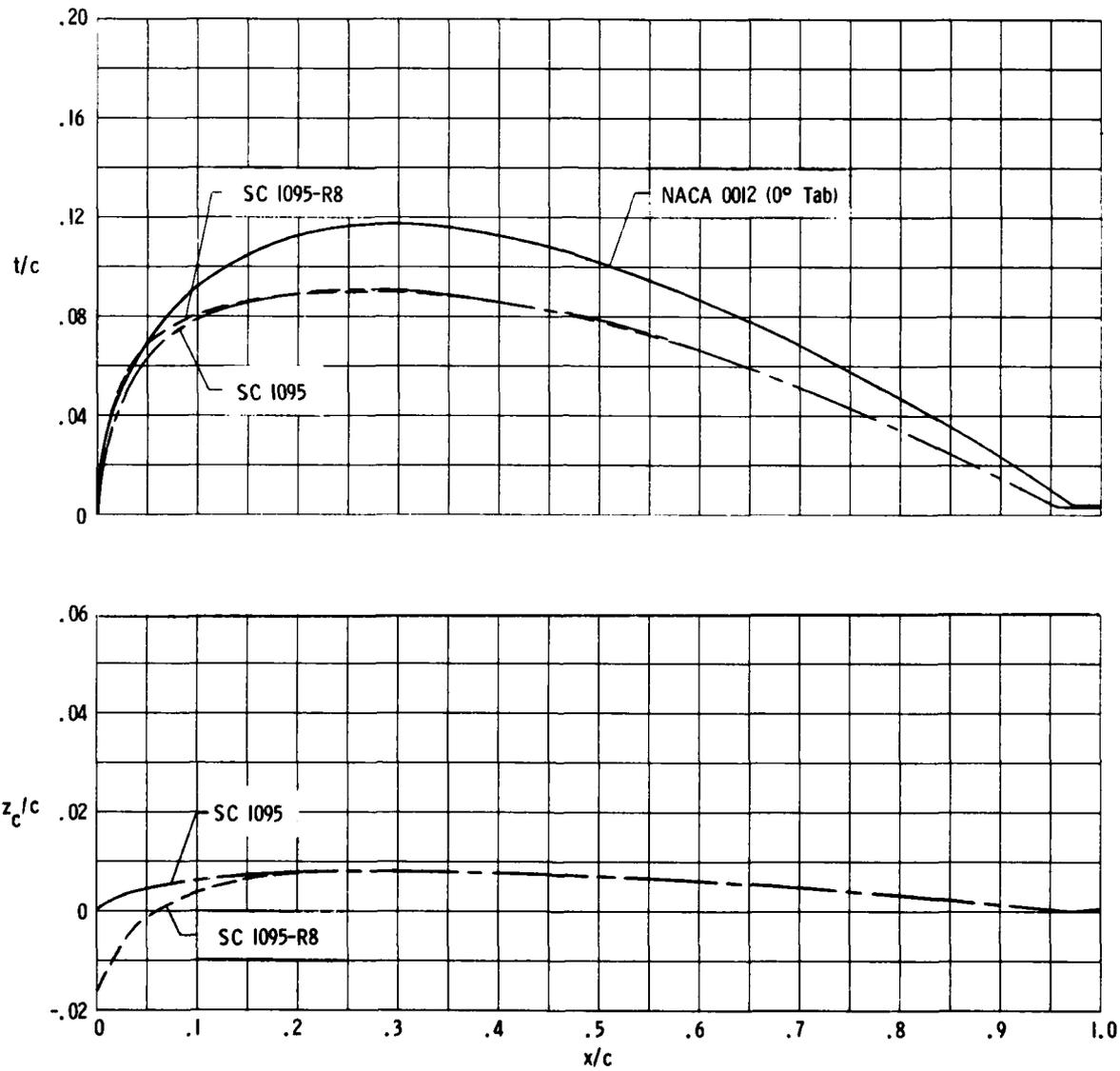
Figure 2.- Airfoil thickness distributions and mean lines.
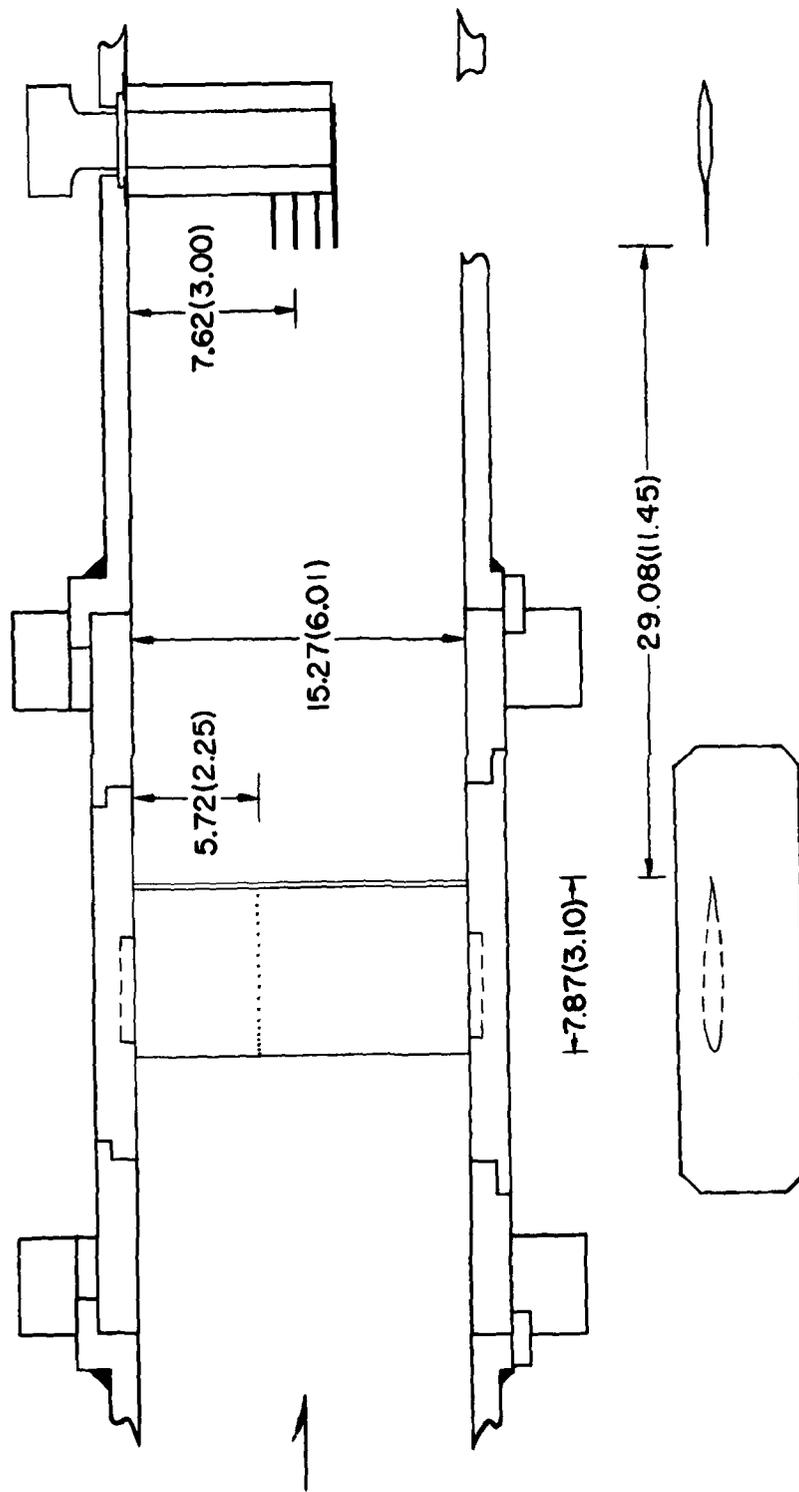
Figure 3.- Model and wake-survey probe installation in Langley 6- by 28-Inch Transonic Tunnel. All dimensions are in cm (in.).

22
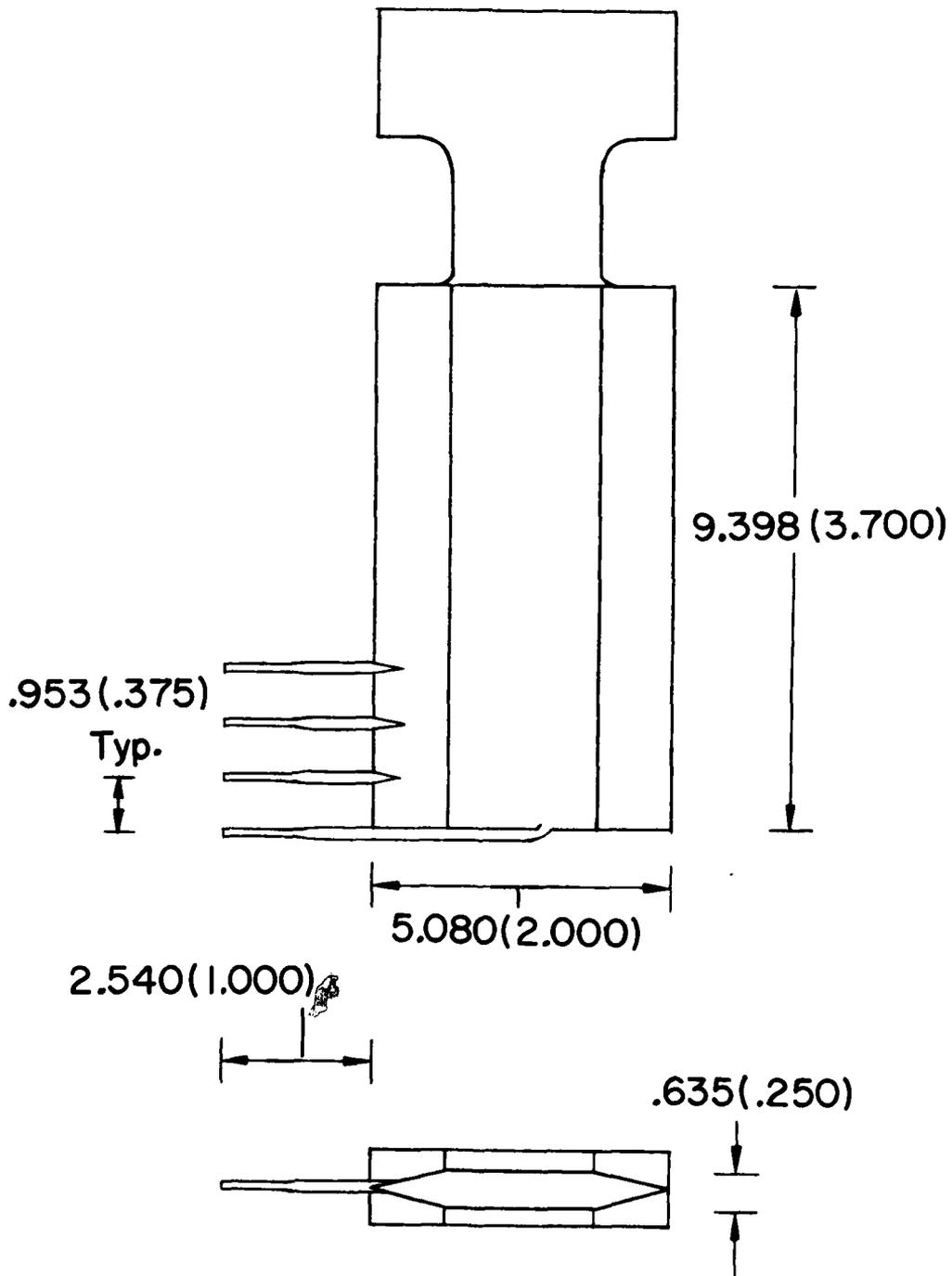
Figure 4.- Wake-survey probe used in Langley 6- by 28-Inch Transonic Tunnel.
All dimensions are in cm (in.).

23
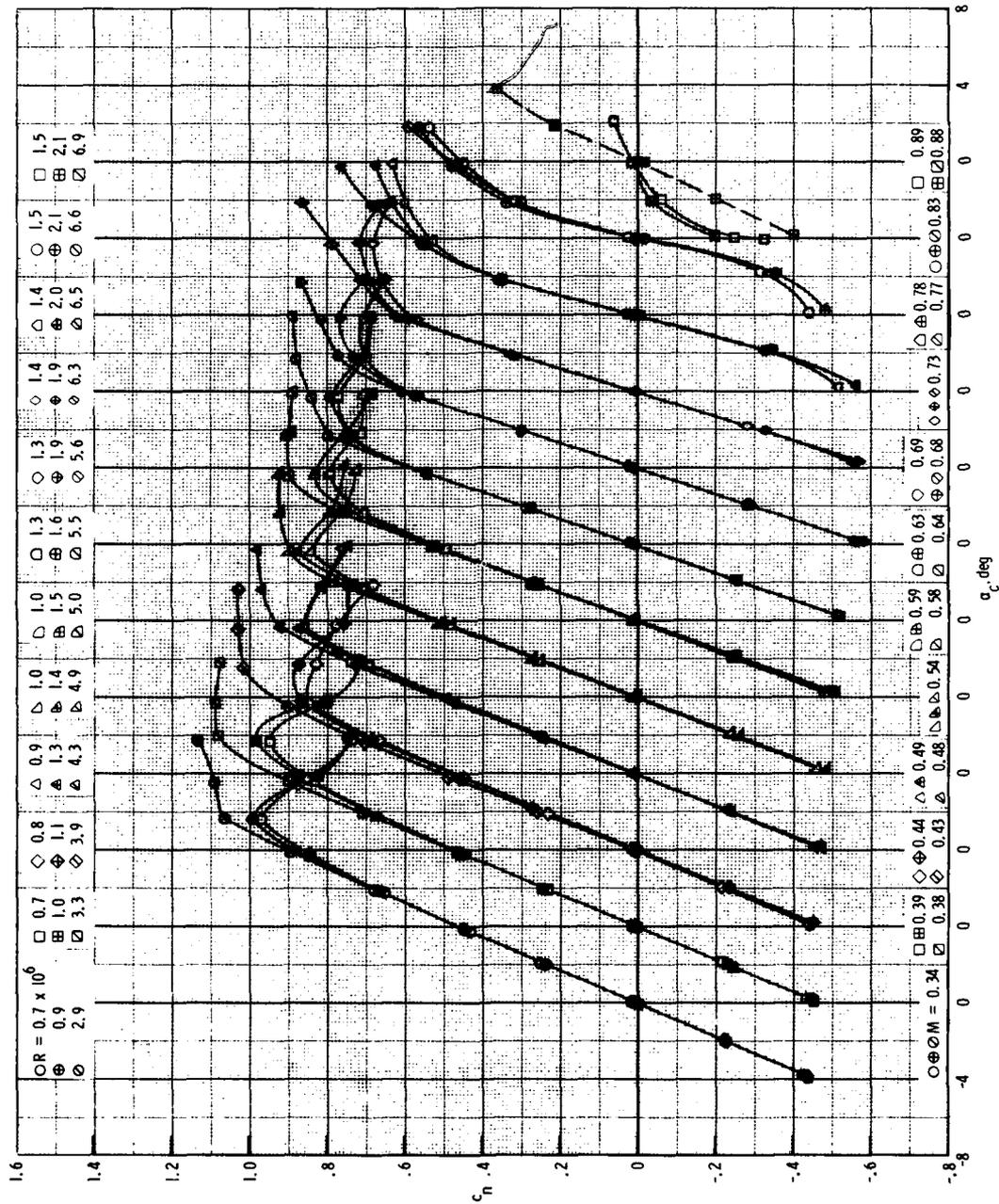
(a) Section normal-force coefficients.

Figure 5.- Effect of Reynolds number on aerodynamic characteristics of NACA 0012 (0° Tab) airfoil.

24
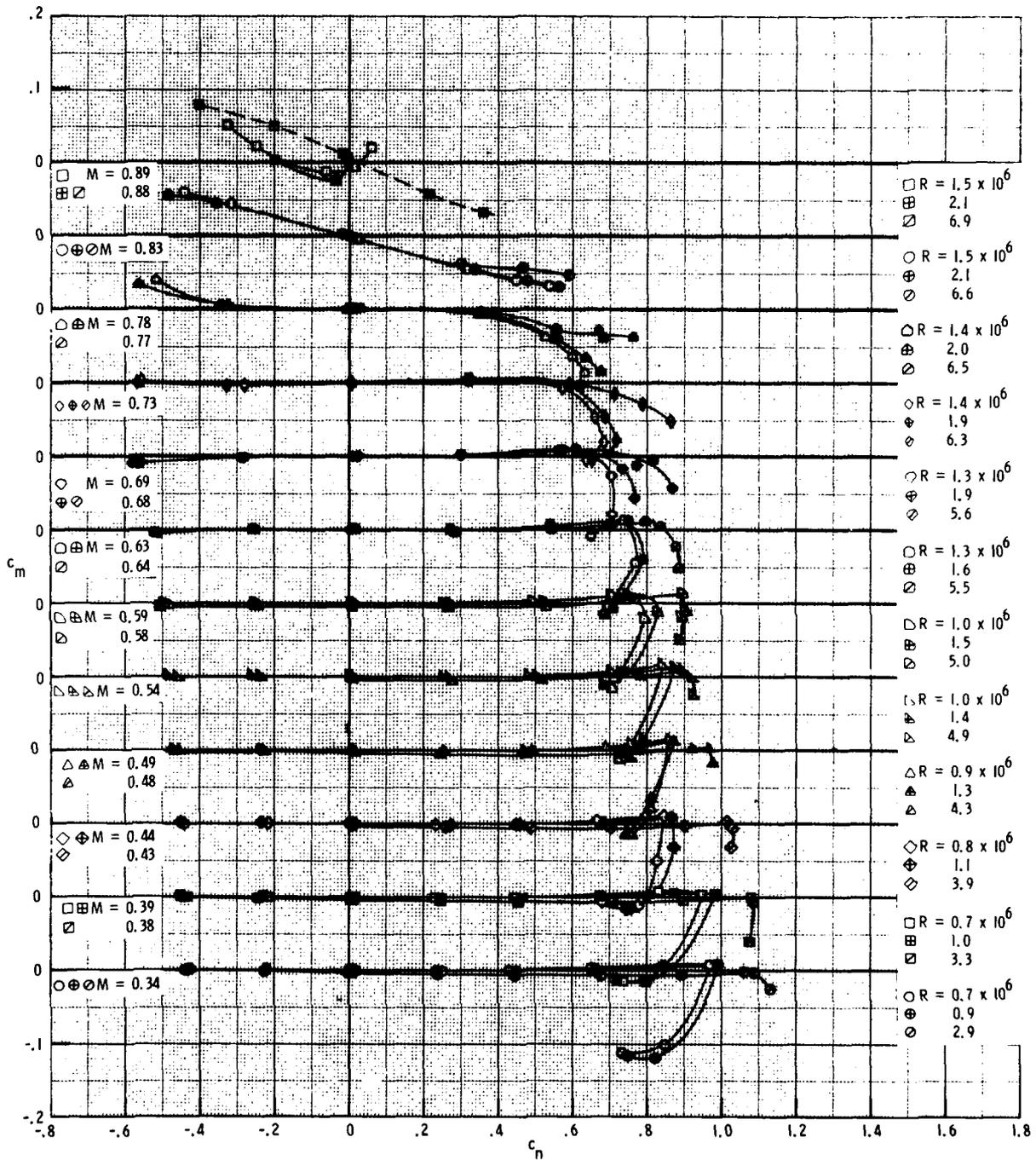
(b) Section pitching-moment coefficients.

Figure 5.- Continued.
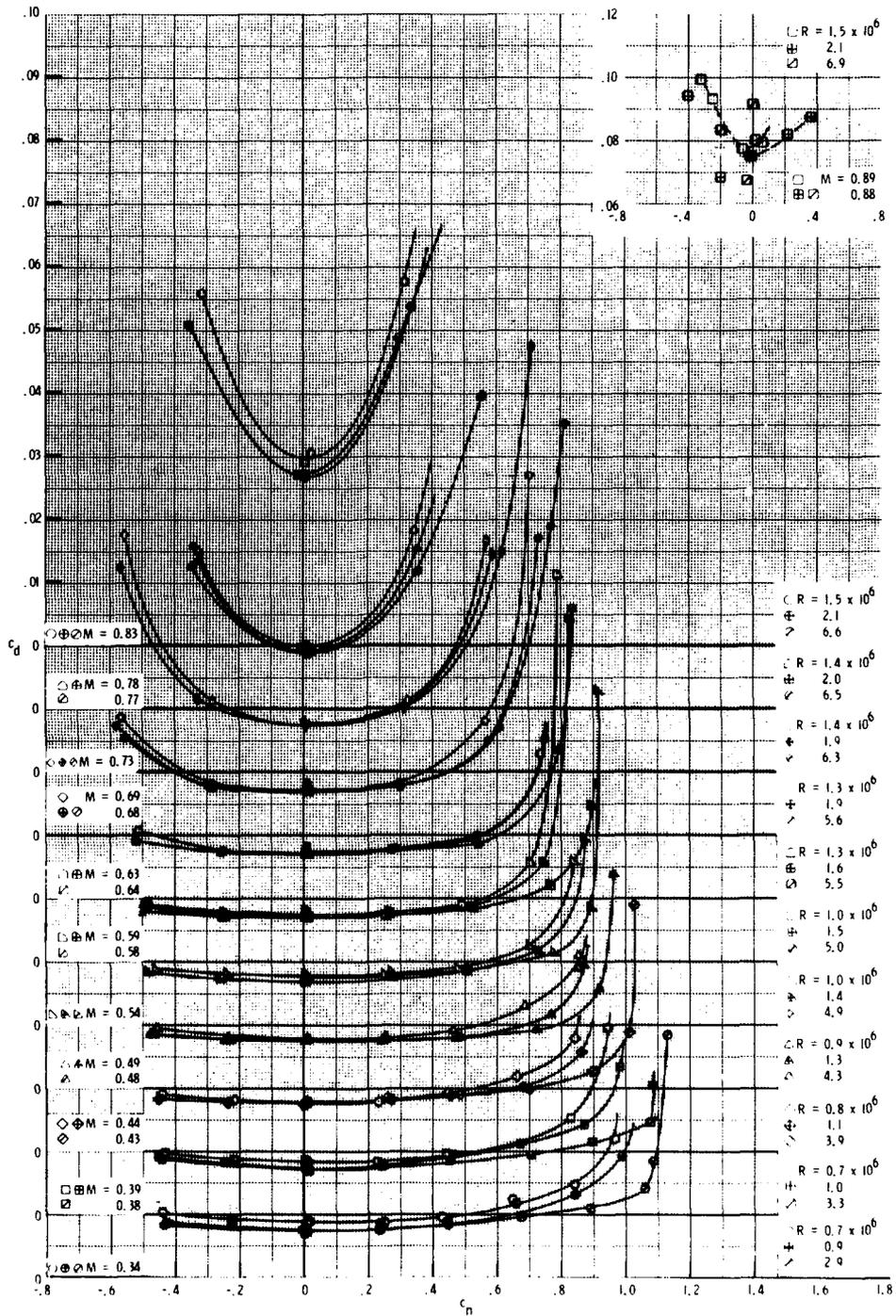
(c) Section drag coefficients.

Figure 5.- Concluded.
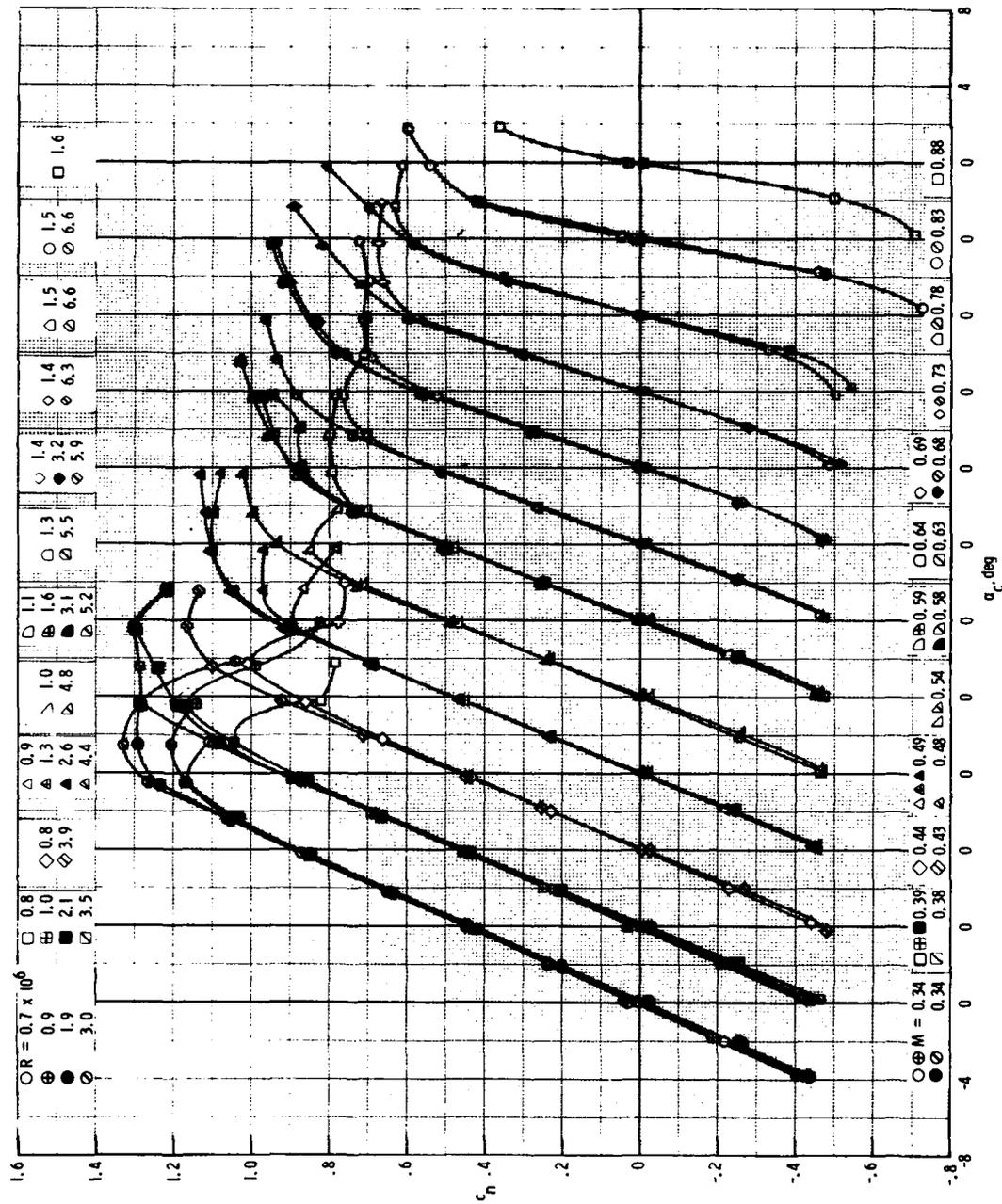
(a) Section normal-force coefficients.

Figure 6.- Effect of Reynolds number on aerodynamic characteristics of SC 1095-R8 airfoil.

27
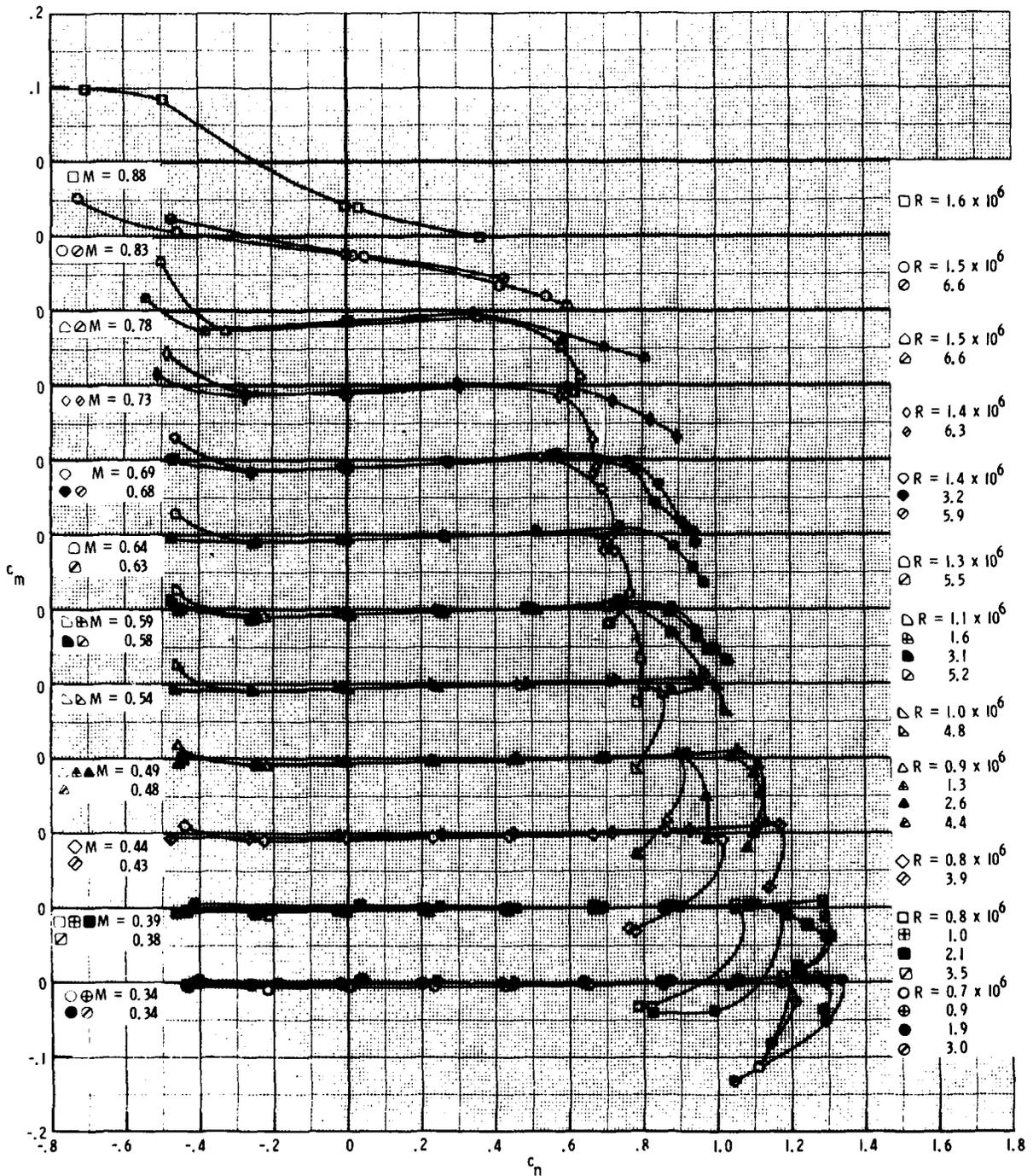
(b) Section pitching-moment coefficients.

Figure 6.- Continued.
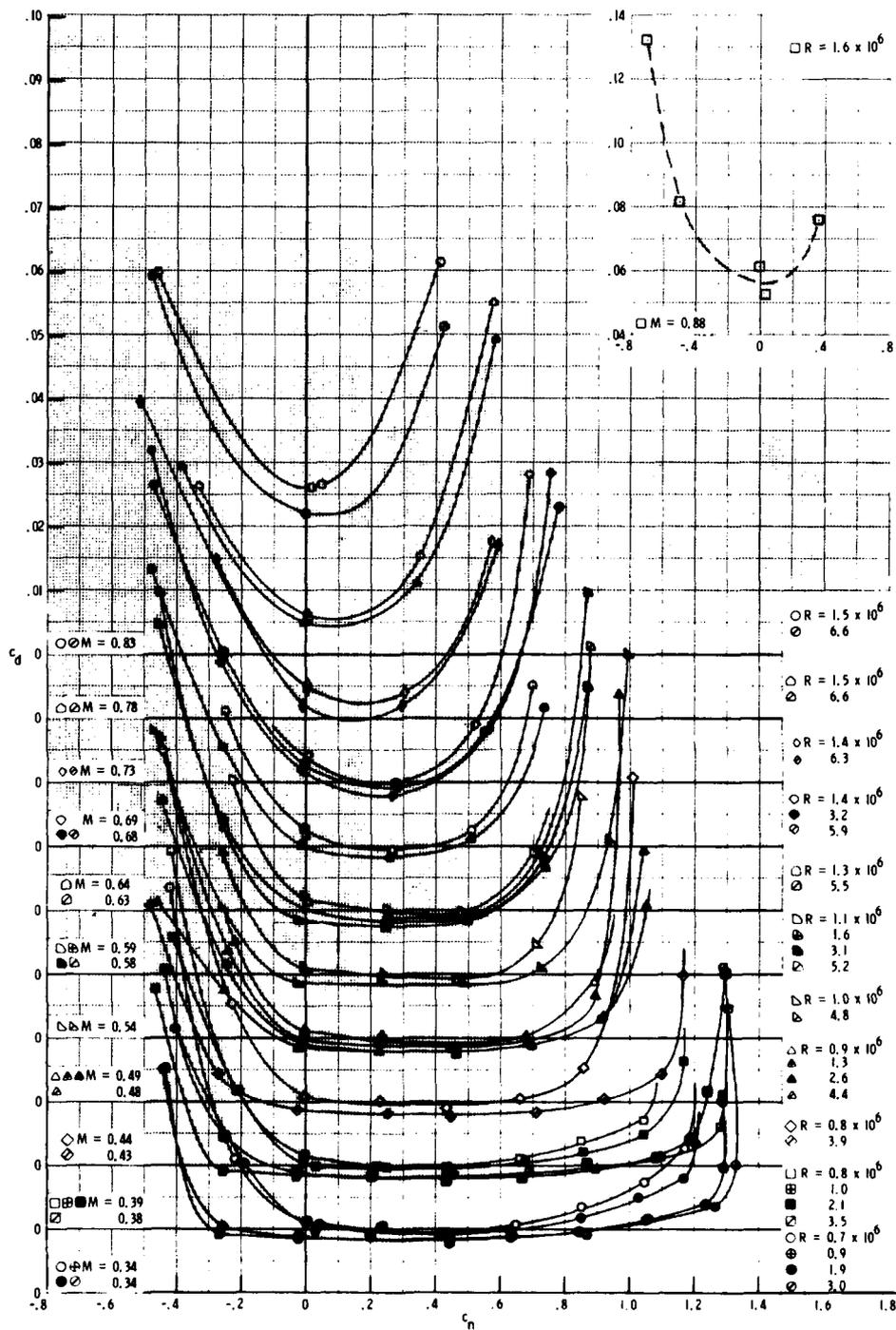
(c) Section drag coefficients.

Figure 6.- Concluded.
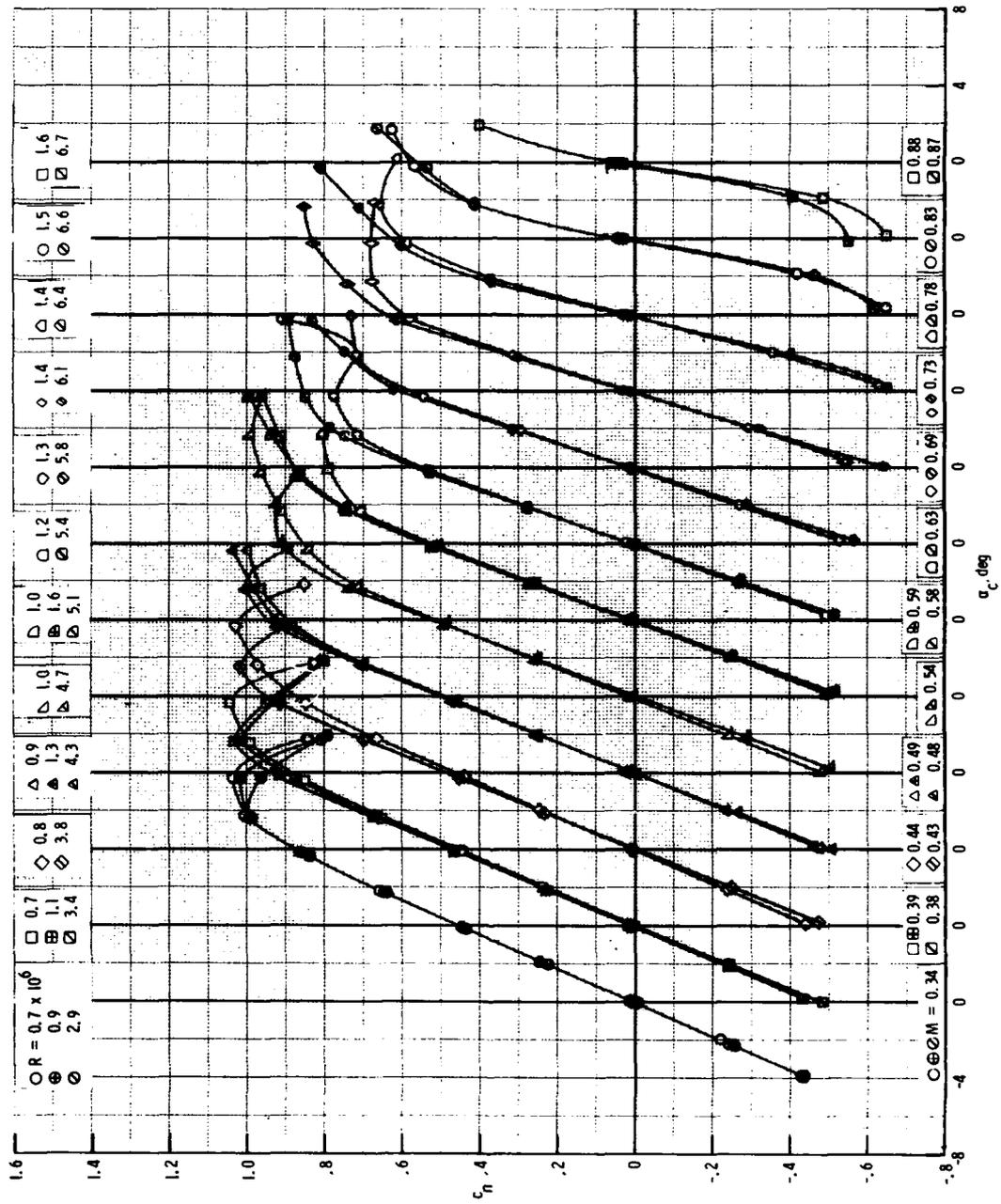
(a) Section normal-force coefficients.

Figure 7.- Effect of Reynolds number on aerodynamic characteristics of SC 1095 airfoil.
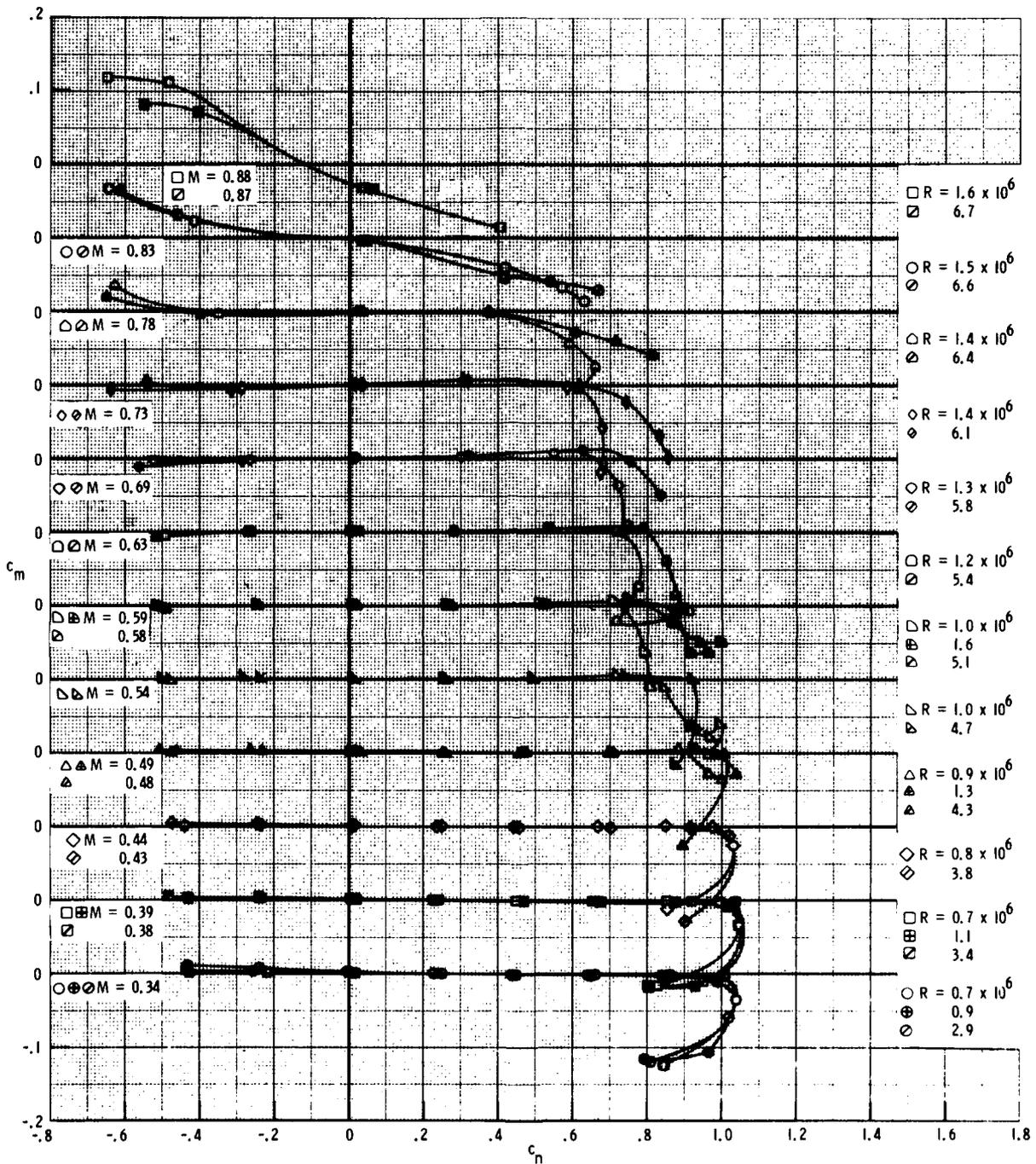
(b) Section pitching-moment coefficients.

Figure 7.- Continued.

31
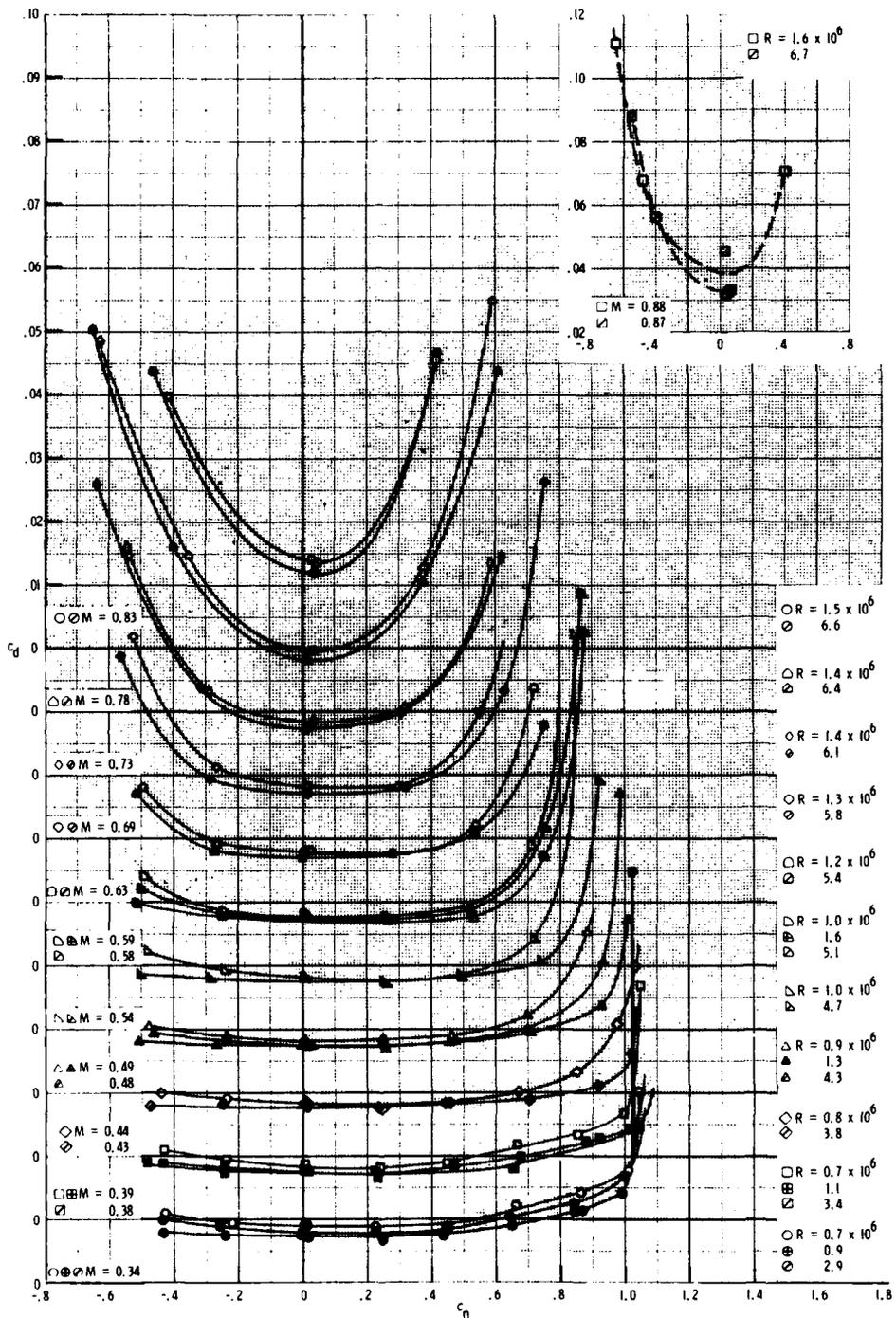
(c) Section drag coefficients.

Figure 7.- Concluded.
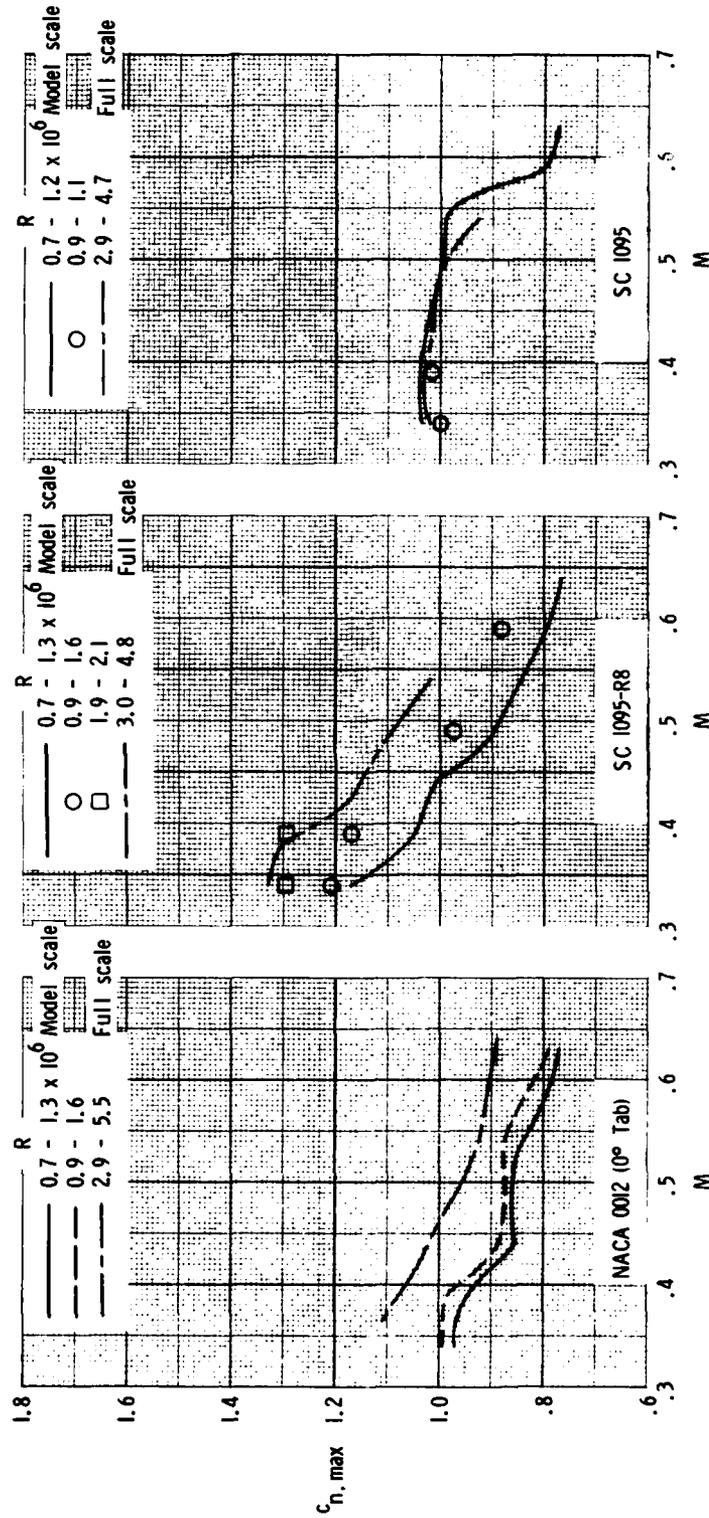
Figure 8.- Effect of Reynolds number on variation of maximum section normal-force coefficient with Mach number of NACA 0012 (0° Tab), SC 1095-R8, and SC 1095 airfoils.
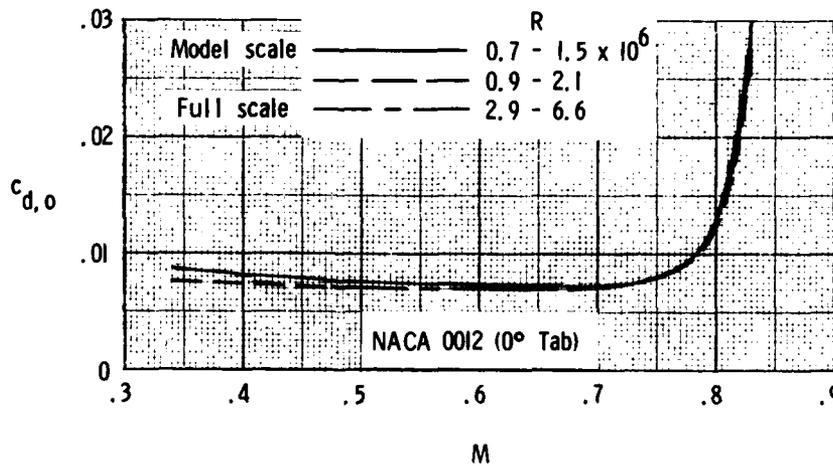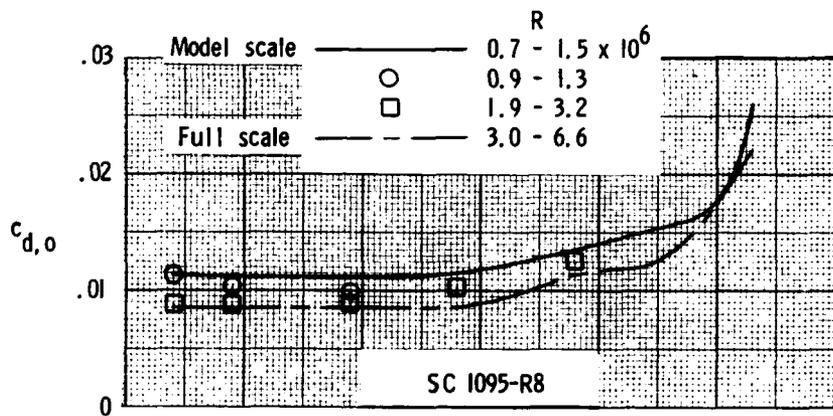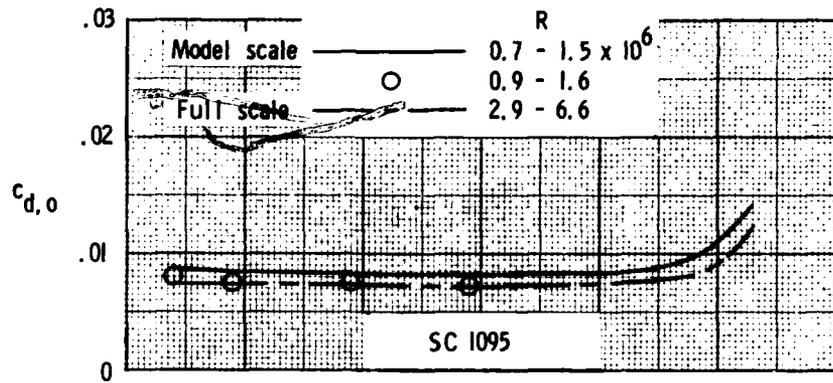
Figure 9.- Effect of Reynolds number on section drag coefficient at zero normal force of NACA 0012 (0° Tab), SC 1095-R8, and SC 1095 airfoils.

34
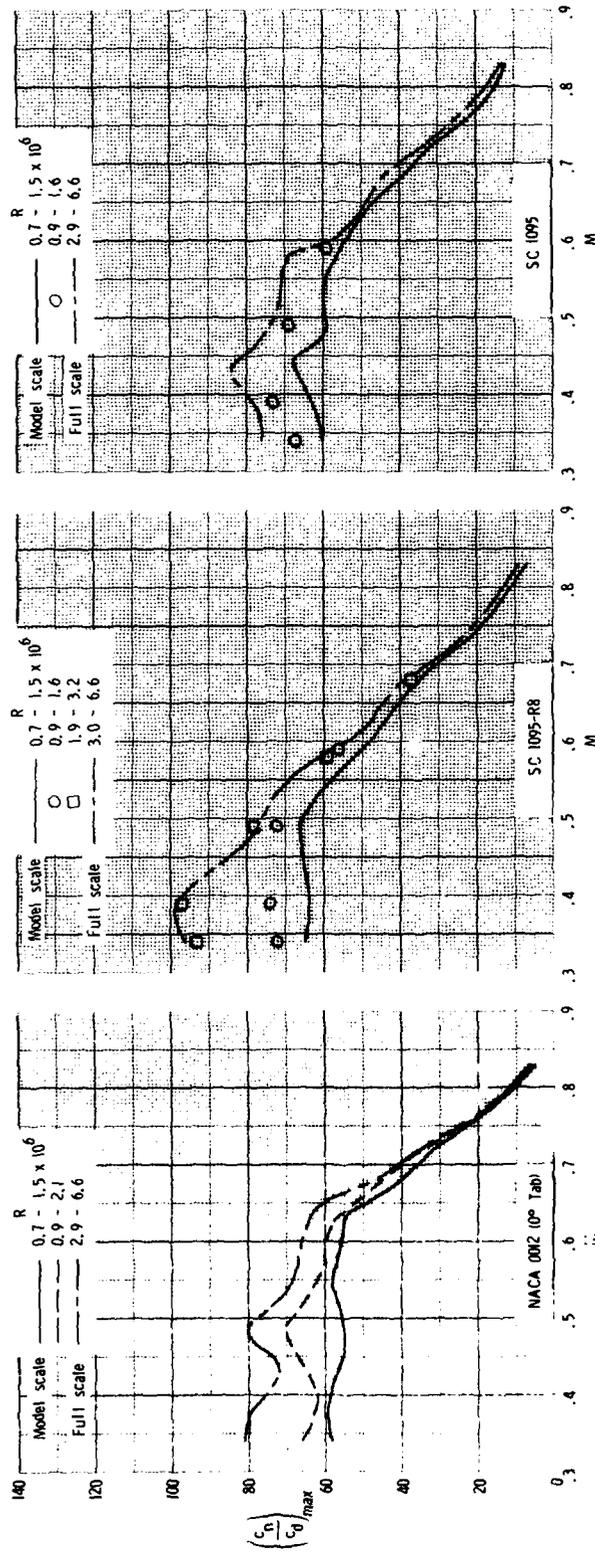
Figure 10.- Effect of Reynolds number on variation of maximum section normal-force—drag ratio with Mach number of NACA 0012 (0° Tab), SC 1095-R8, and SC 1095 airfoils.
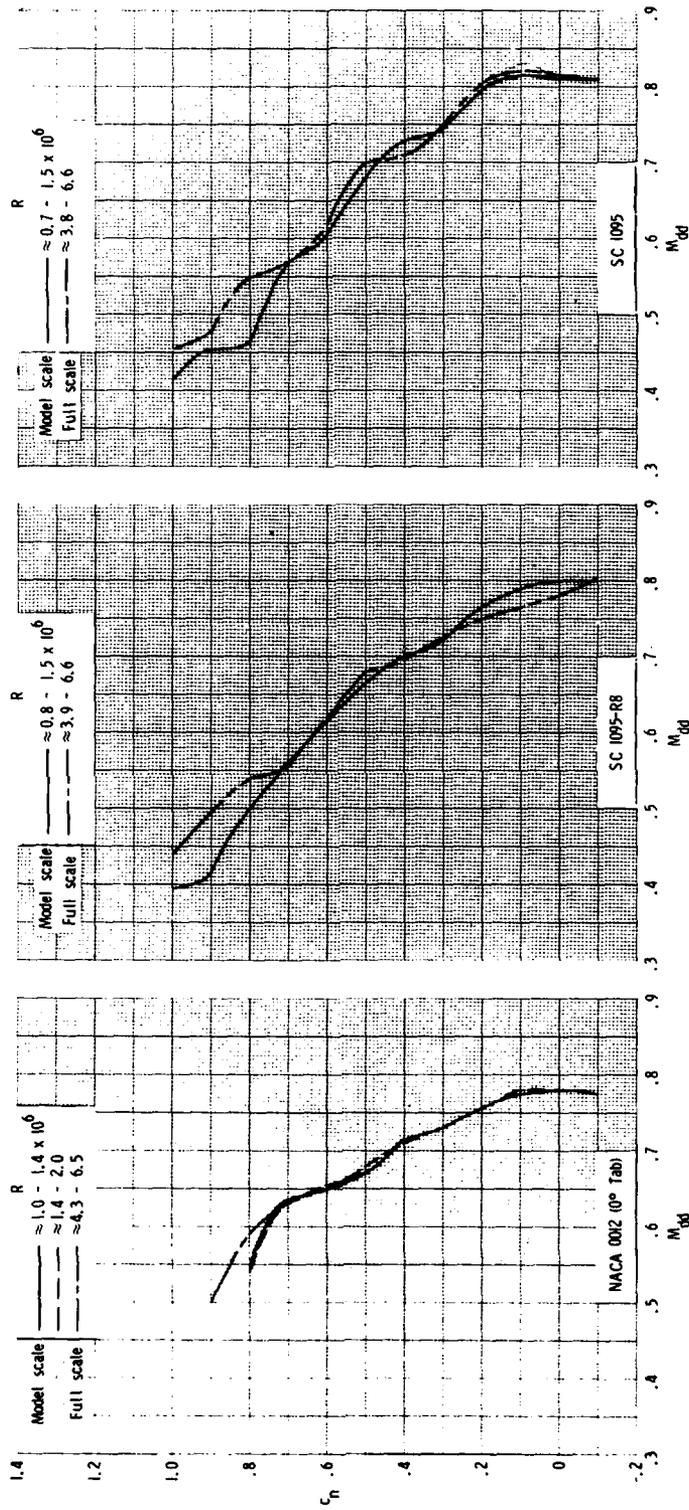
Figure 11.- Effect of Reynolds number on variation of section normal-force coefficient with drag-divergence Mach number of NACA 0012 (0° Tab), SC 1095-R8, and SC 1095 airfoils.

36
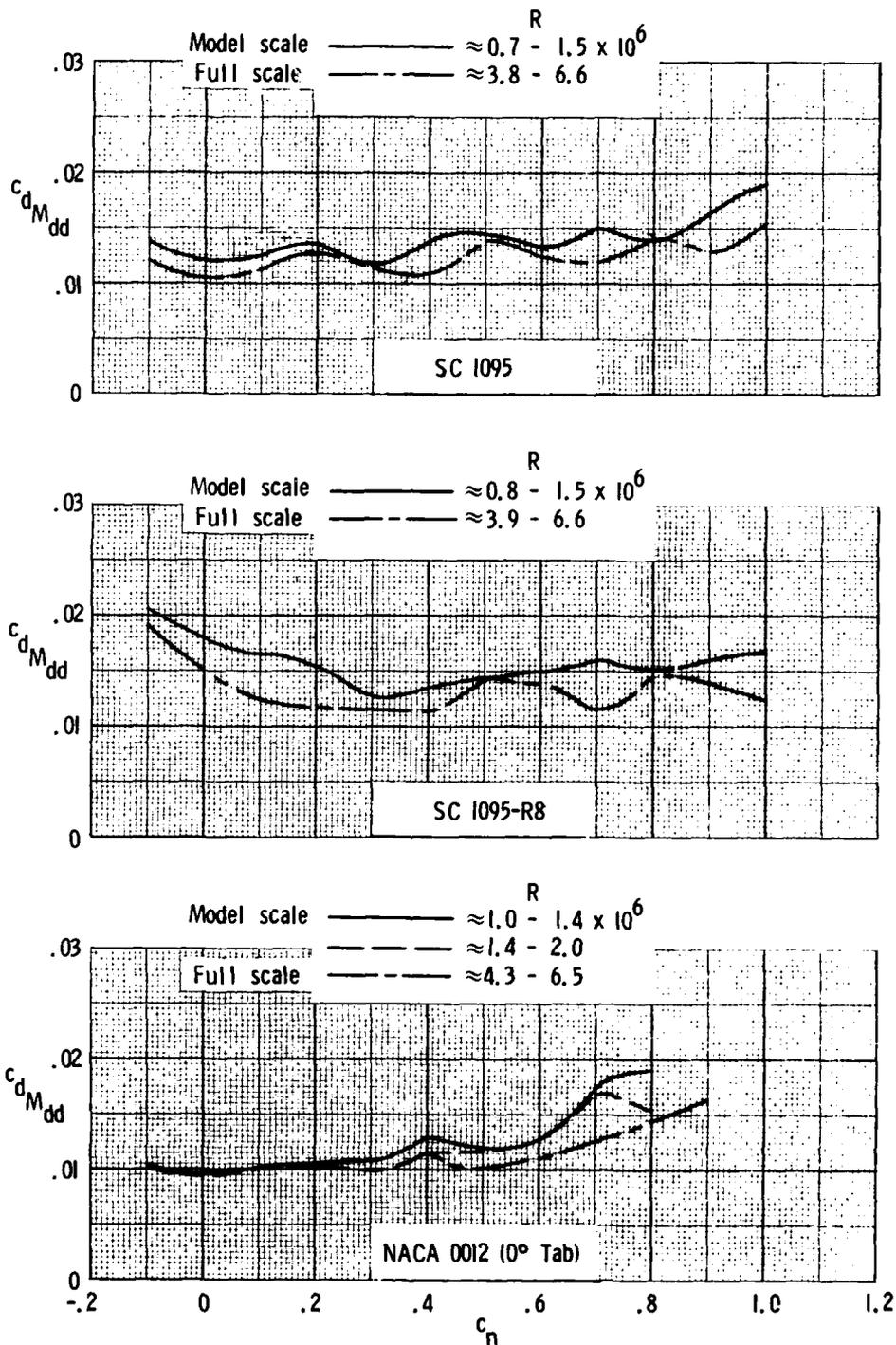
Figure 12.- Effect of Reynolds number on section drag coefficient at drag-divergence Mach number of NACA 0012 (0° Tab), SC 1095-R8, and SC 1095 airfoils.

M	$C_{p,sonic}$		α	α_c	c_n	M	R
.38	-4.12	○	10.2	9.7	.95	.39	.7
.39	-3.88	□	10.7	10.0	1.08	.38	3.3
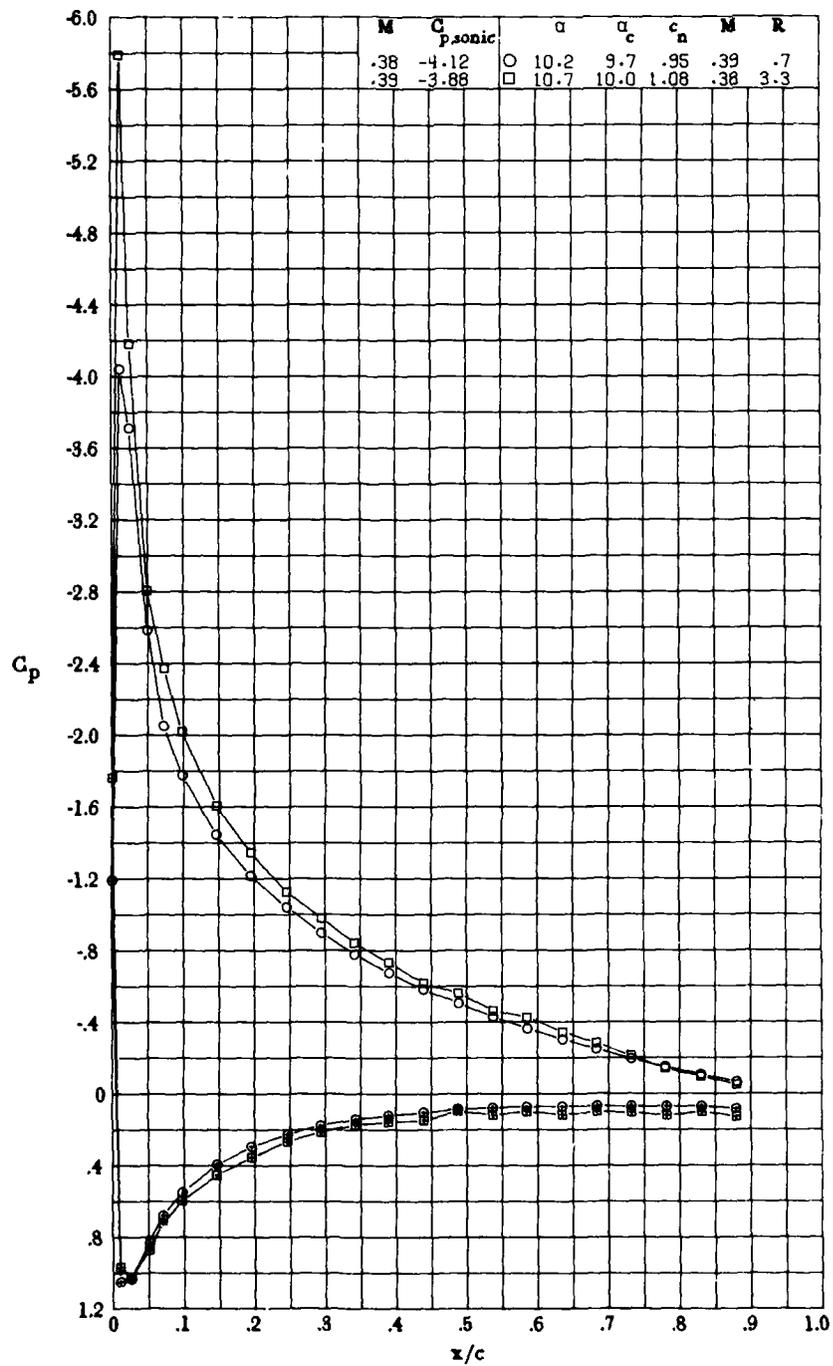
(a) $\alpha_c \approx 10^\circ$.

Figure 13.- Effect of Reynolds number on chordwise pressure distribution
of NACA 0012 (0° Tab) airfoil.   Symbols with plus sign inside indicate
lower surface.   R given in millions.
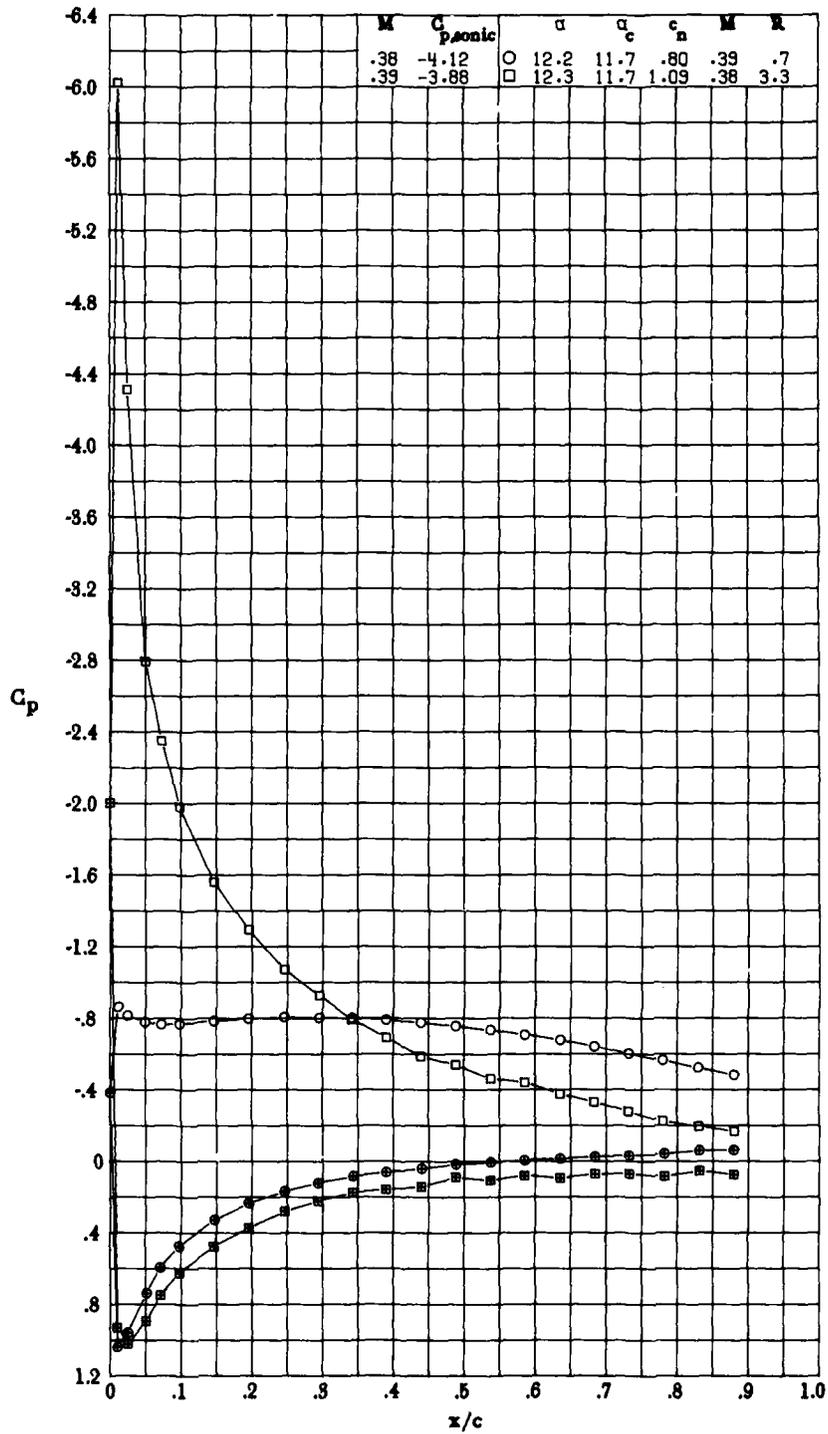
(b) $\alpha_c = 11.7°$.

Figure 13.- Concluded.

	M	$C_{p,sonic}$		α	α_c	c_n	M	R
	.38	-4.12	O	10.2	9.6	1.05	.39	.8
	.39	-3.88	□	10.3	9.6	1.10	.38	3.5
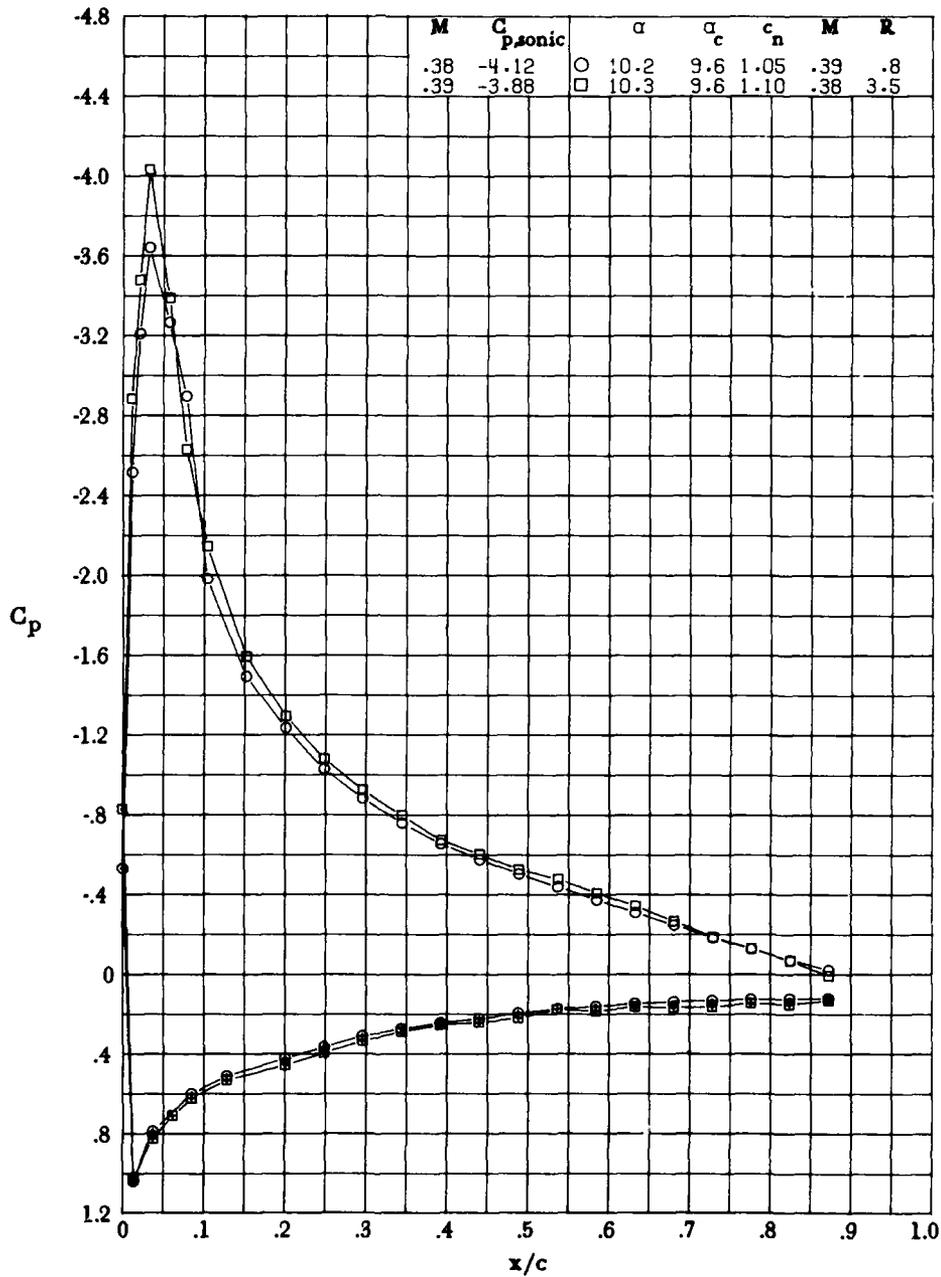
(a) $\alpha_c = 9.6^\circ$.

Figure 14.- Effect of Reynolds number on chordwise pressure distribution of SC 1095-R8 airfoil.   Symbols with plus sign inside indicate lower surface. R given in millions.
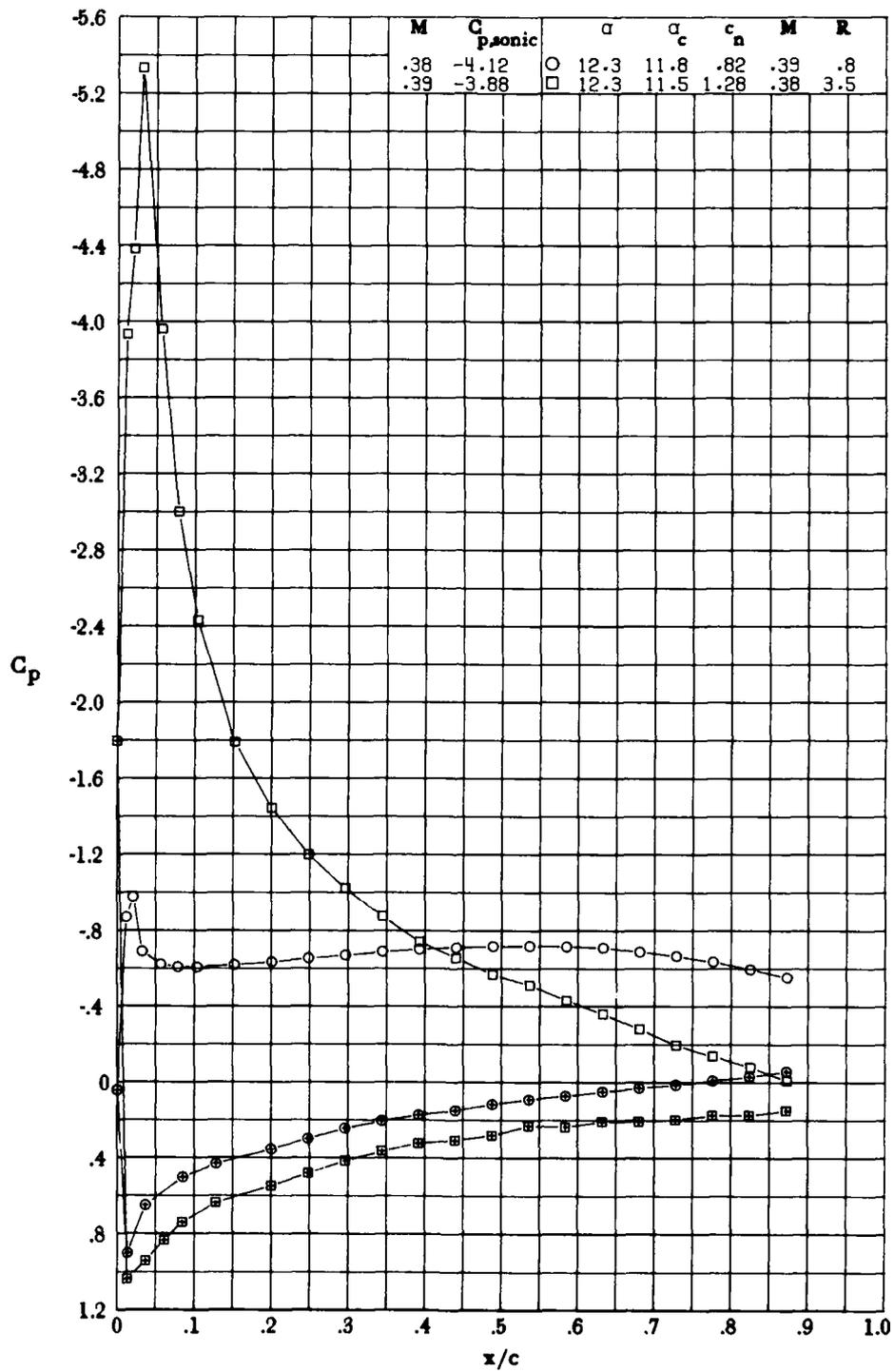
(b) $\alpha_c \approx 12°$.

Figure 14.- Concluded.

	M	$C_{p,sonic}$		α	α_c	c_n	M	R
	.38	-4.12	○	10.2	9.6	.99	.39	.7
	.39	-3.88	□	10.3	9.6	1.04	.38	3.4

(a) $\alpha_c = 9.6^o$.
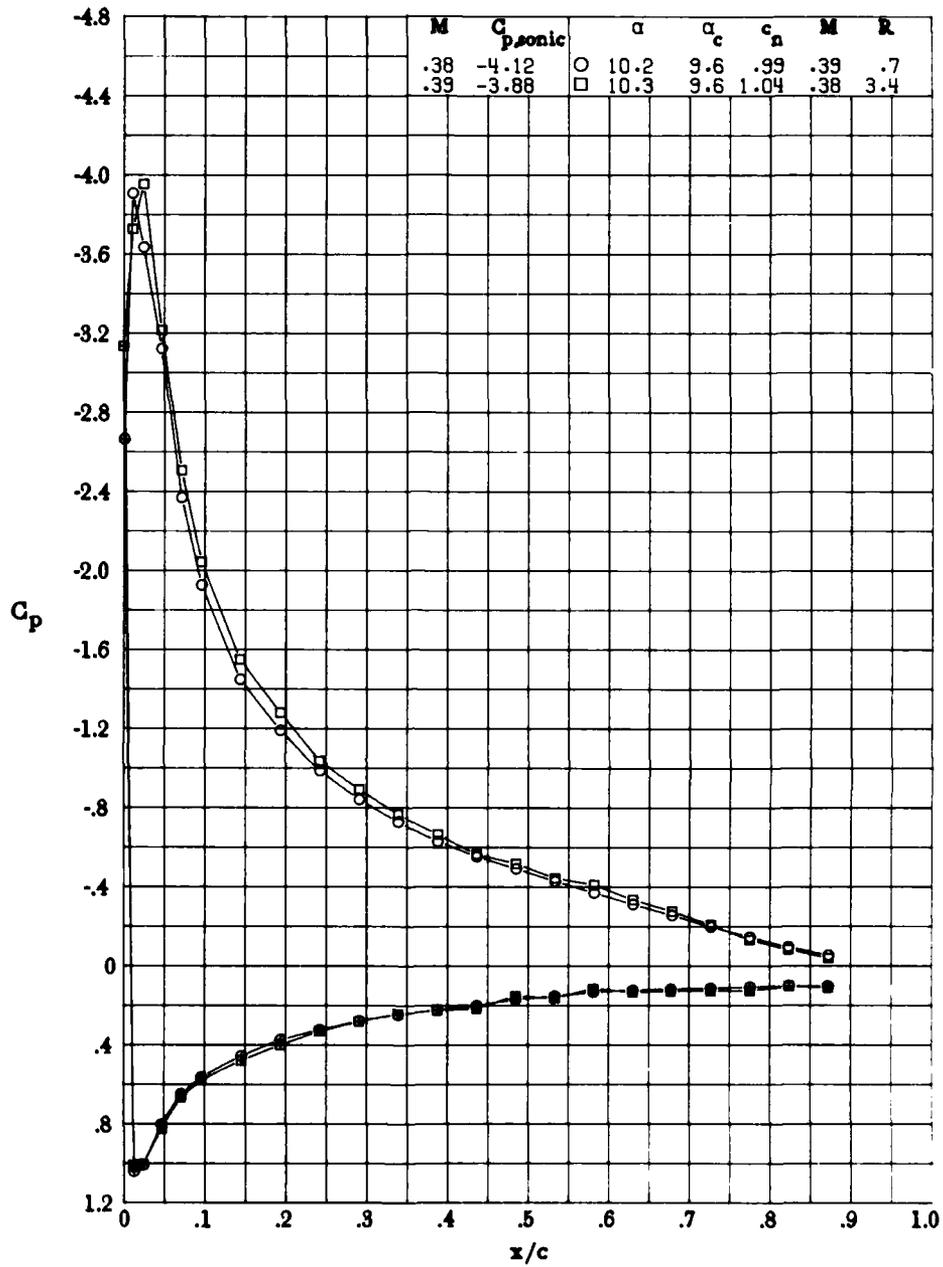
Figure 15.- Effect of Reynolds number on chordwise pressure distribution of SC 1095 airfoil. Symbols with plus sign inside indicate lower surface. R given in millions.

42

M	$C_{p,sonic}$		α	α_c	c_n	M	R
.38	-4.12	O	12.3	11.7	1.05	.39	.7
.39	-3.88	□	12.2	11.6	.95	.38	3.4
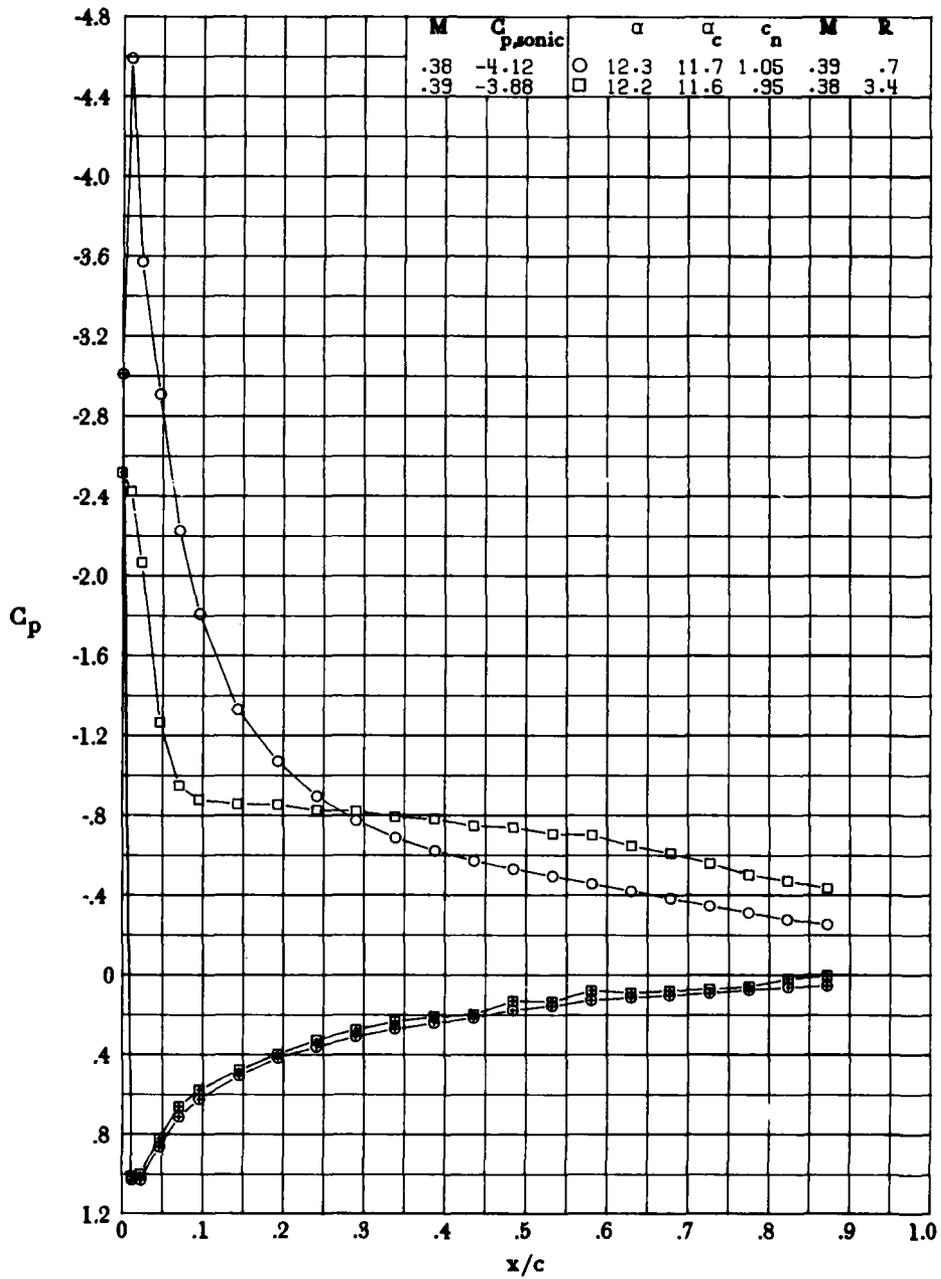
(b) $\alpha_c \approx 12°$.

Figure 15.- Concluded.
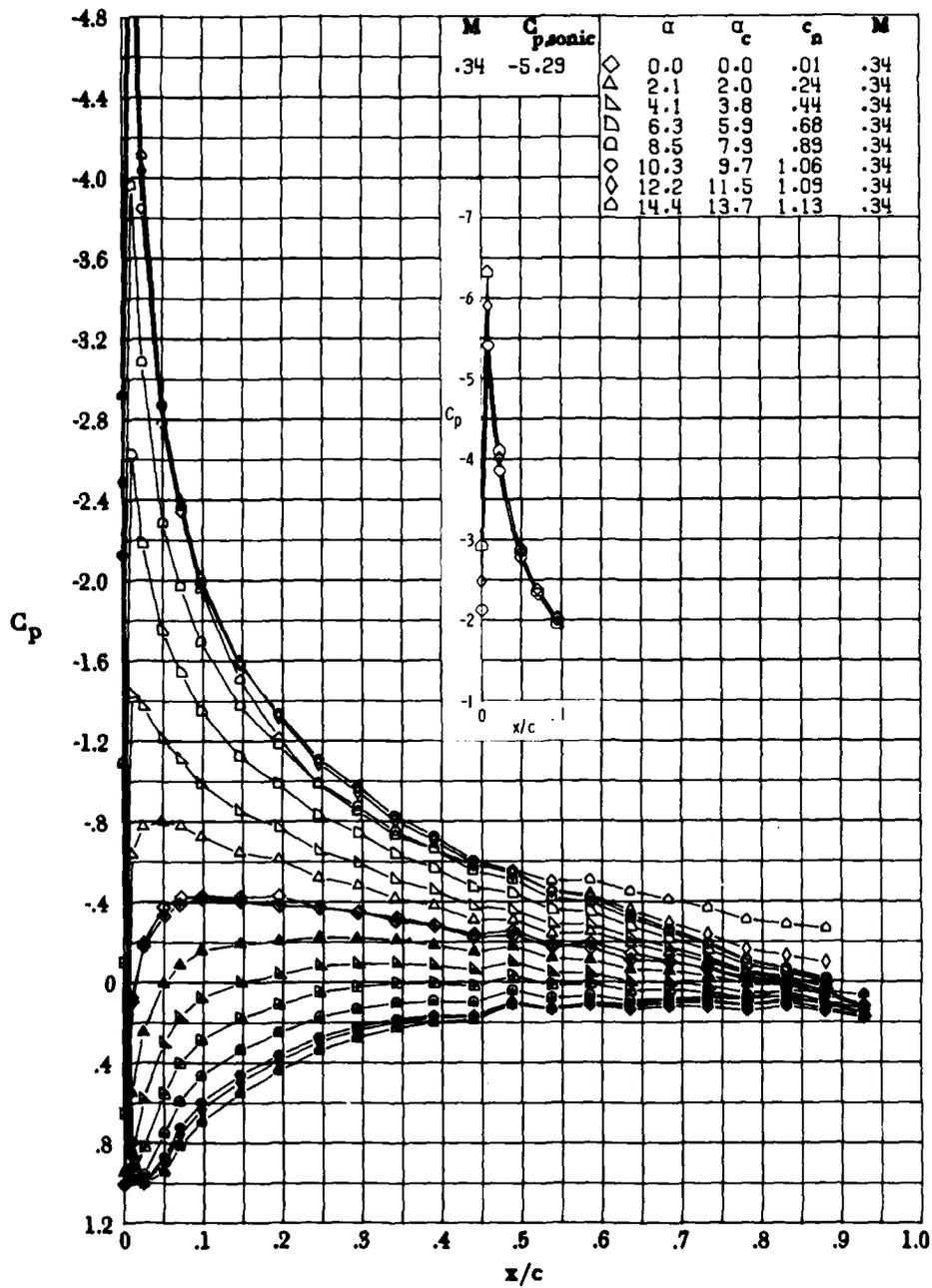
(a) M = 0.34; R ≈ 2.9 × 10⁶.

Figure 16.- Effect of angle of attack on chordwise pressure distribution of
NACA 0012 (0° Tab) airfoil. Symbols with plus sign inside indicate lower
surface.

44

M	$C_{p,sonic}$	α	α_c	c_n	M
.38	-4.12	◇ -.1	-.1	0.00	.38
		△ 2.1	2.0	.25	.38
		◁ 4.1	3.8	.45	.38
		▷ 6.4	5.9	.71	.38
		◻ 8.2	7.6	.90	.38
		○ 10.7	10.0	1.08	.38
		◇ 12.3	11.7	1.09	.38
		△ 14.5	13.8	1.07	.38

C_p

C_p

x/c

x/c
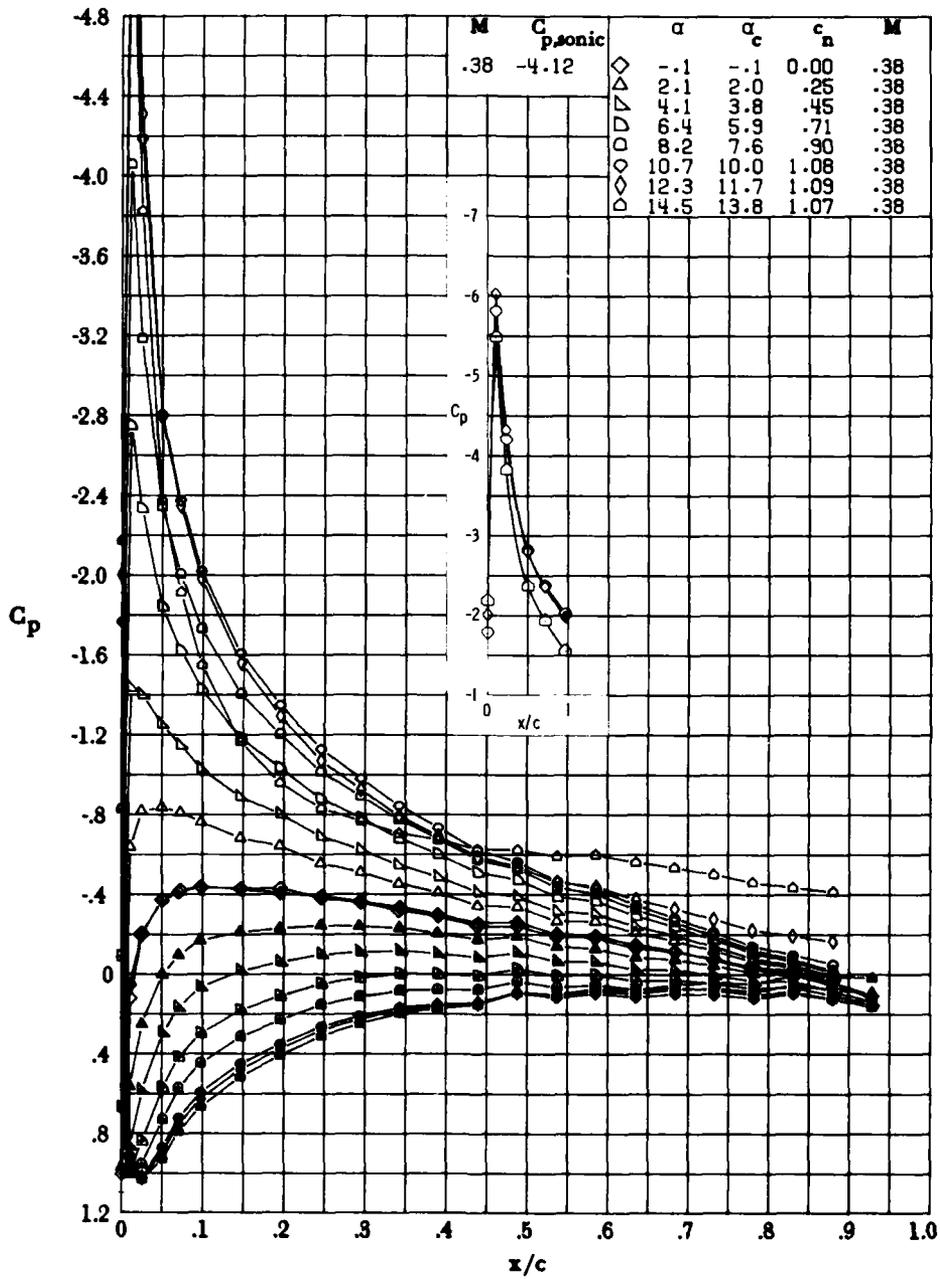
(b) $M = 0.38$; $R \approx 3.3 \times 10^6$.

Figure 16.- Continued.

45
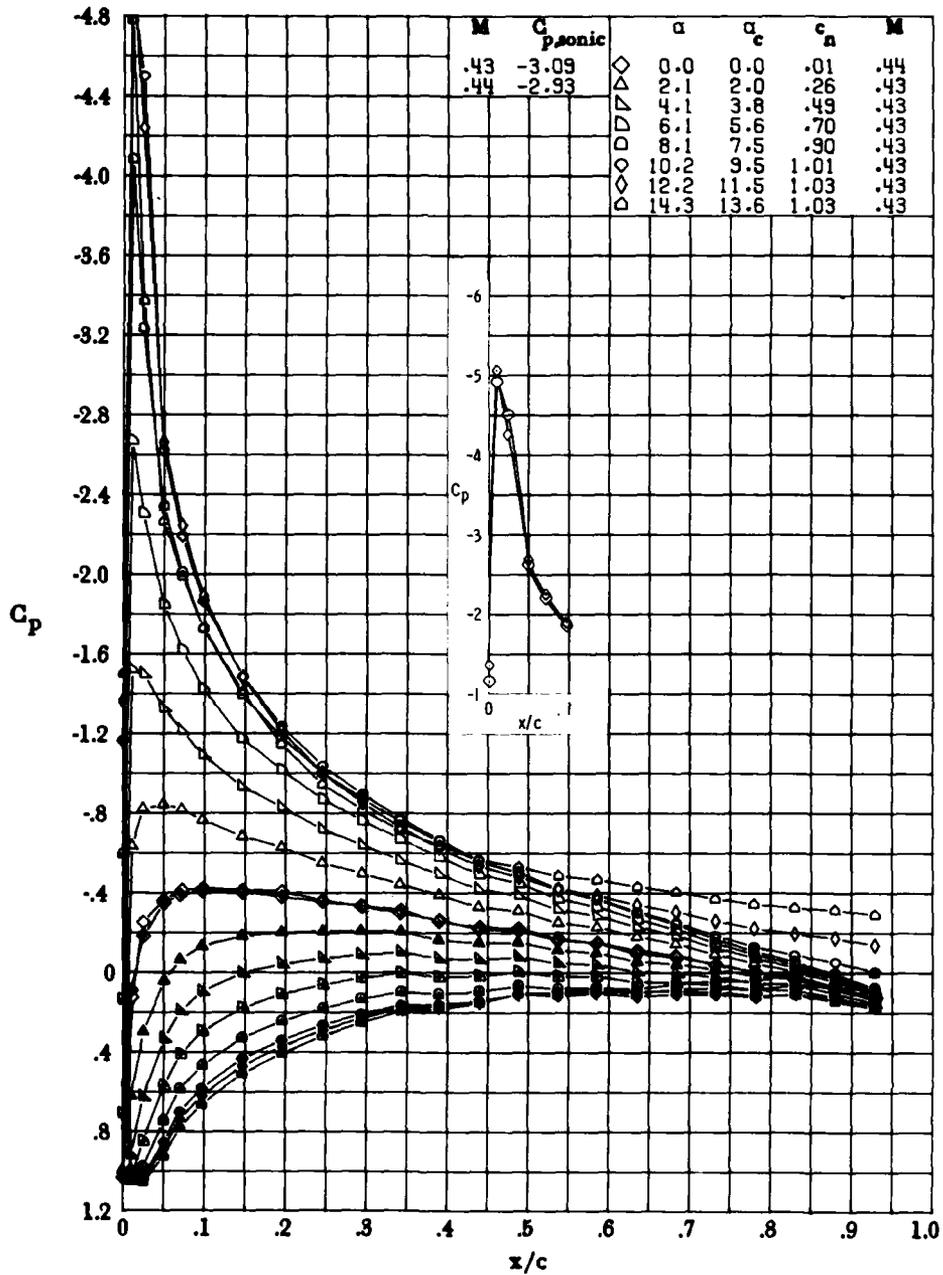
(c) $M \approx 0.43$; $R \approx 3.9 \times 10^6$.

Figure 16.- Continued.
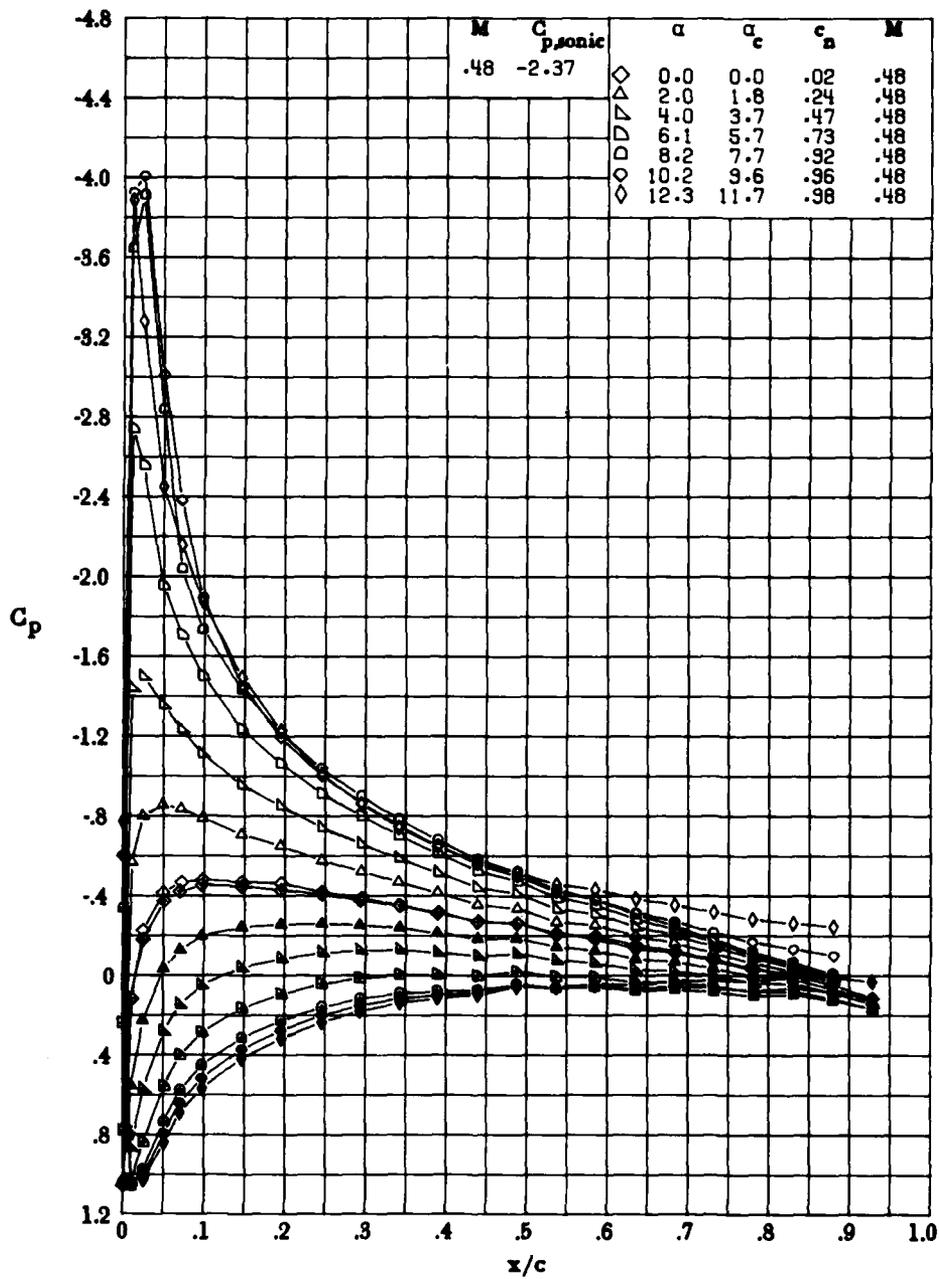
(d)   M = 0.48;   R ≈ 4.3 × 10⁶.

Figure 16.- Continued.
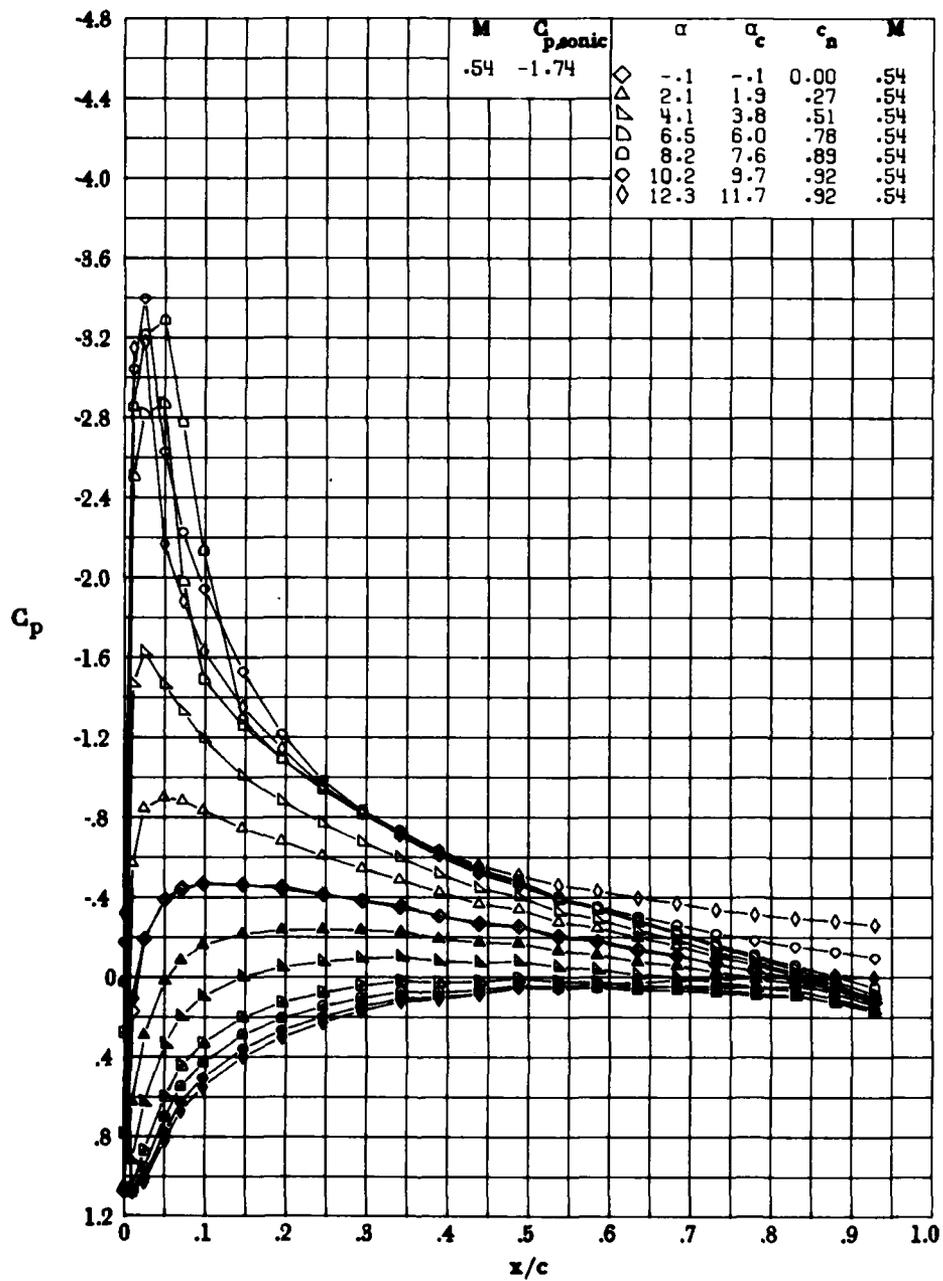
(e)   M = 0.54;   R ≈ 4.9 × 10⁶.

Figure 16.- Continued.
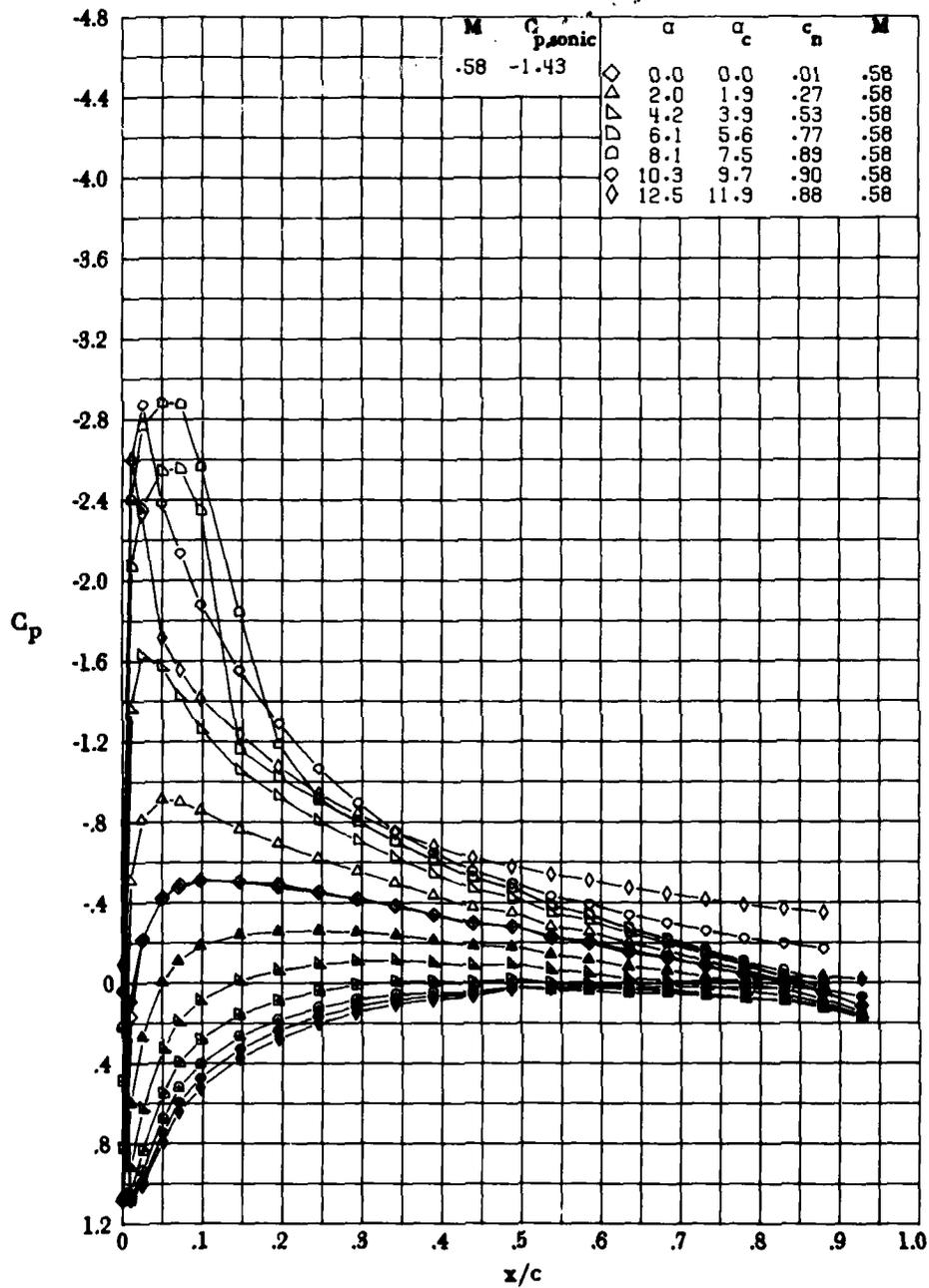
(f) M ≈ 0.58; R ≈ 5.0×10^6.

Figure 16.- Continued.
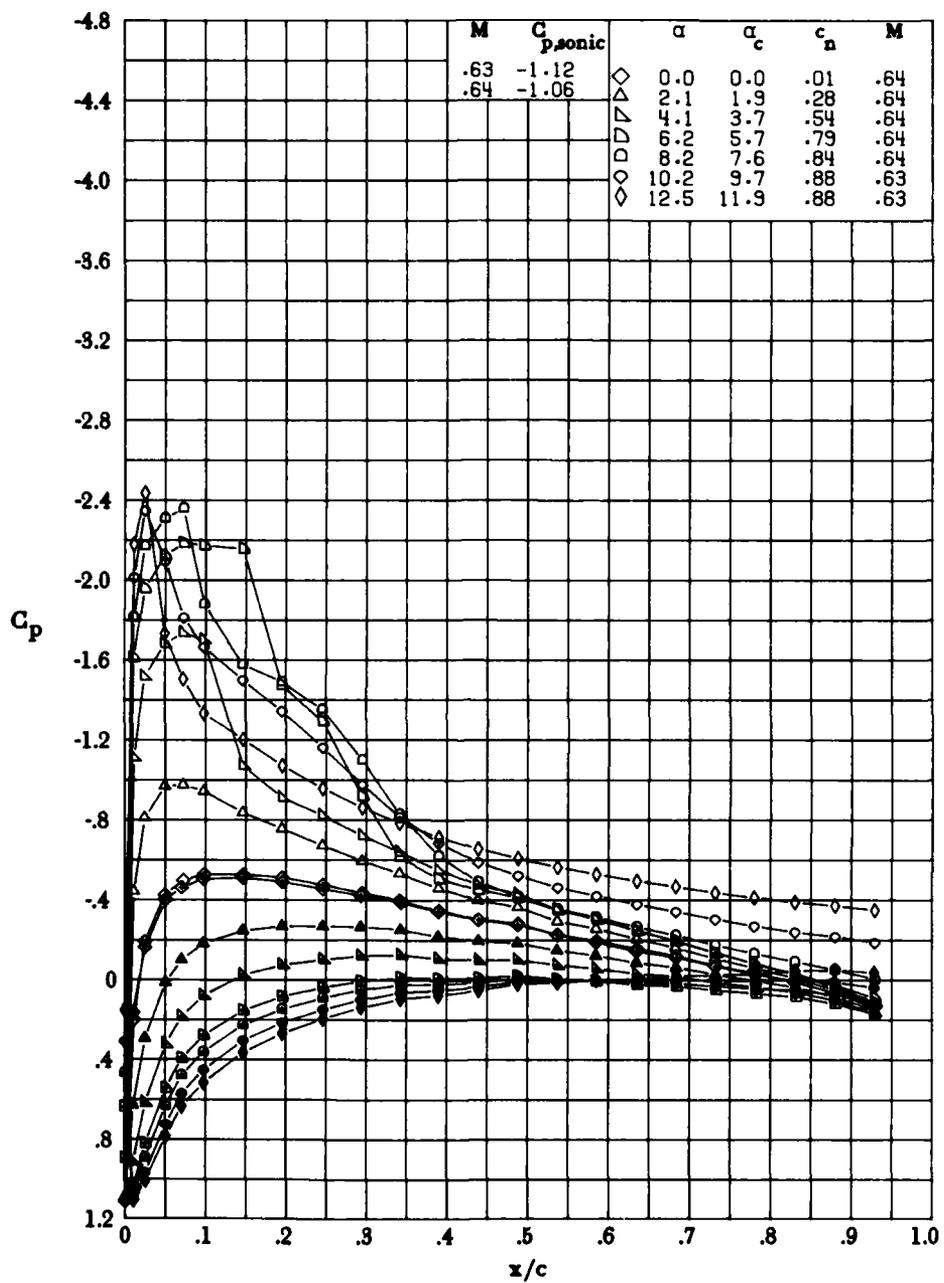
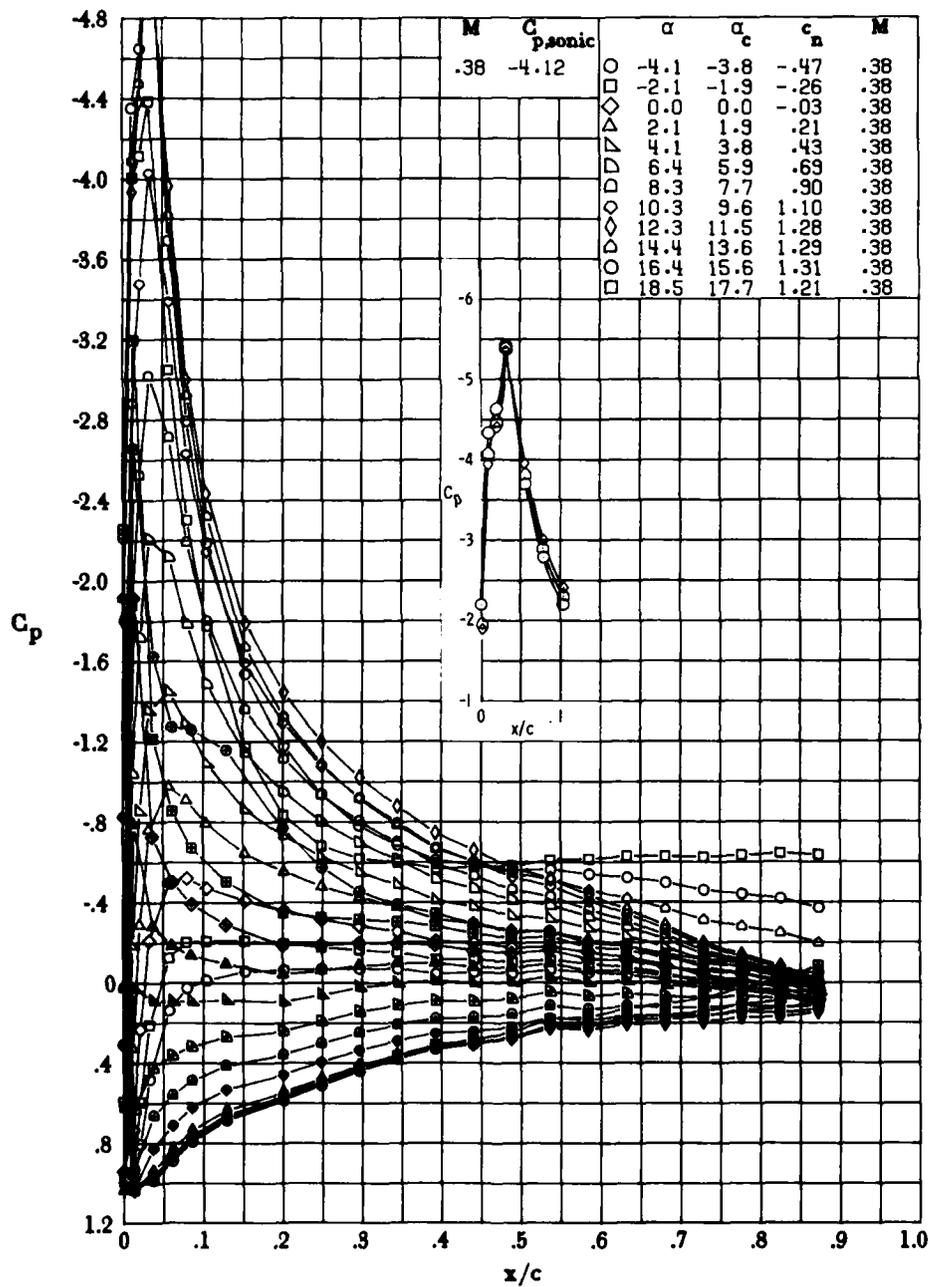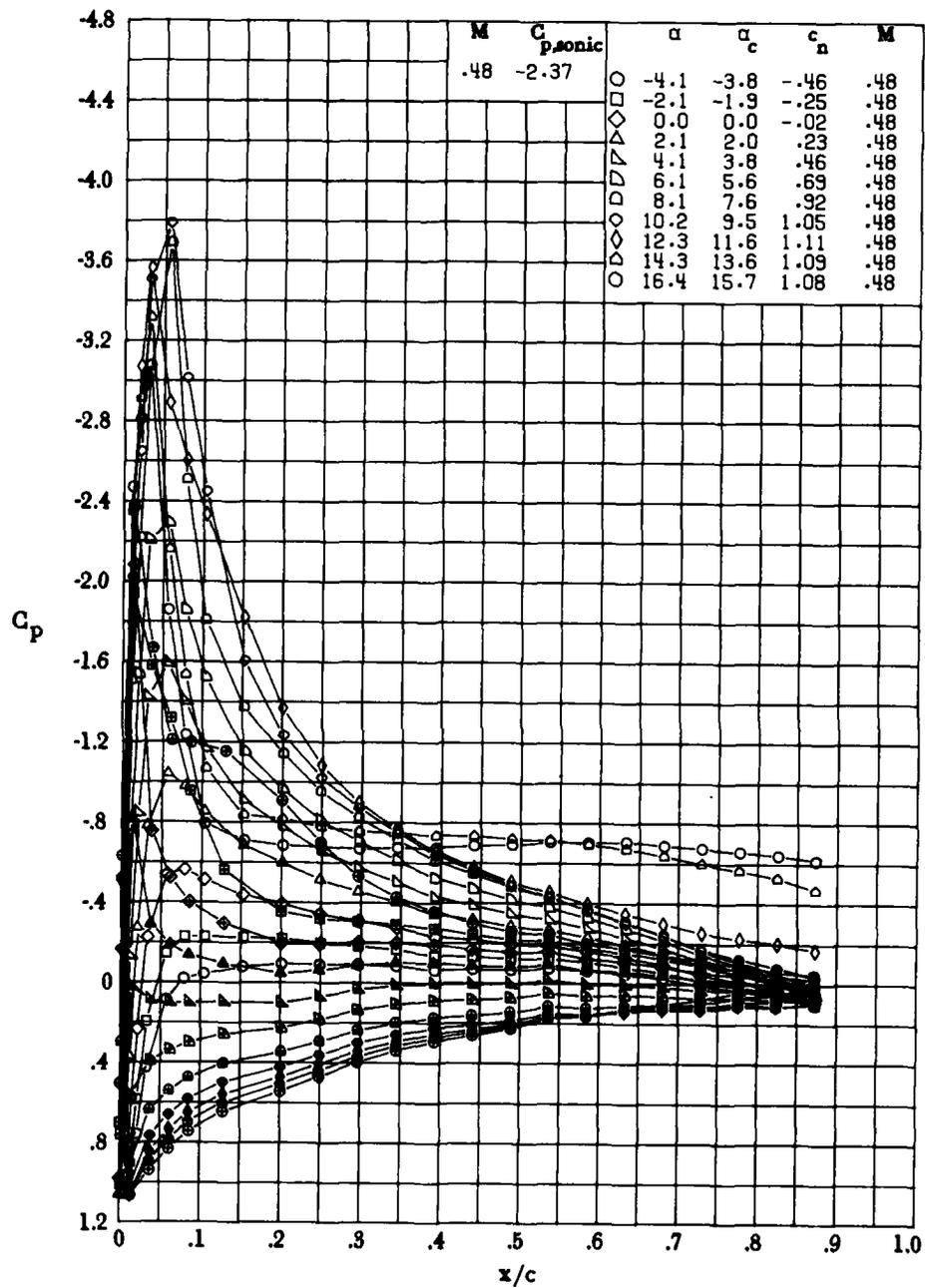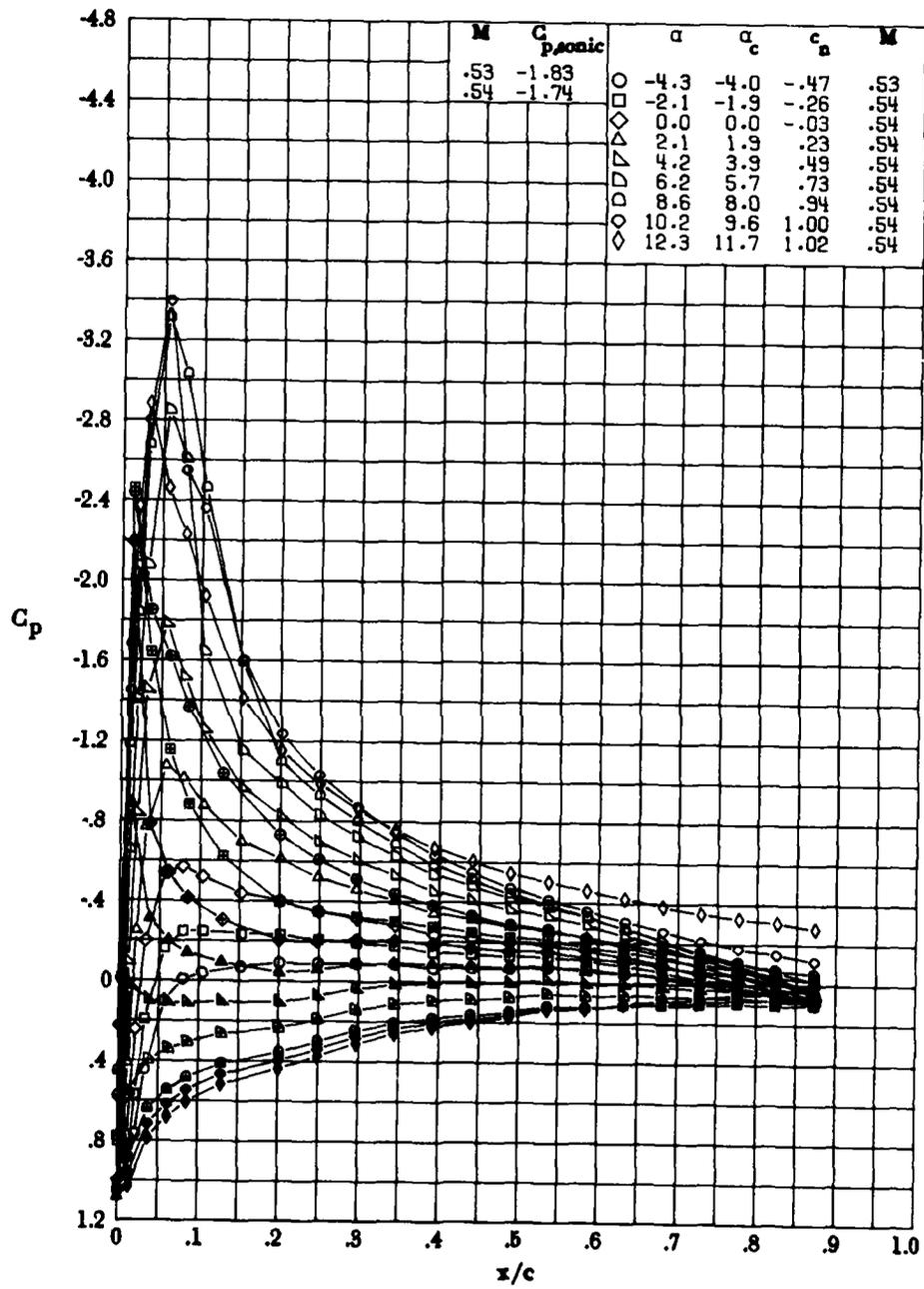(g) $M \approx 0.64$; $R \approx 5.5 \times 10^6$.

Figure 16.- Continued.
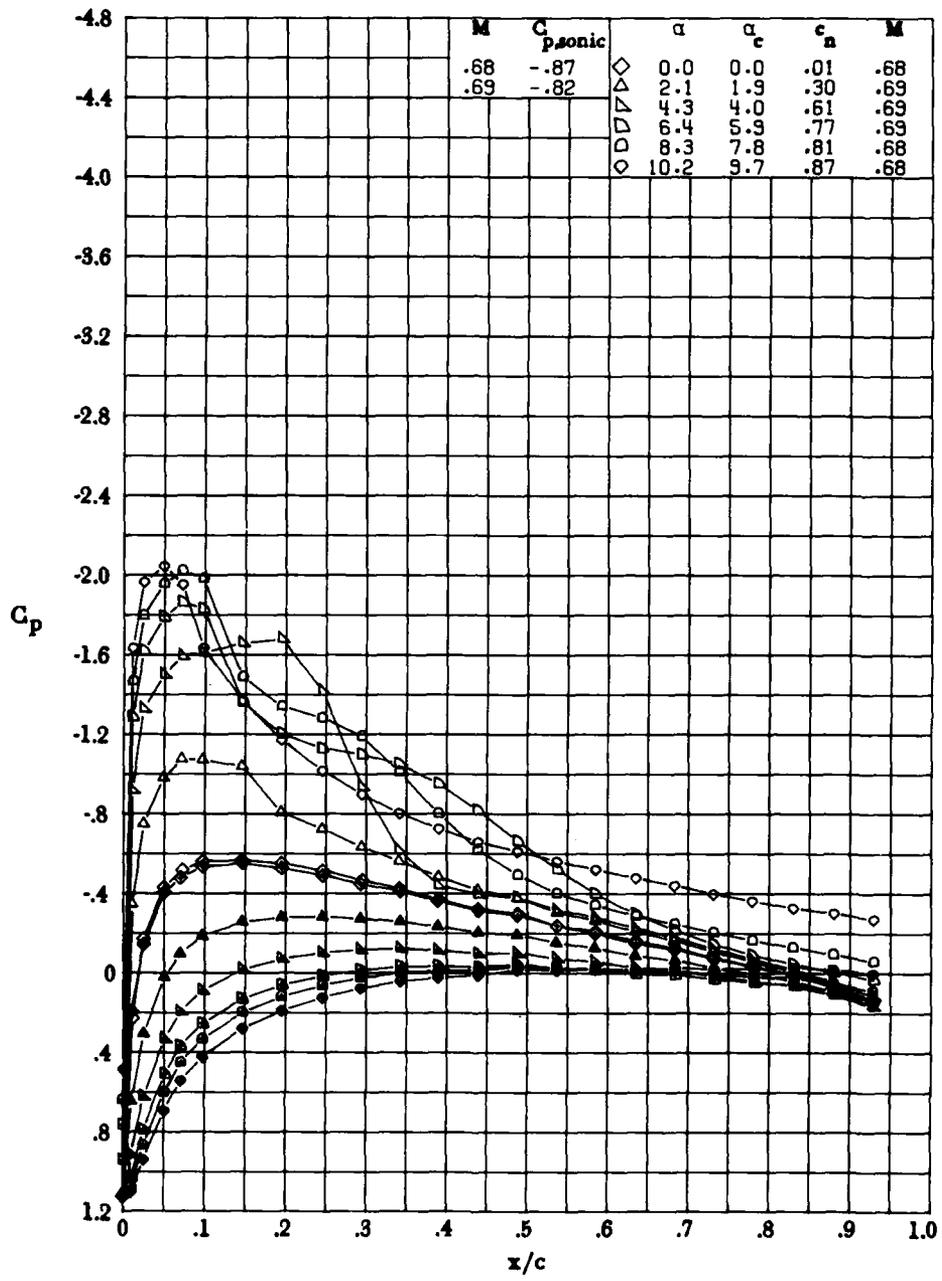
(h) $M \approx 0.68$; $R \approx 5.6 \times 10^6$.

Figure 16.- Continued.
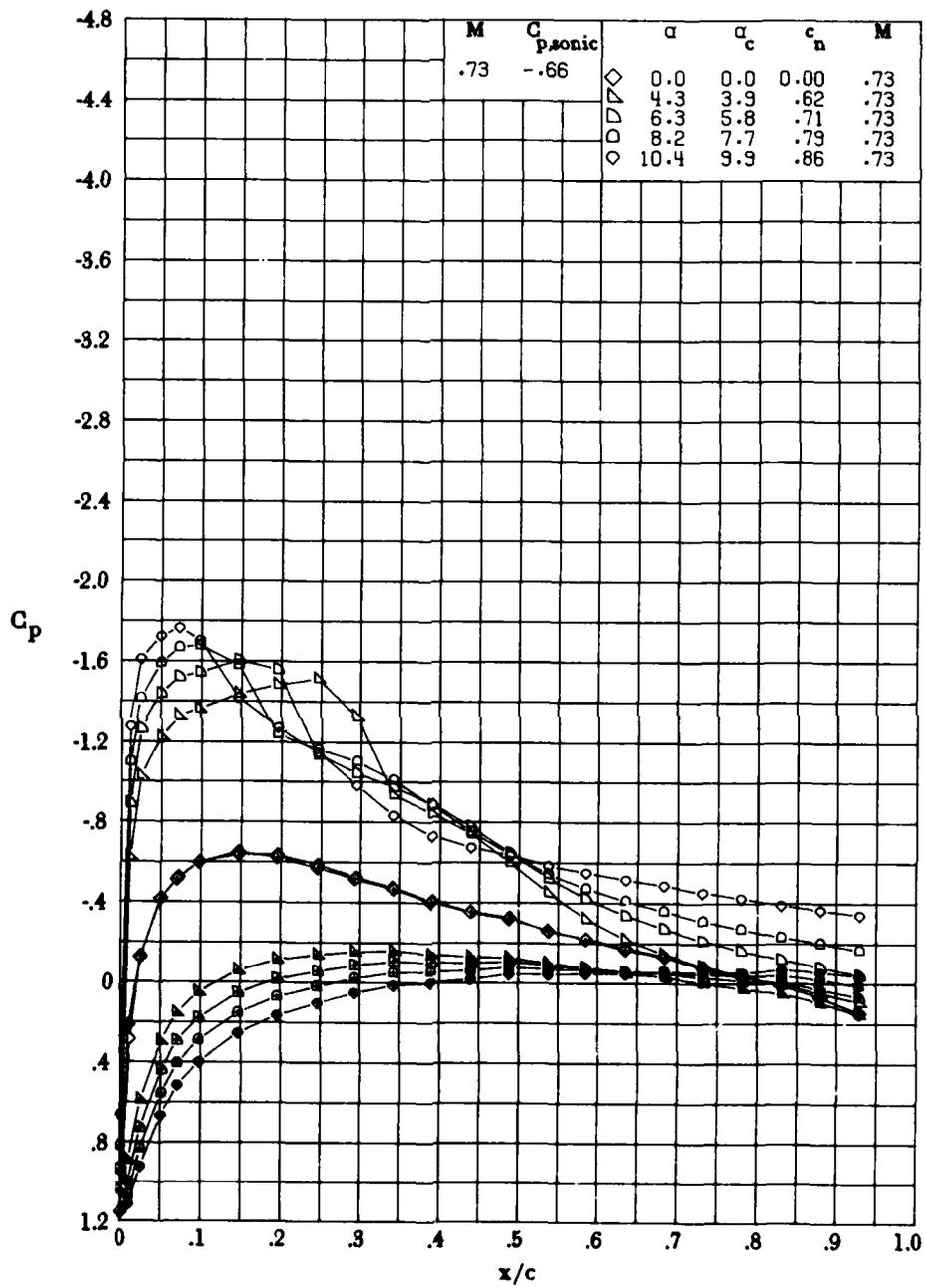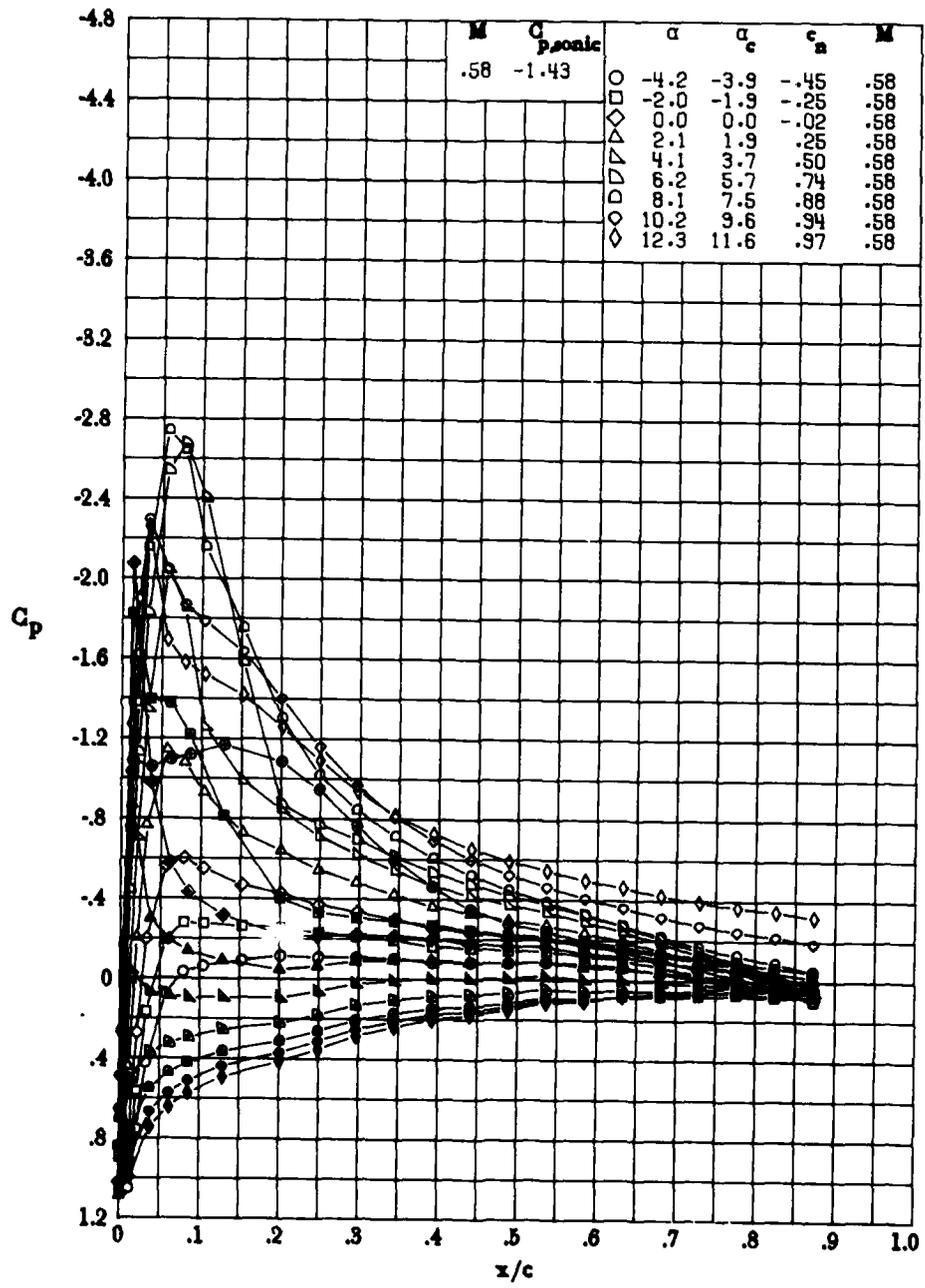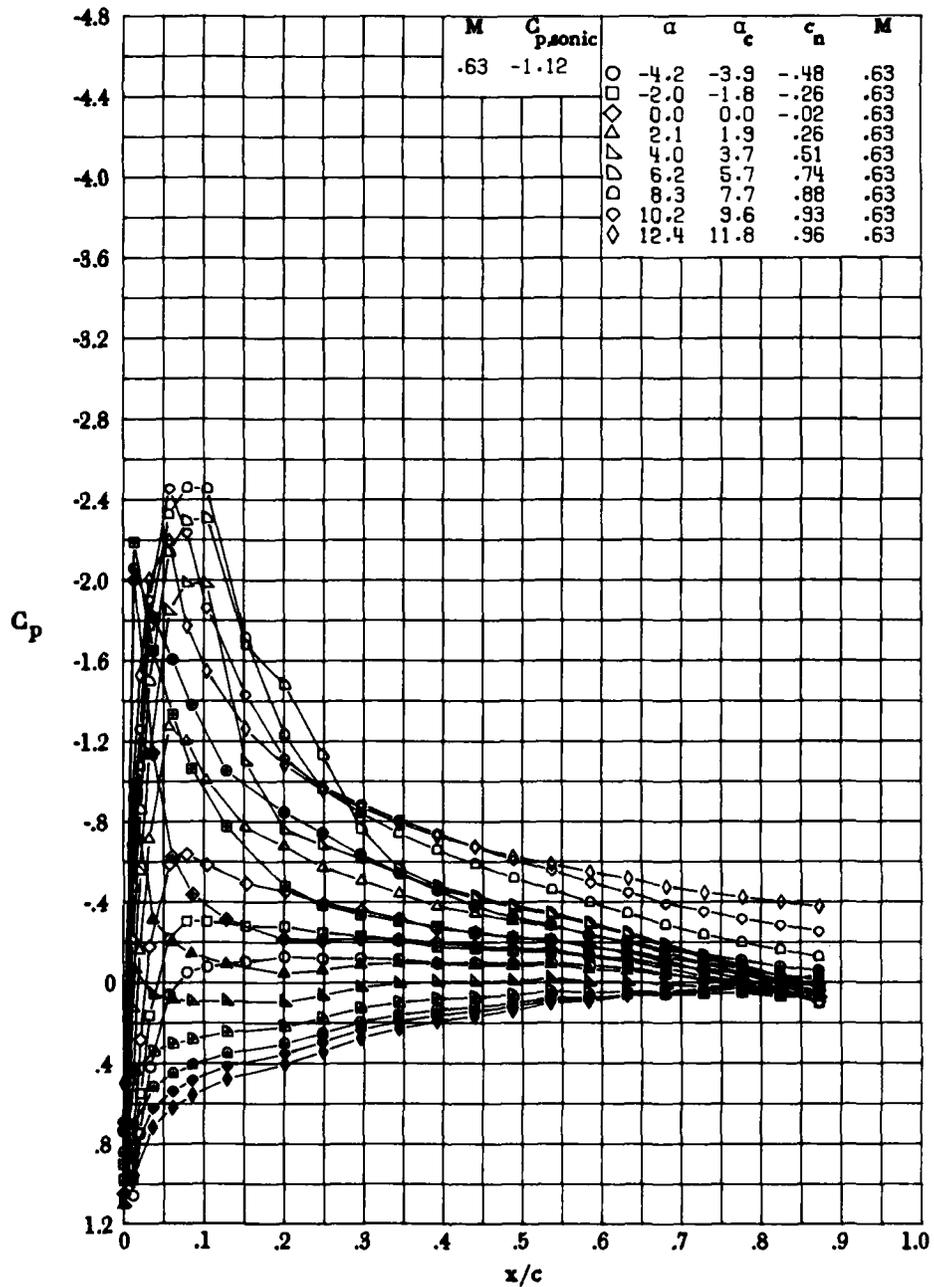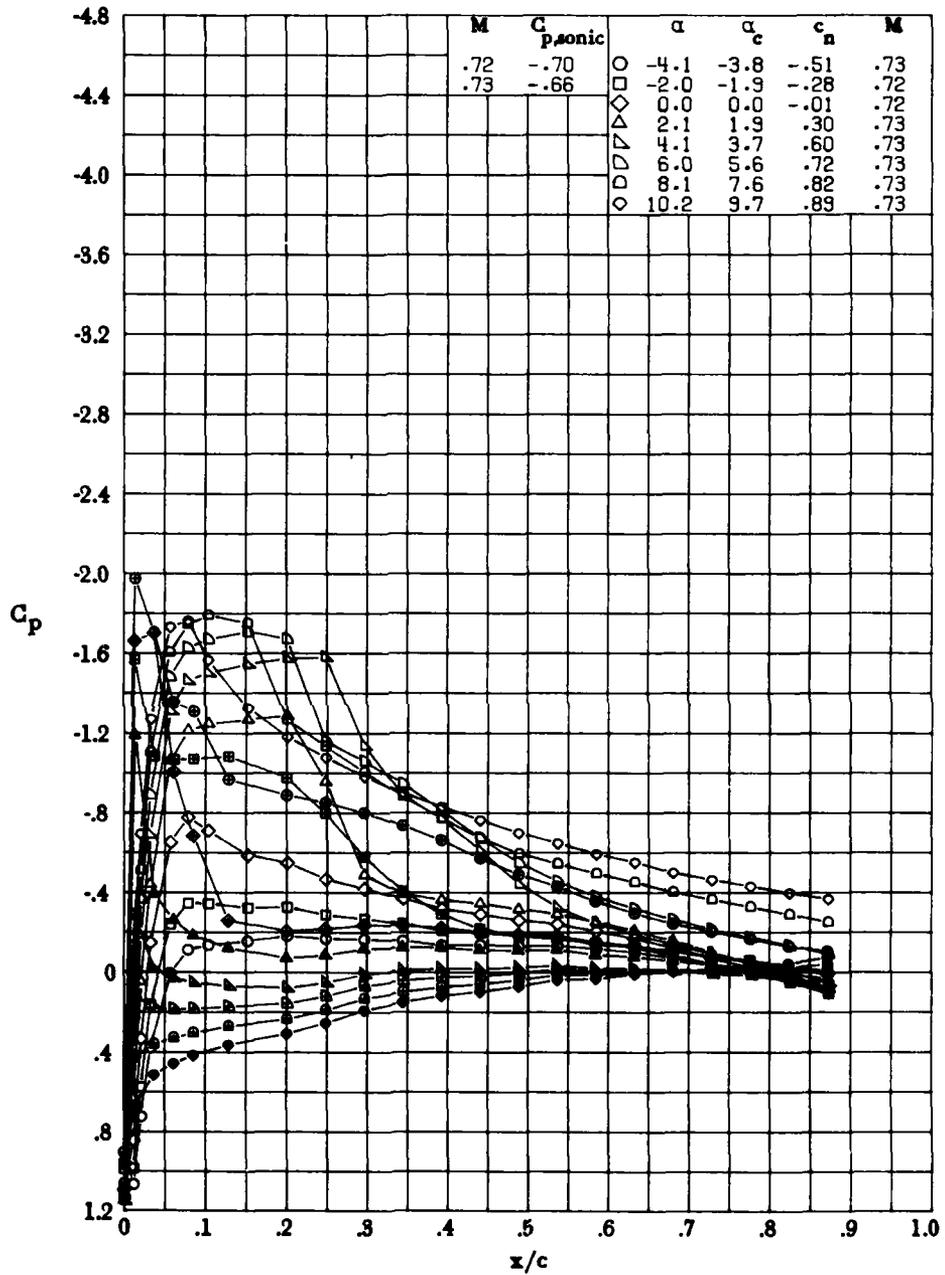
(i) M = 0.73; R ≈ 6.3 × 10^6.

Figure 16.- Continued.
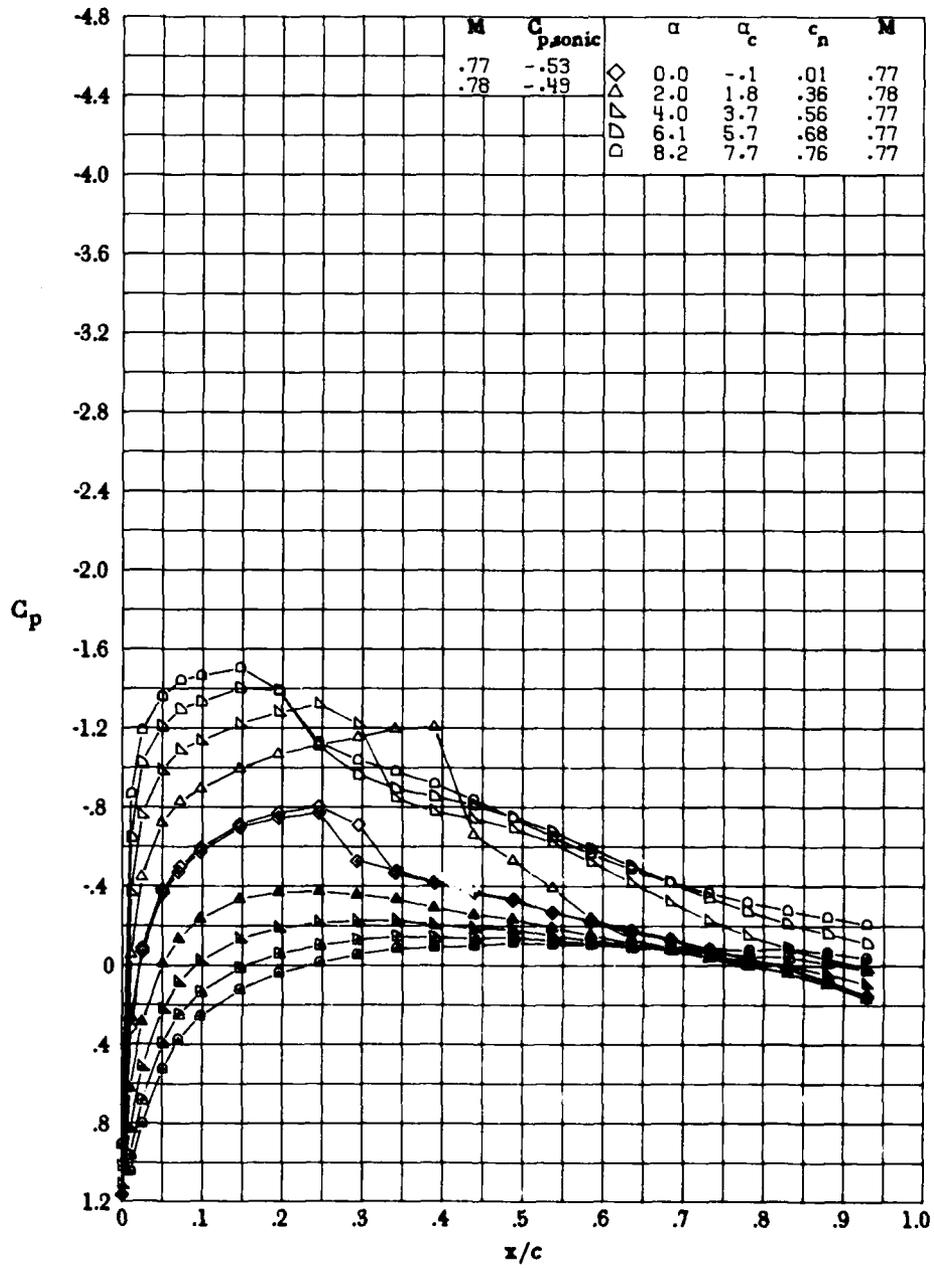
(j) M ≈ 0.77; R ≈ 6.5 × 10⁶.

Figure 16.- Continued.
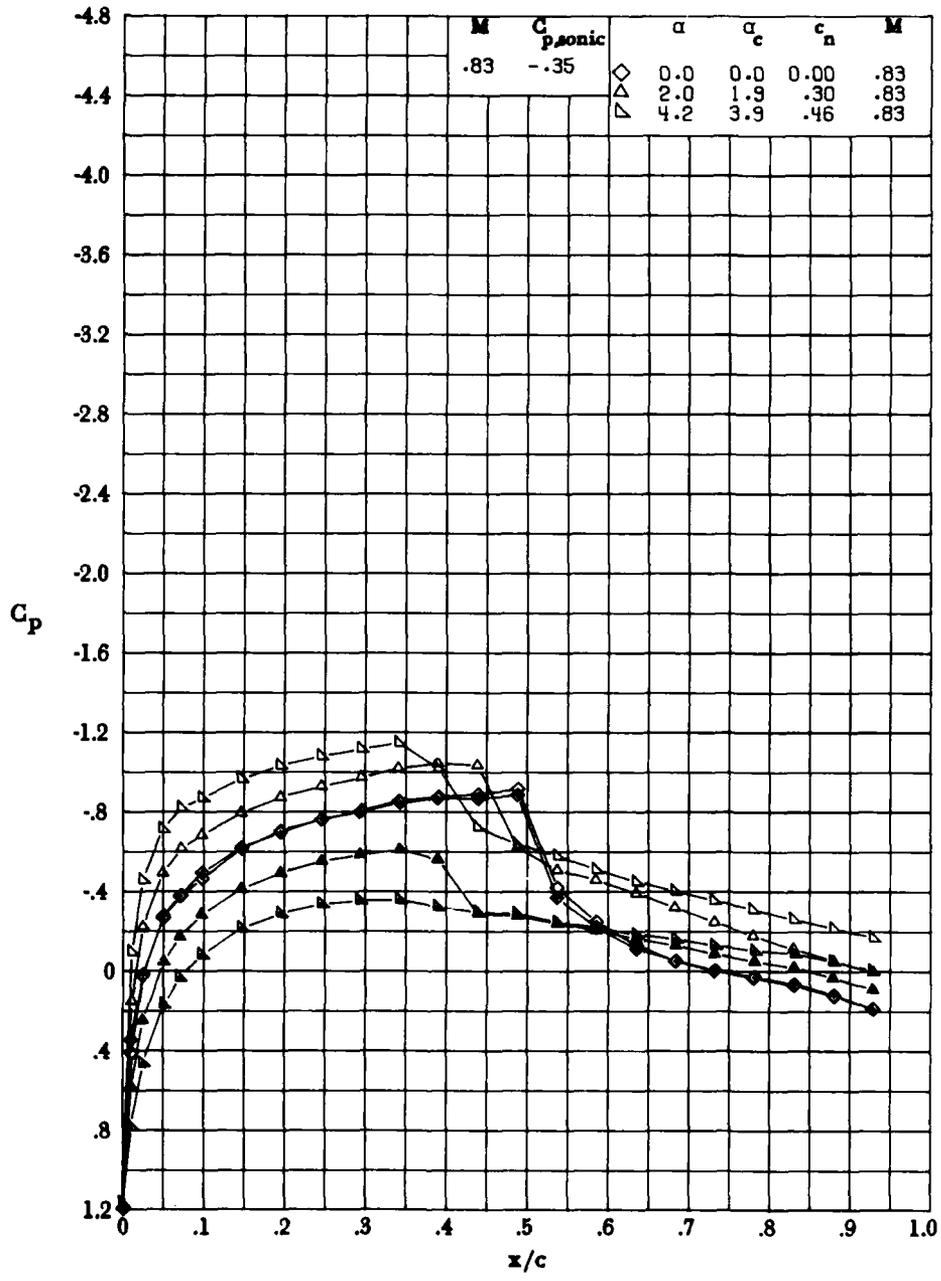
(k) M = 0.83; R ≈ 6.6 × 10⁶.

Figure 16.- Continued.
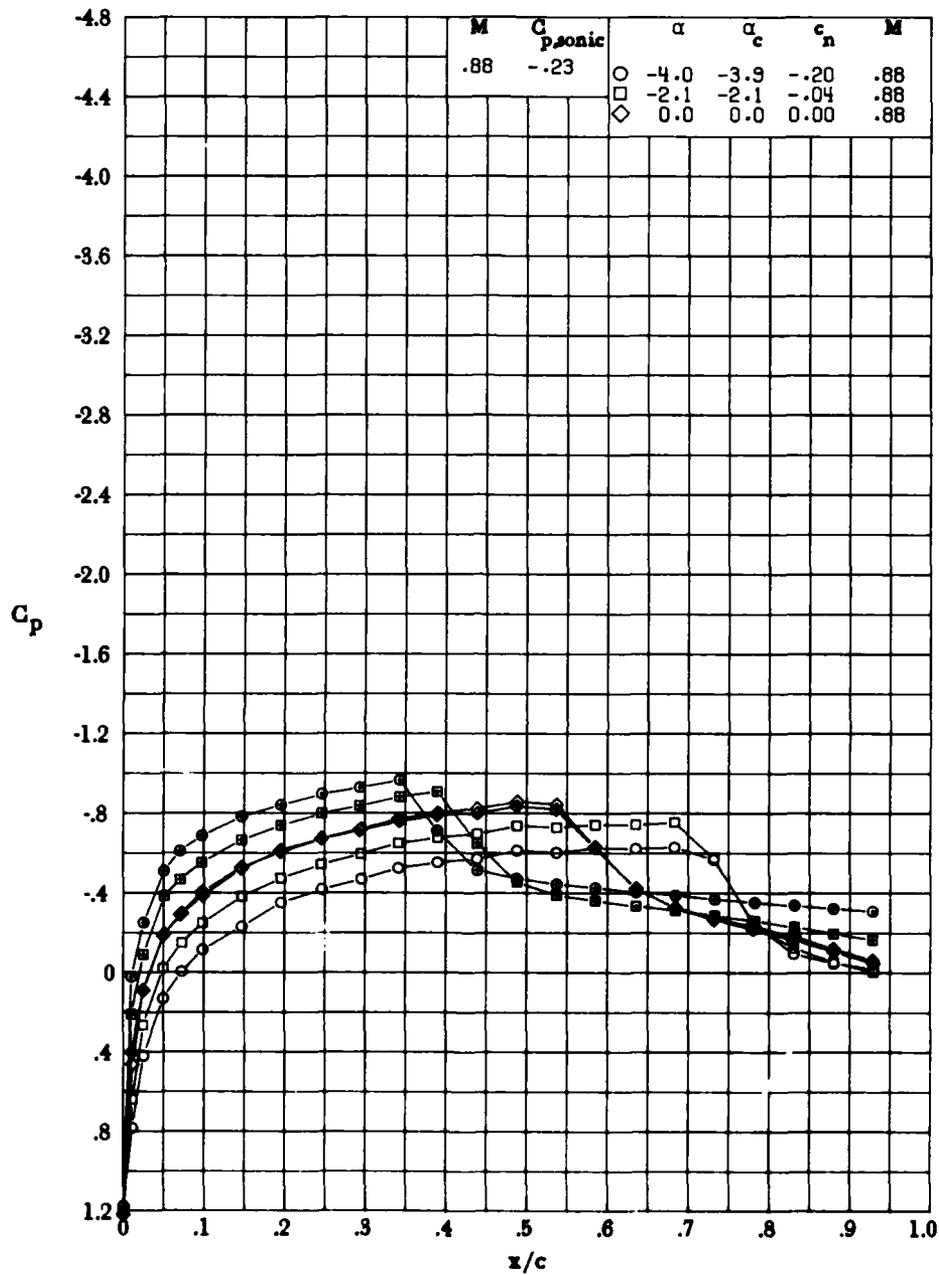
(1) M = 0.88; R ≈ 6.9 × 10^6.

Figure 16.- Concluded.

M	$C_{p,sonic}$		α	$α_c$	c_n	M
.33	-5.65	○	-4.1	-3.8	-.43	.34
.34	-5.29	□	-2.2	-2.1	-.27	.34
		◇	0.0	0.0	-.02	.34
		△	2.1	2.0	.20	.34
		◁	4.1	3.8	.42	.34
		▷	6.1	5.7	.64	.33
		◻	8.4	7.8	.87	.34
		◐	10.2	9.5	1.05	.34
		◇	12.3	11.5	1.27	.33
		△	14.3	13.4	1.33	.34
		○	16.5	15.7	1.29	.34
		□	18.5	17.8	1.04	.34
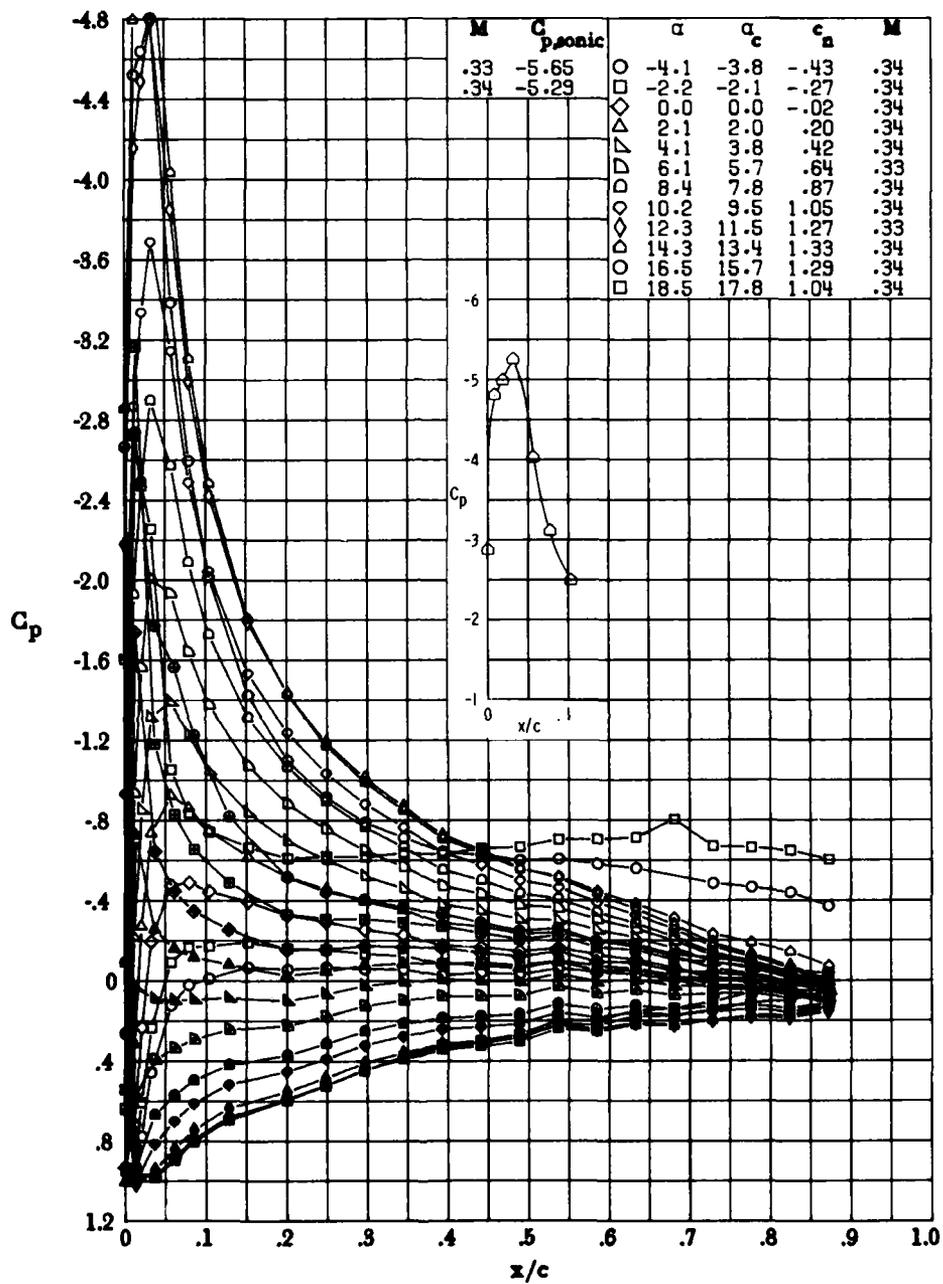
(a) $M \approx 0.33;$ $R \approx 3.0 \times 10^6.$

Figure 17.- Effect of angle of attack on chordwise pressure distribution of SC 1095-R8 airfoil. Symbols with plus sign inside indicate lower surface.

(b) M = 0.38; R ≈ 3.5 × 10⁶.

Figure 17.- Continued.

M	$C_{p,sonic}$		α	α_c	c_n	M
.43	-3.09					
.44	-2.93					
		○	-4.5	-4.2	-.48	.43
		□	-2.2	-2.0	-.27	.43
		◇	0.0	0.0	-.03	.43
		△	2.4	2.2	.25	.43
		◁	4.1	3.8	.45	.44
		▷	6.4	6.0	.71	.43
		▽	8.3	7.8	.92	.43
		◇	10.3	9.6	1.10	.43
		◇	12.4	11.7	1.17	.44

C_p

x/c
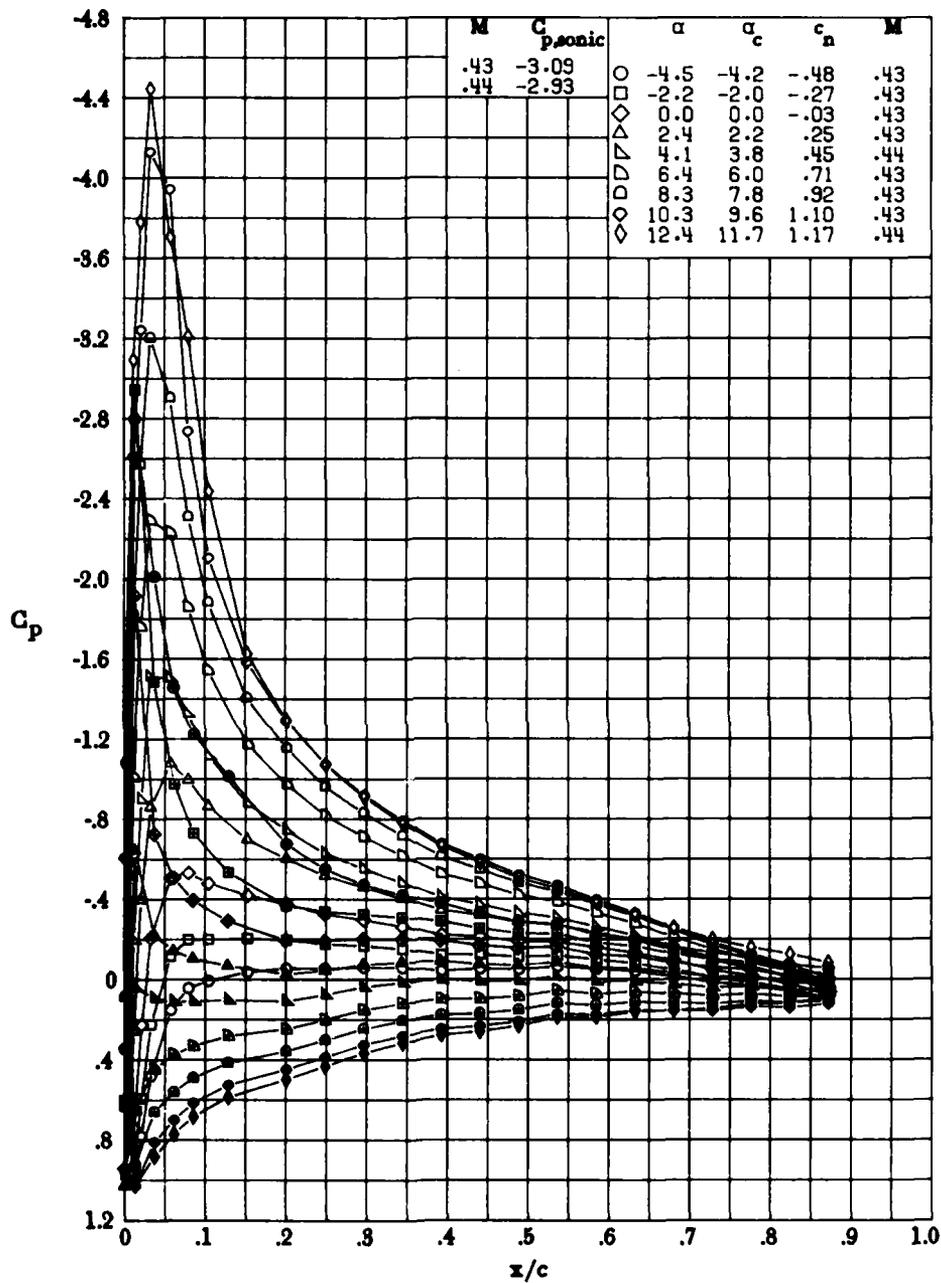
(c) $M \approx 0.43$; $R \approx 3.9 \times 10^6$.

Figure 17.- Continued.

58

(d)   M = 0.48;   R ~ 4.4 × 10⁶.

Figure 17.- Continued.

59

(e) $M \approx 0.54$; $R \approx 4.8 \times 10^6$.

Figure 17.- Continued.

(f) M = 0.58; R ≈ 5.2 × 10⁶.

Figure 17.- Continued.

(g) $M = 0.63$; $R \approx 5.5 \times 10^6$.

Figure 17.- Continued.

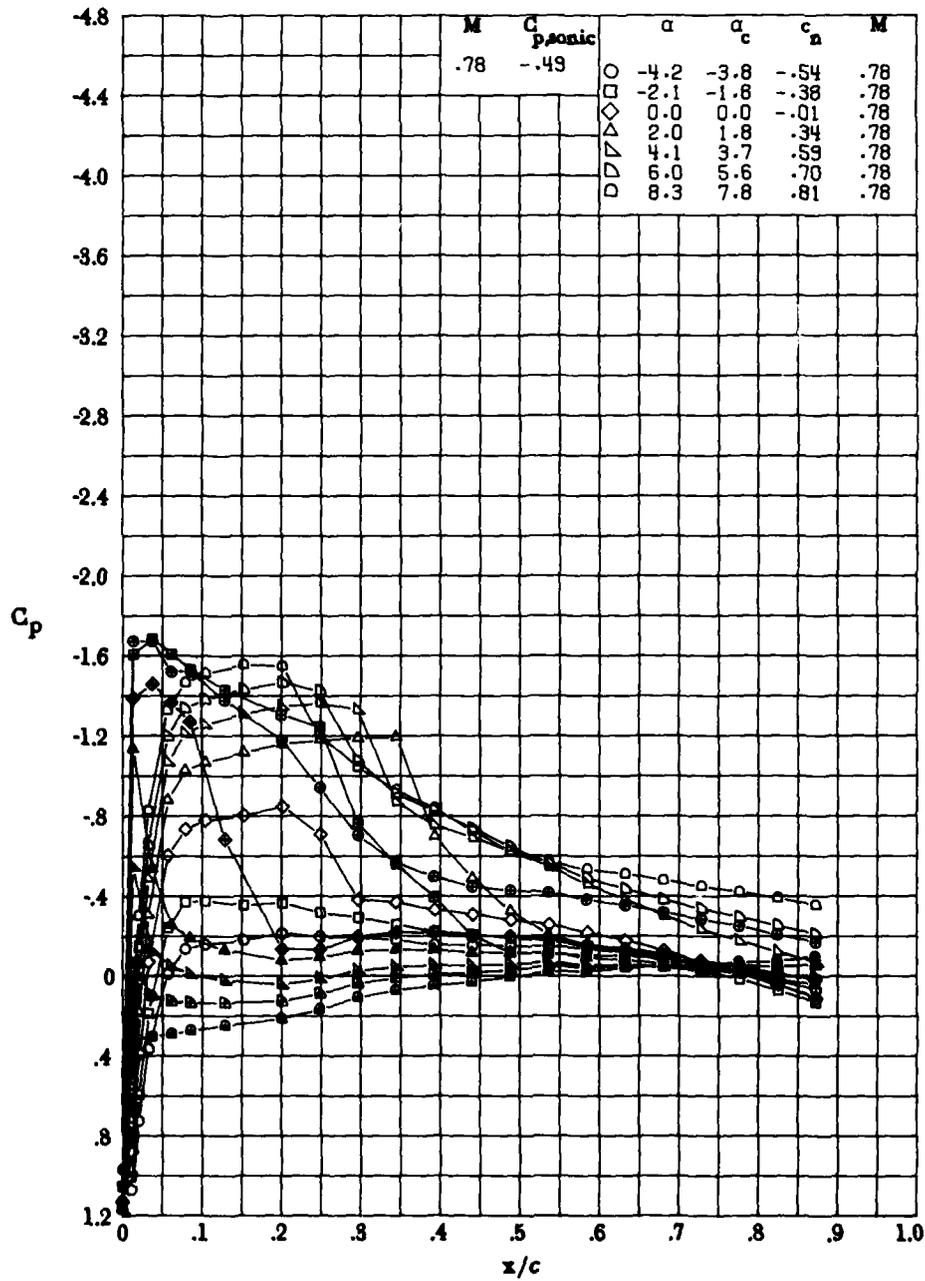|	M	$C_{p,sonic}$		α	α_c	c_n	M
	.67	-.91					
	.68	-.87					
○				-4.1	-3.8	-.48	.67
□				-2.0	-1.8	-.26	.68
◇				0.0	0.0	-.02	.68
△				2.0	1.9	.27	.68
◁				4.2	3.9	.57	.68
▷				6.4	5.9	.76	.68
◻				8.2	7.7	.84	.68
○				10.2	9.7	.90	.68
◇				12.4	11.8	.94	.68
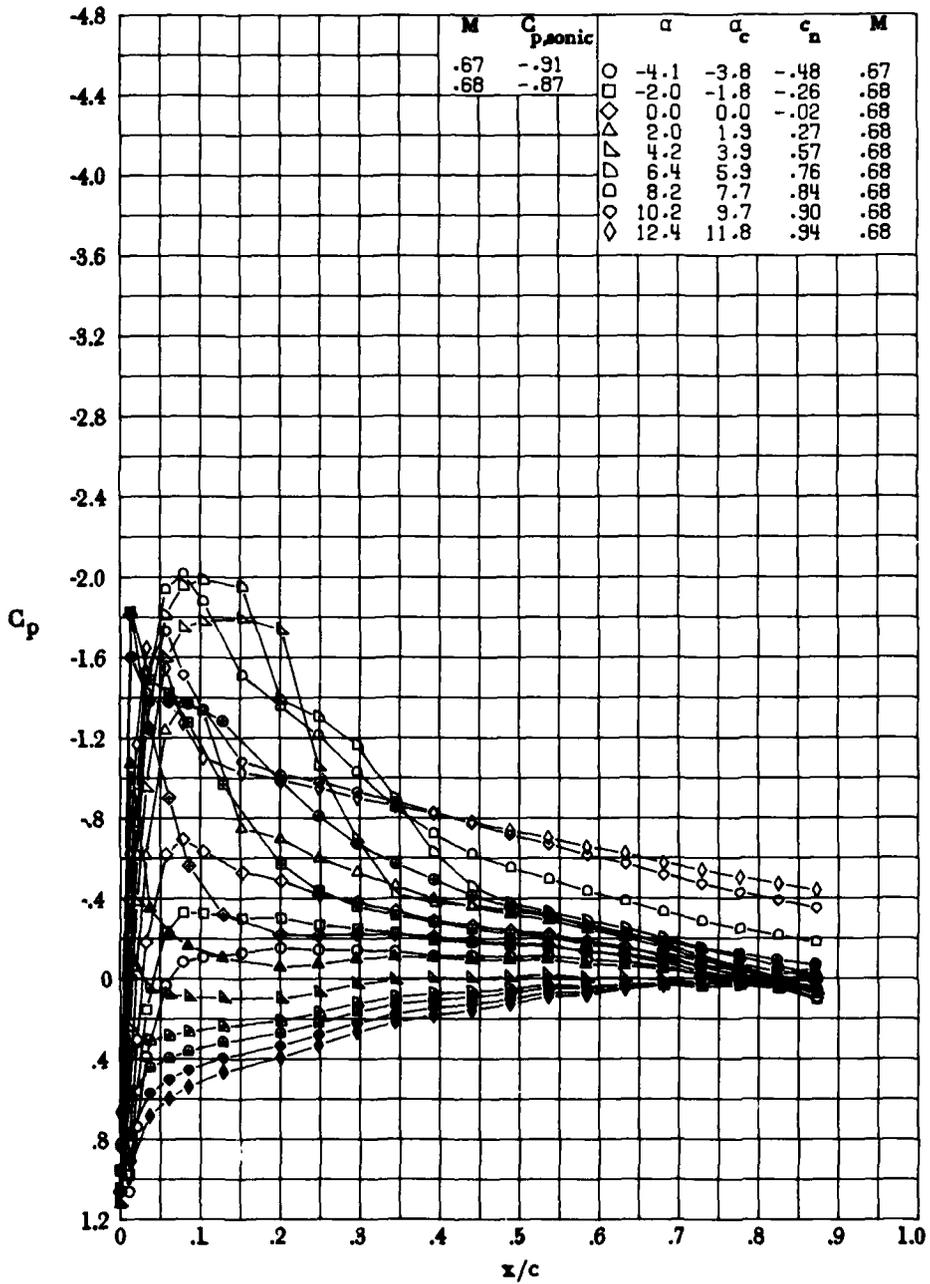
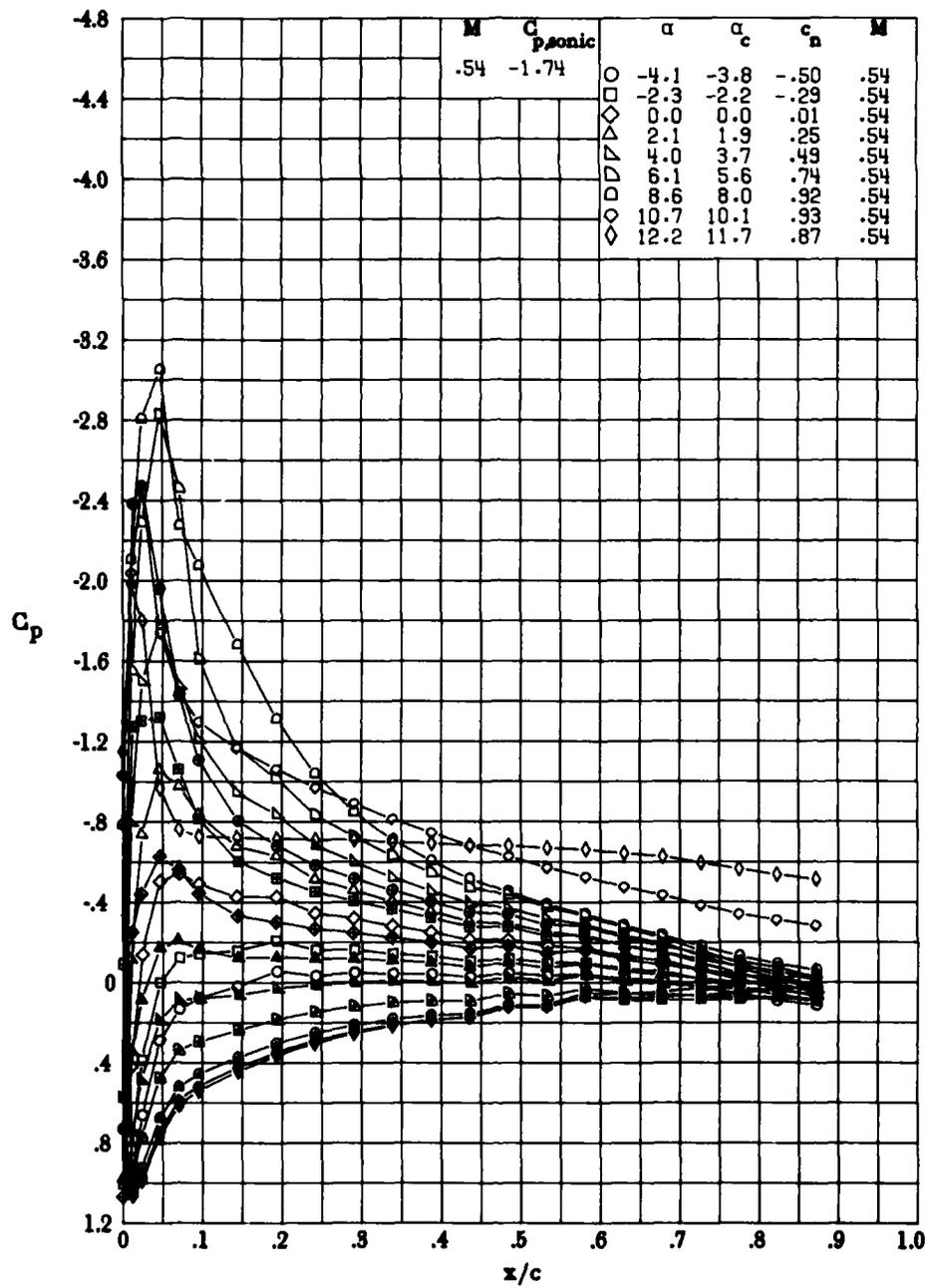(h) $M \approx 0.68$; $R \approx 5.9 \times 10^6$.

Figure 17.- Continued.

63

(i) $M \approx 0.73$; $R \approx 6.3 \times 10^6$.

Figure 17.- Continued.

M	$C_{p,sonic}$		α	α_c	c_n	M
.78	-.49					
		○ -4.2	-3.8	-.54	.78
		□ -2.1	-1.8	-.38	.78
		◇ 0.0	0.0	-.01	.78
		△ 2.0	1.8	.34	.78
		◁ 4.1	3.7	.59	.78
		◁ 6.0	5.6	.70	.78
		◻ 8.3	7.8	.81	.78

(j)   M = 0.78;   R ≈ 6.6 × 10⁶.

Figure 17.- Continued.

65
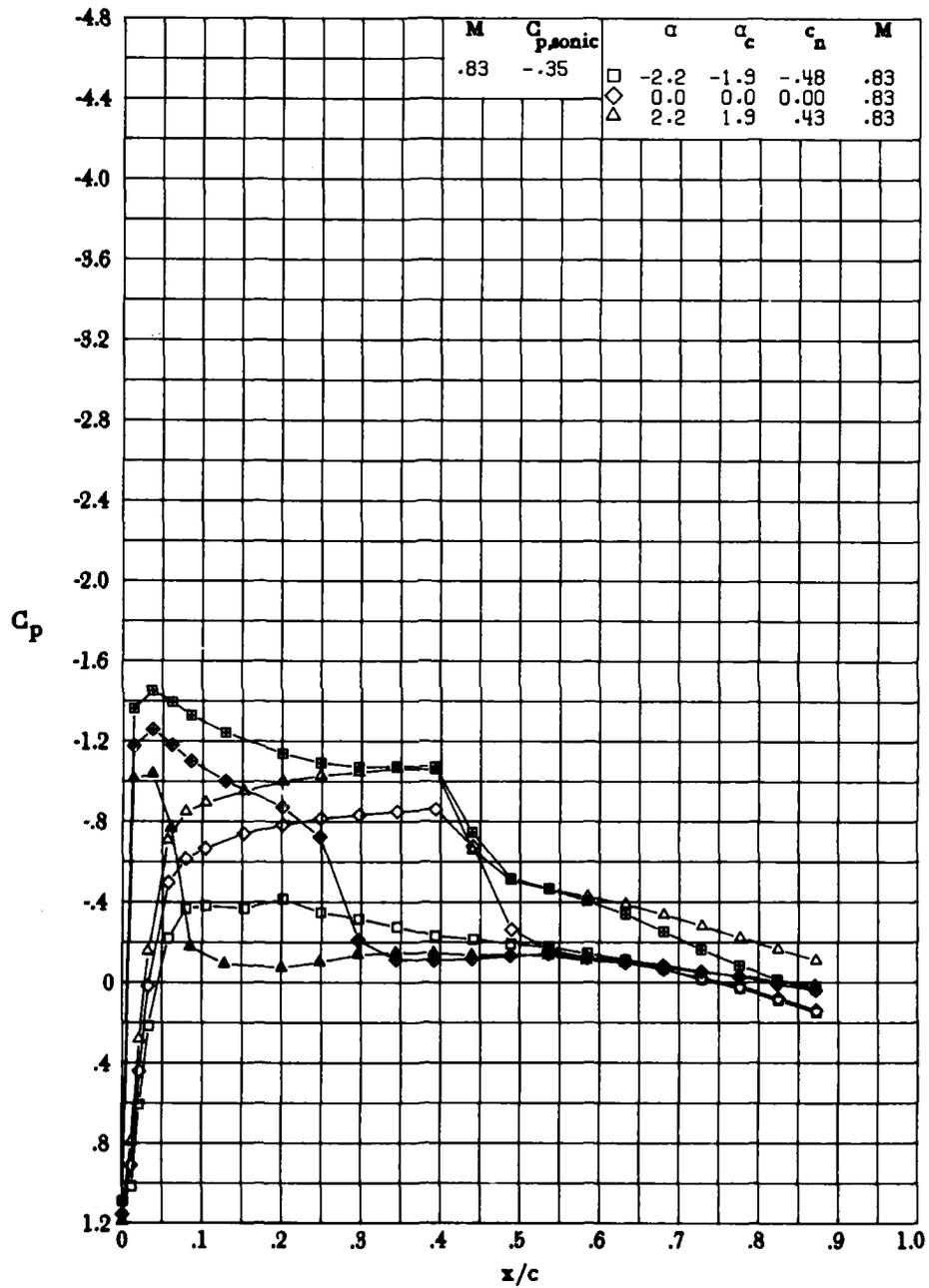
(k)   M = 0.83;   R ≈ 6.6 × 10^6.

Figure 17.- Concluded.

M	$C_{p,sonic}$		α	α_c	c_n	M
.34	-5.29	○	-4.2	-3.9	-.43	.34
		□	-2.4	-2.2	-.24	.34
		◇	0.0	0.0	0.00	.34
		△	2.1	2.0	.23	.34
		▷	4.1	3.8	.44	.34
		◿	6.1	5.7	.65	.34
		◺	8.1	7.6	.84	.34
		⟡	10.3	9.7	.99	.34
		◇	12.4	11.7	1.02	.34
		△	14.2	13.7	.81	.34

C_p

x/c
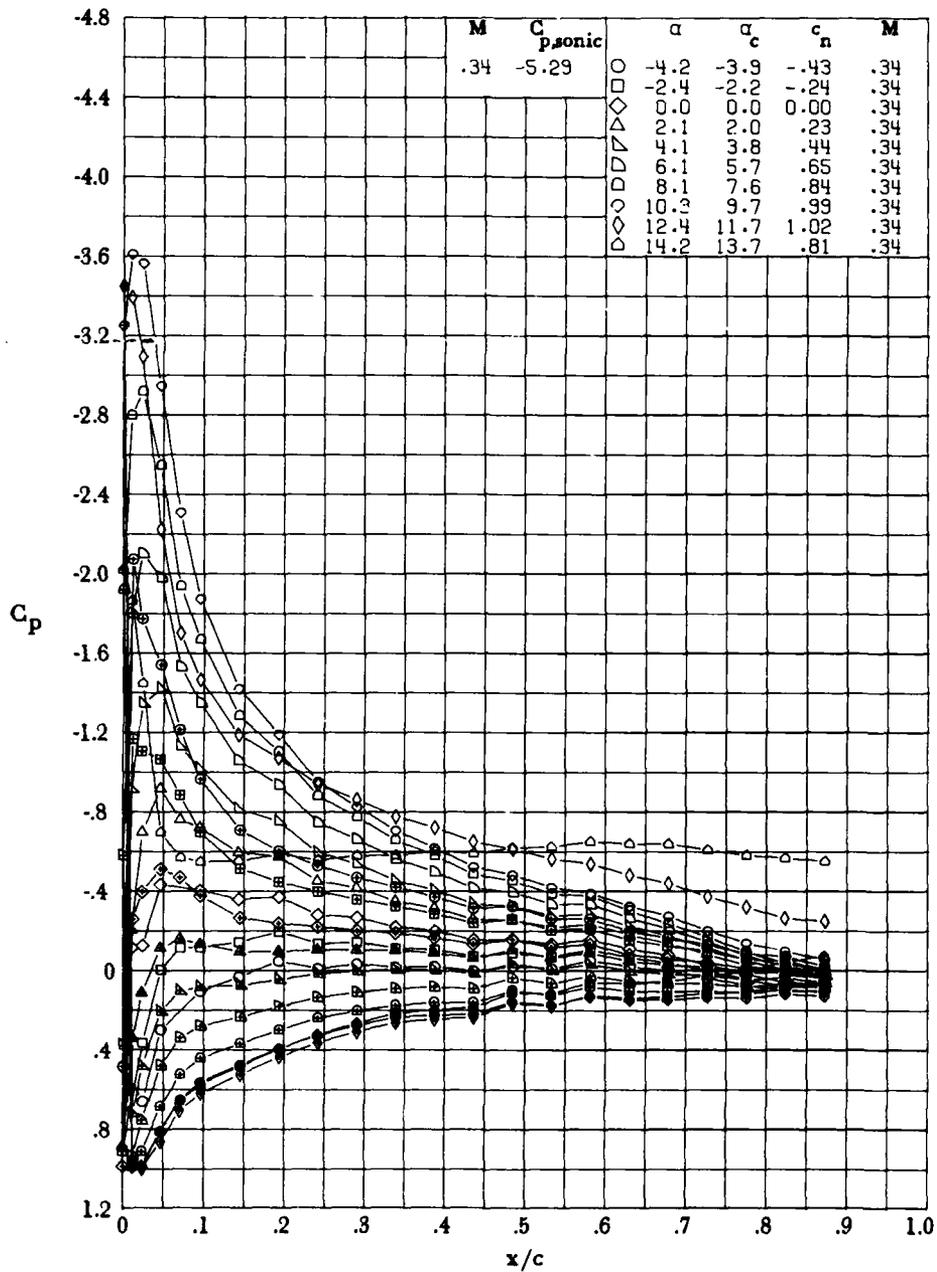
(a)   M = 0.34;   R ≈ 2.9 × 10^6.

Figure 18.- Effect of angle of attack on chordwise pressure distribution of SC 1095 airfoil. Symbols with plus sign inside indicate lower surface.

	M	$C_{p,sonic}$		α	α_c	c_n	M
	.38	-4.12	○	-4.3	-4.0	-.48	.38
	.39	-3.88	□	-2.1	-2.0	-.24	.38
			◇	0.0	0.0	0.00	.38
			△	2.0	1.9	.23	.39
			◁	4.2	3.9	.47	.38
			▷	6.0	5.6	.65	.39
			◁	8.4	7.9	.92	.38
			○	10.3	9.6	1.04	.38
			◇	12.2	11.6	.95	.38
			△	14.4	13.9	.80	.38
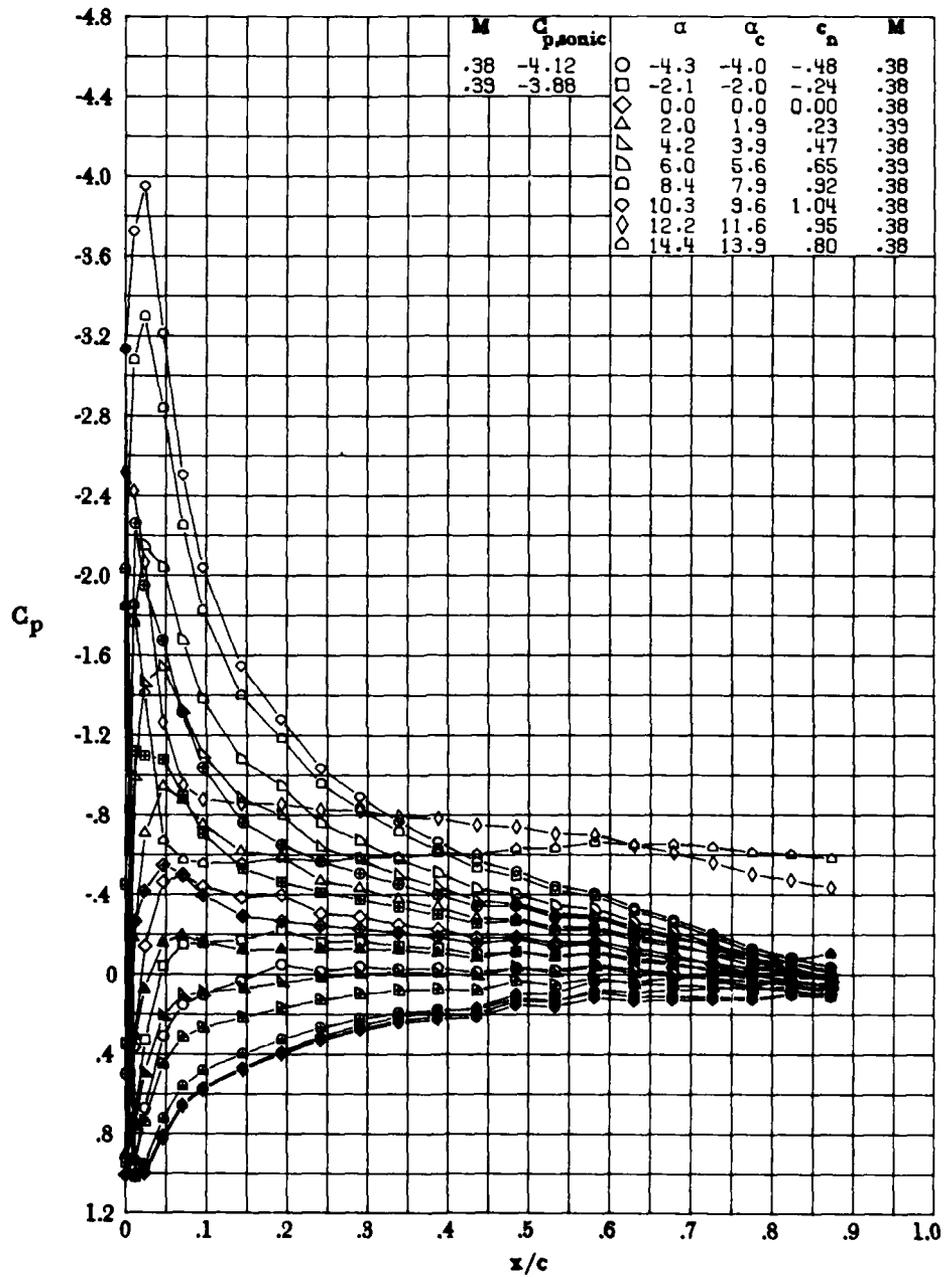
(b) $M \approx 0.38$; $R \approx 3.4 \times 10^6$.

Figure 18.- Continued.

68
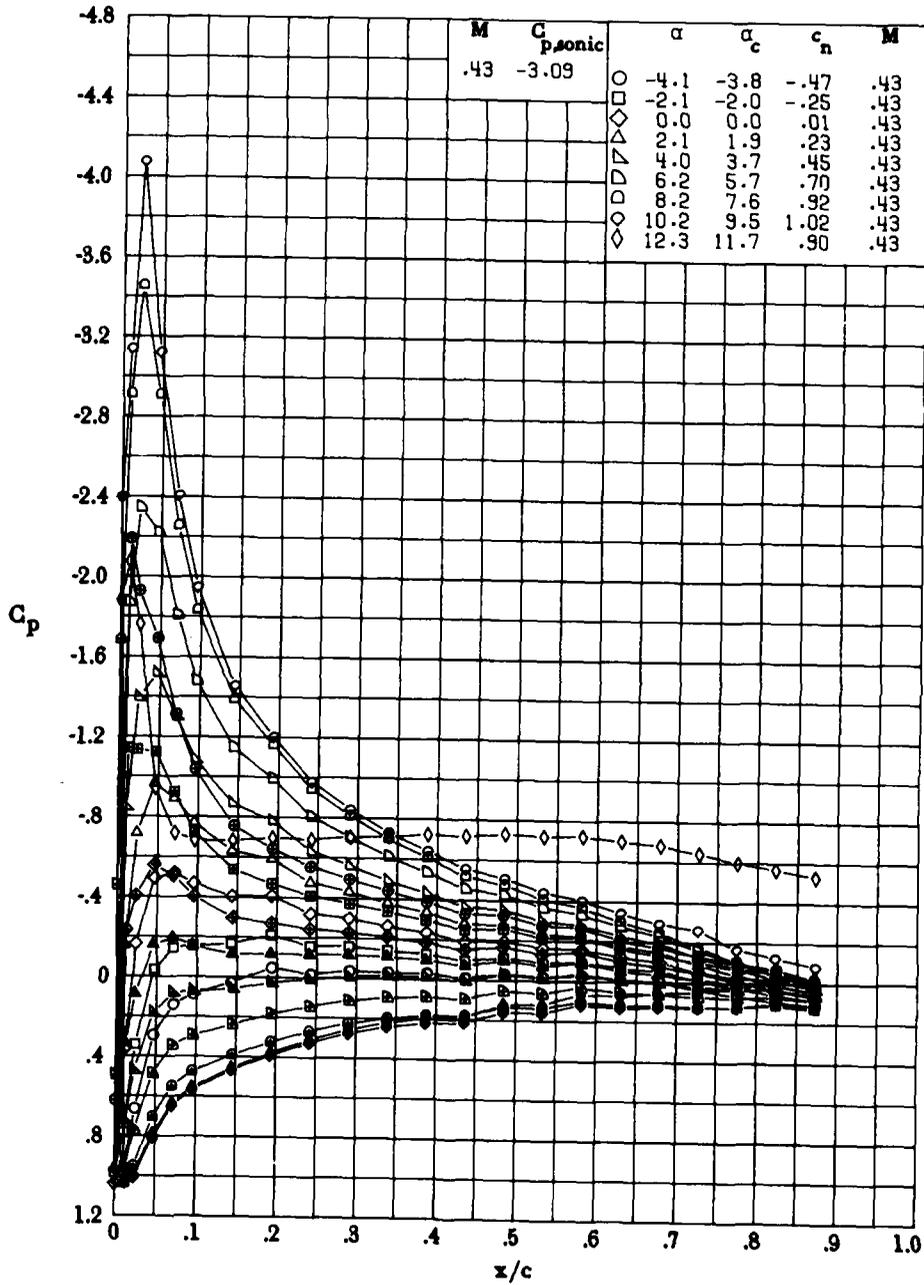
(c) M = 0.43; R ≈ 3.8 × 10⁶.

Figure 18.- Continued.
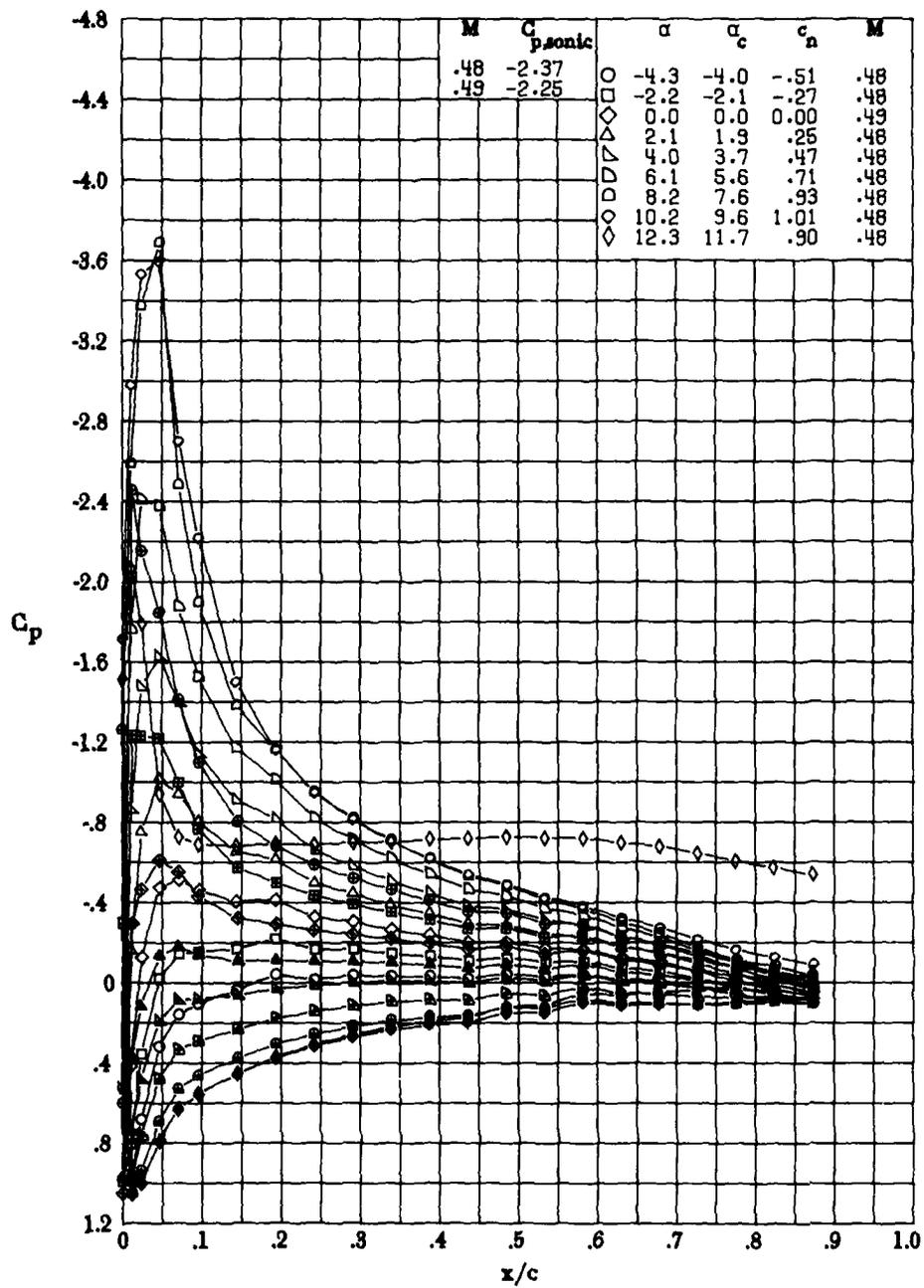
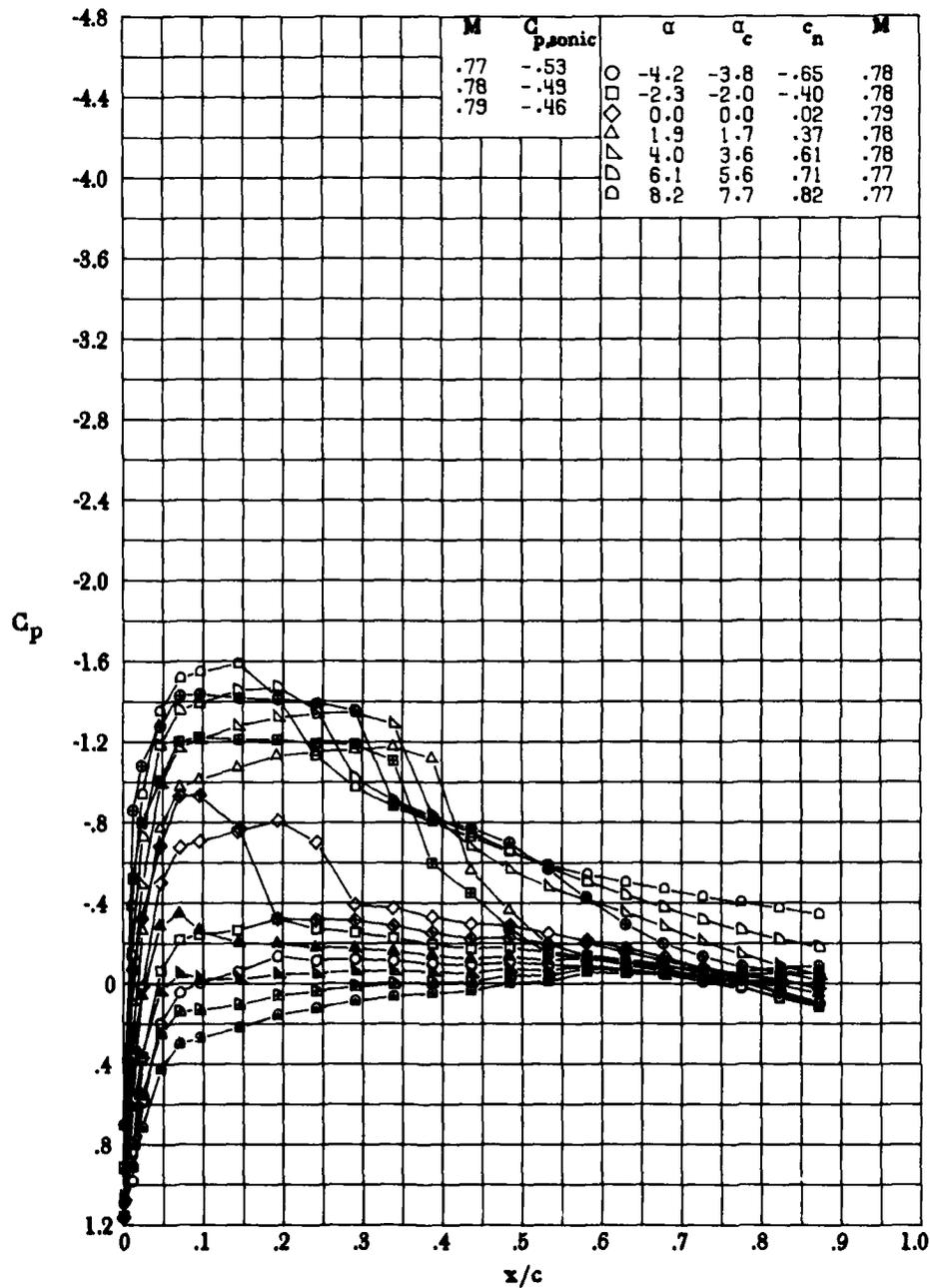(d) $M \approx 0.48$; $R \approx 4.3 \times 10^6$.

Figure 18.- Continued.

70

(e) M = 0.54; R ~ 4.7 × 10⁶.

Figure 18.- Continued.

M	$C_{p,sonic}$		α	α_c	c_n	M
.58	-1.43					
		○	-4.1	-3.8	-.52	.58
		△	2.1	1.9	.26	.58
		◁	4.2	3.8	.53	.58
		◻	6.2	5.7	.75	.58
		◻	8.1	7.5	.87	.58
		○	10.2	9.6	.92	.58
		◇	12.3	11.7	.96	.58

C_p

x/c
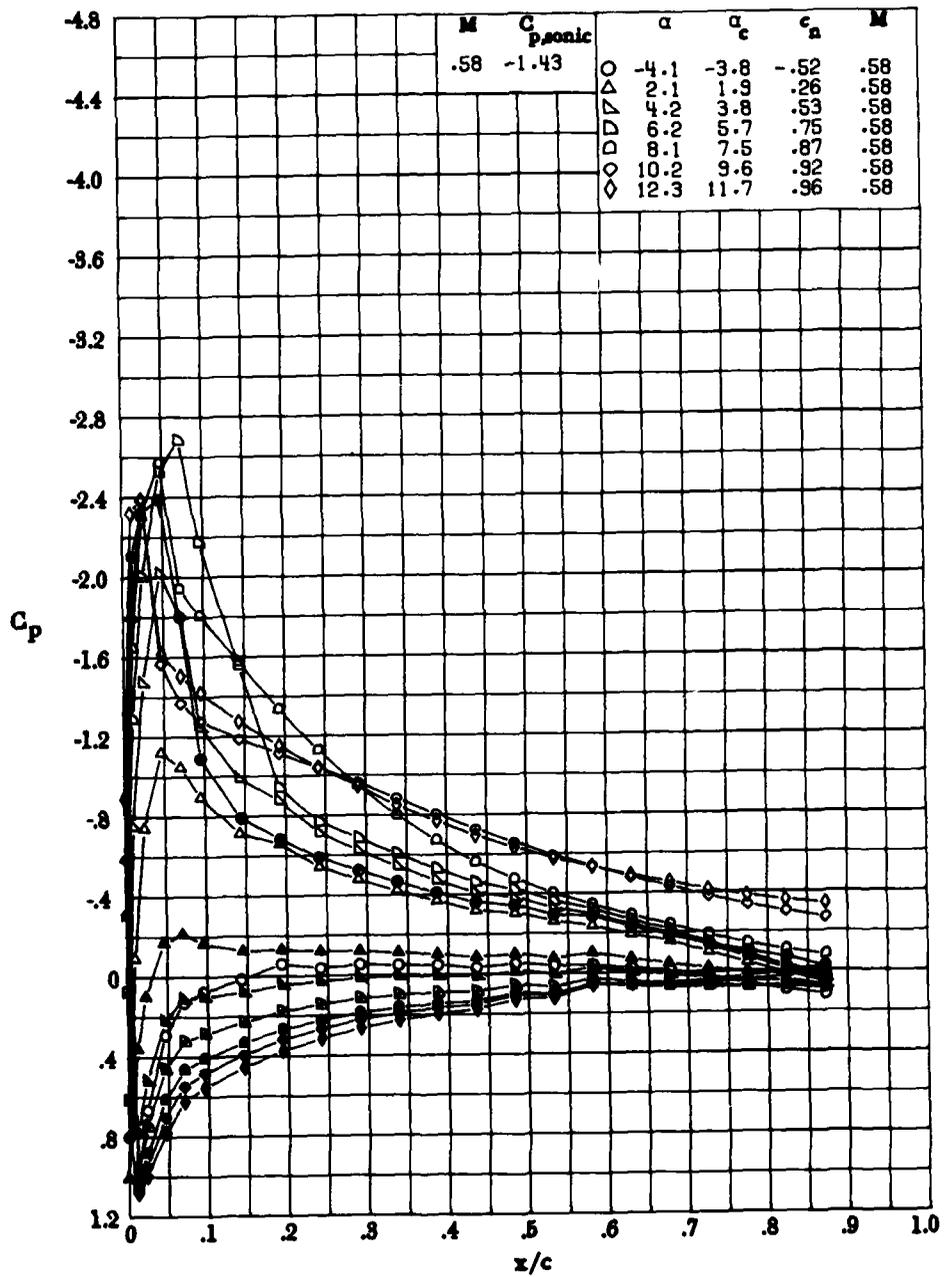
(f)   M = 0.58;   R ≈ 5.1 × 10⁶.

Figure 18.- Continued.
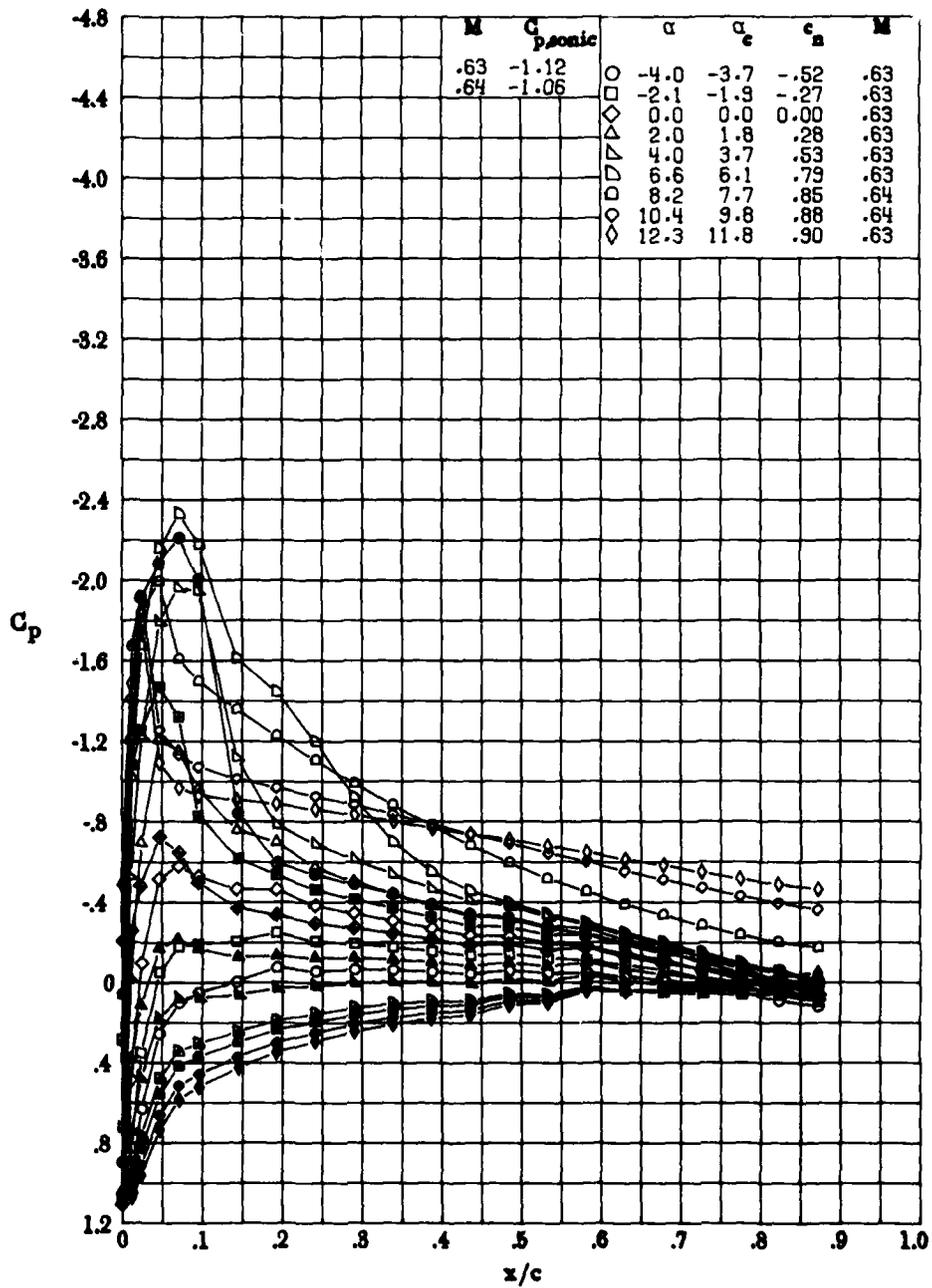
(g) M ~ 0.63; R ~ 5.4 × 10⁶.

Figure 18.- Continued.
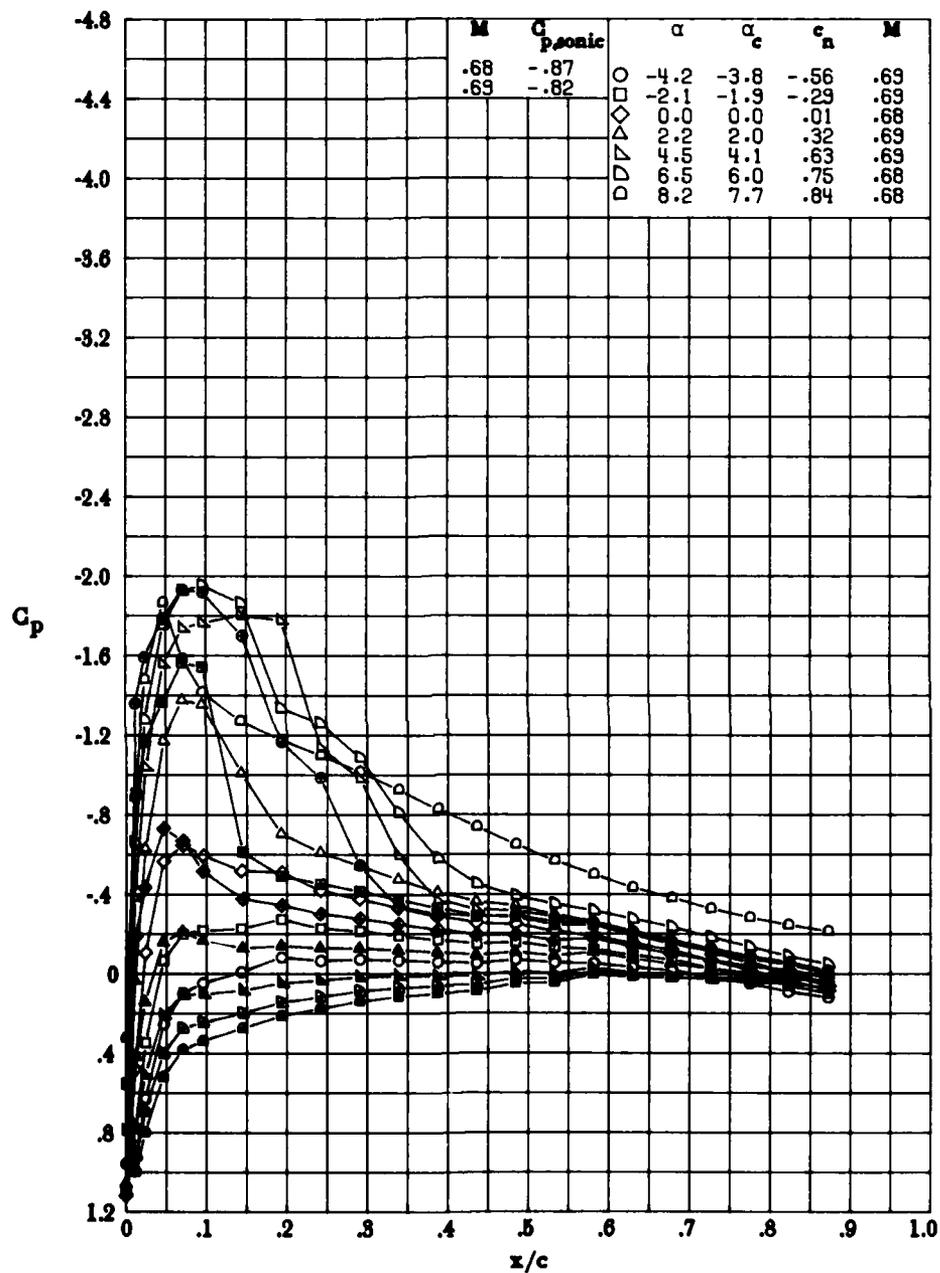
(h) M ≈ 0.69; R ≈ 5.8 × 10⁶.

Figure 18.- Continued.

74

C_p

x/c
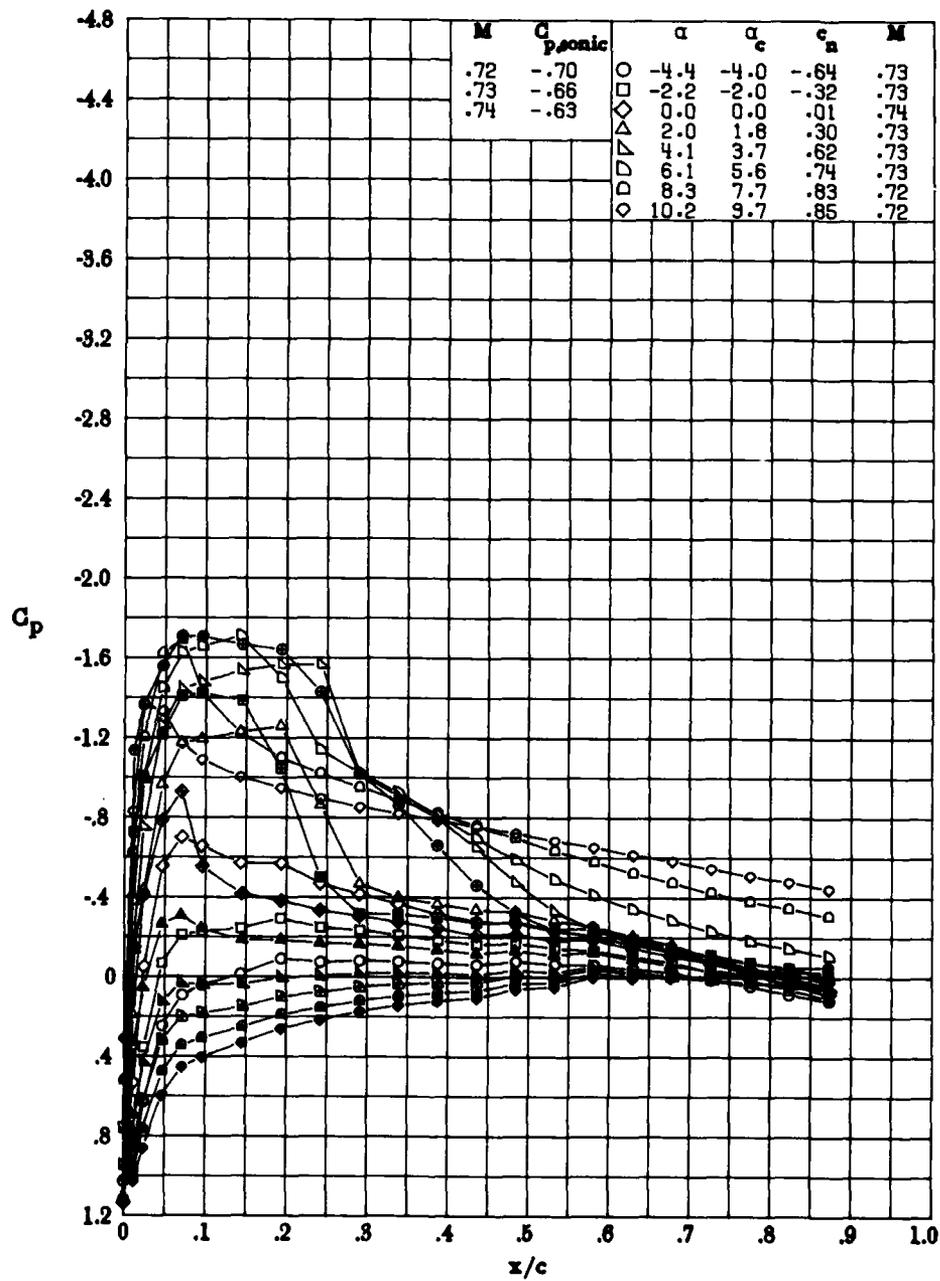
(i)   M ≈ 0.73;   R ≈ 6.1 × 10⁶.

Figure 18.- Continued.

75

(j) M ≈ 0.78; R ≈ 6.4 × 10^6.

Figure 18.- Continued.
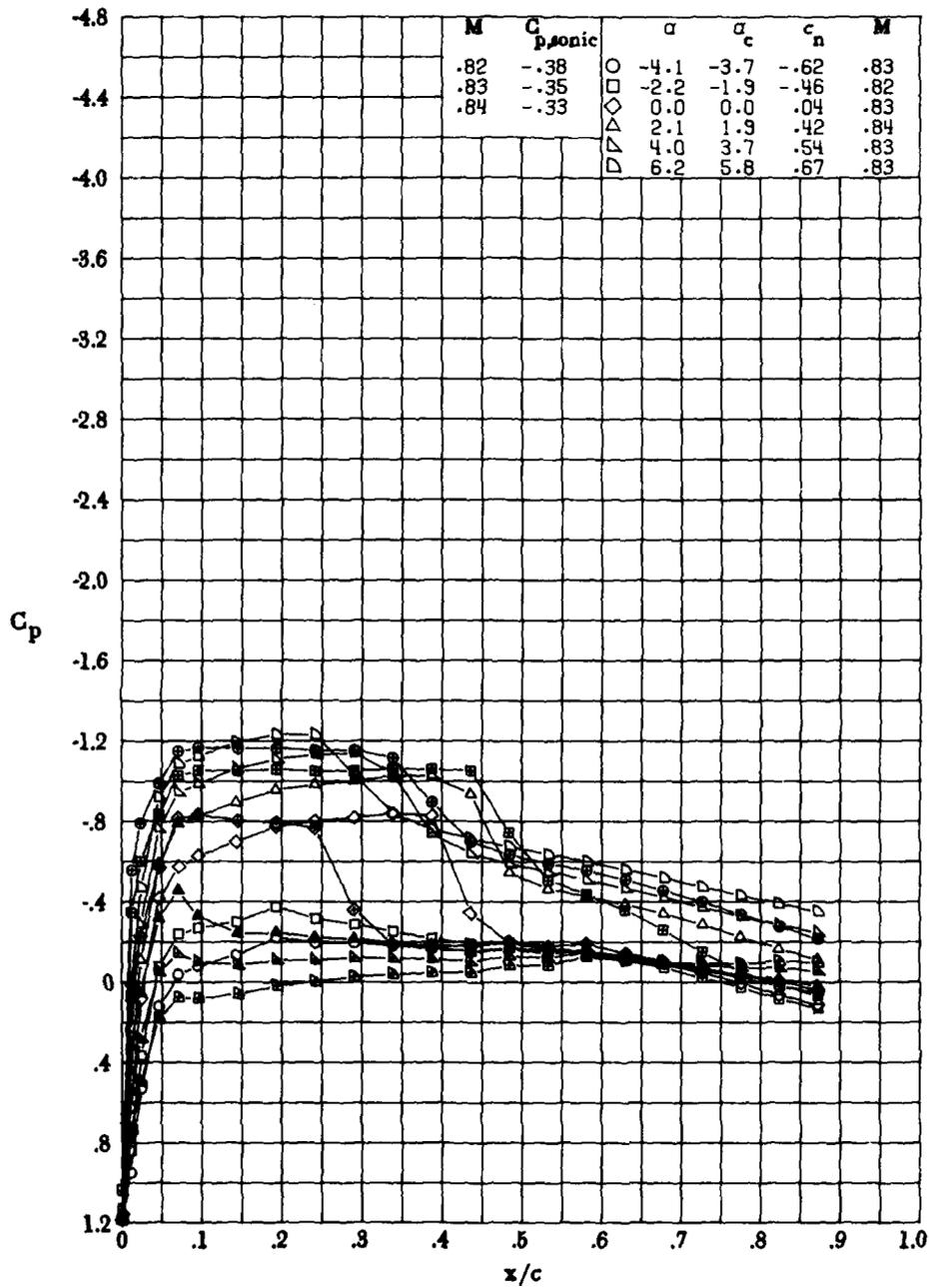
(k) $M \approx 0.83$; $R \approx 6.6 \times 10^6$.

Figure 18.- Continued.
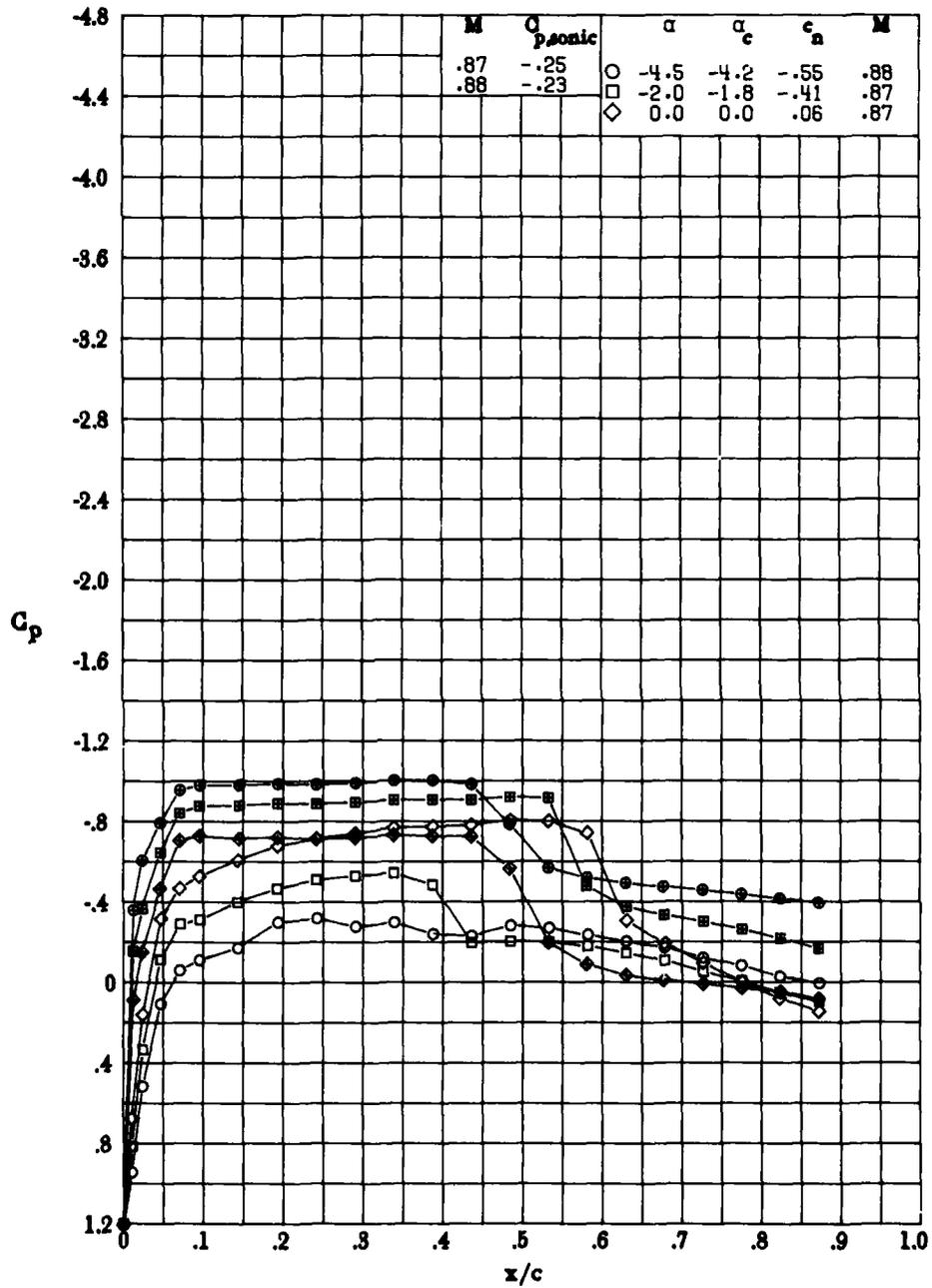
(1)   M ≈ 0.87;   R ≈ 6.7 × 10^6.

Figure 18.- Concluded.

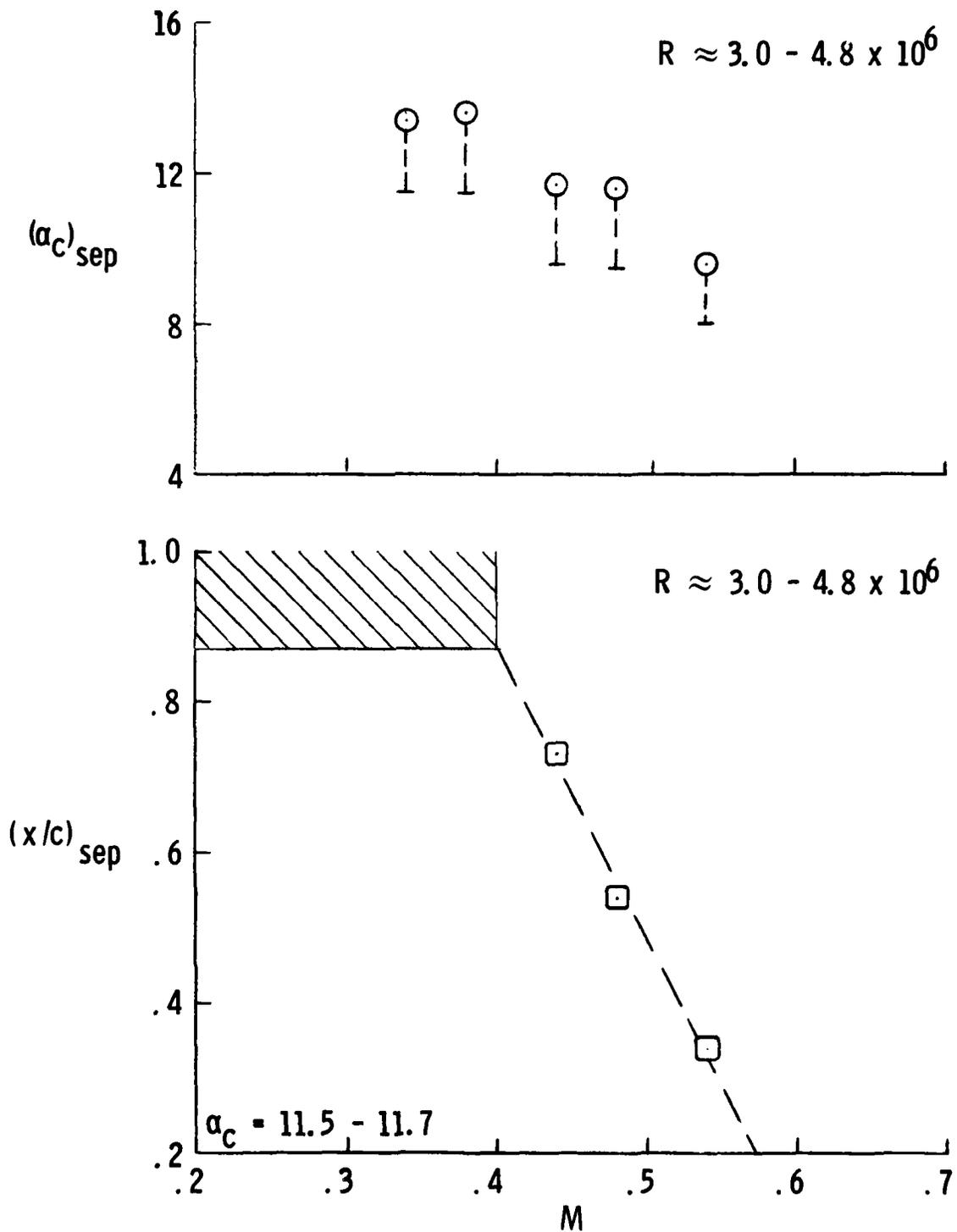Figure 19.- Effect of Mach number on angle of attack at which boundary-layer separation first occurs and on separation point of SC 1095-R8 airfoil.
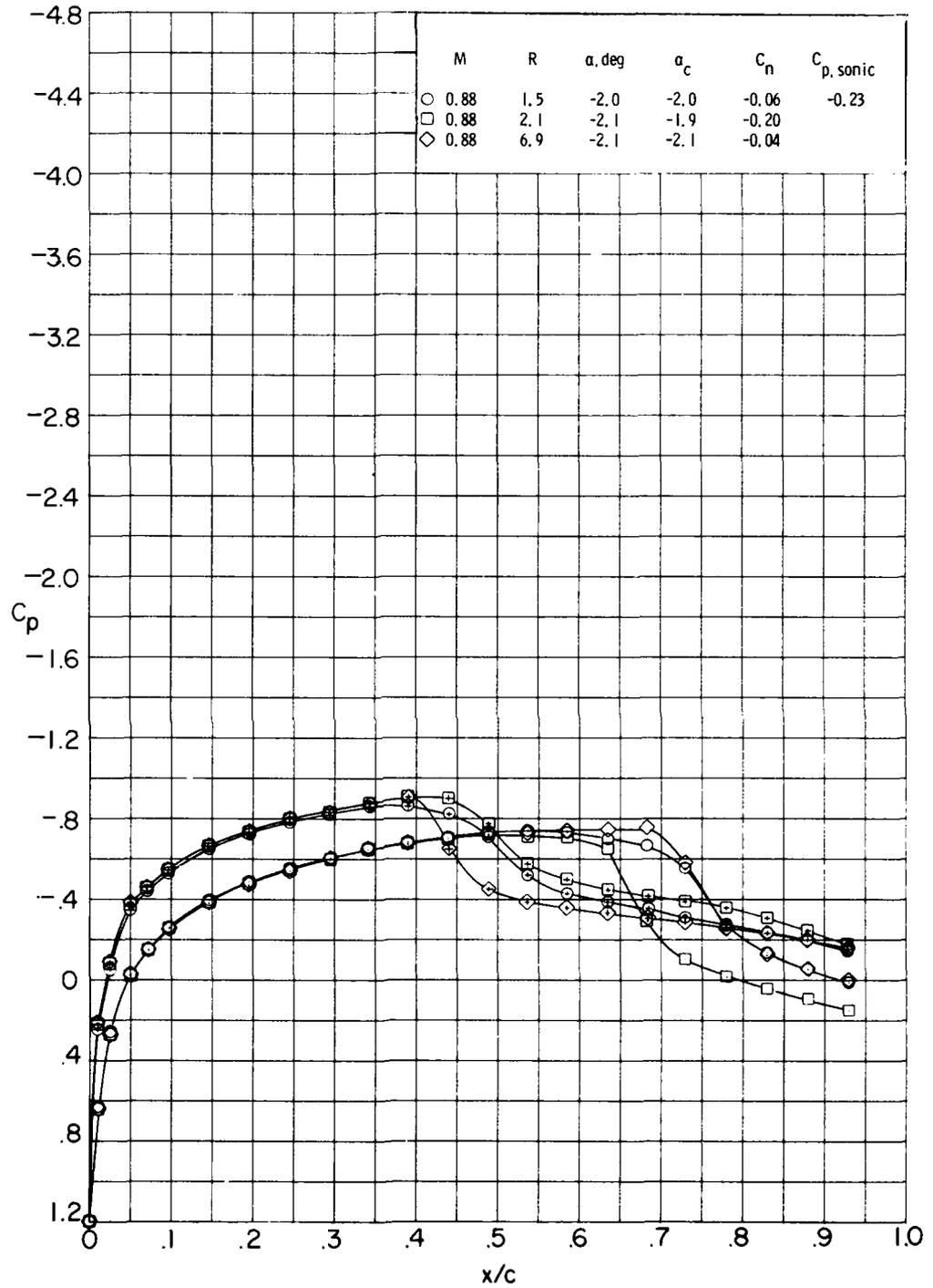
Figure 20.- Effect of Reynolds number on shock wave location on NACA 0012 (0° Tab) airfoil. Symbols with plus sign inside indicate lower surface. R given in millions.
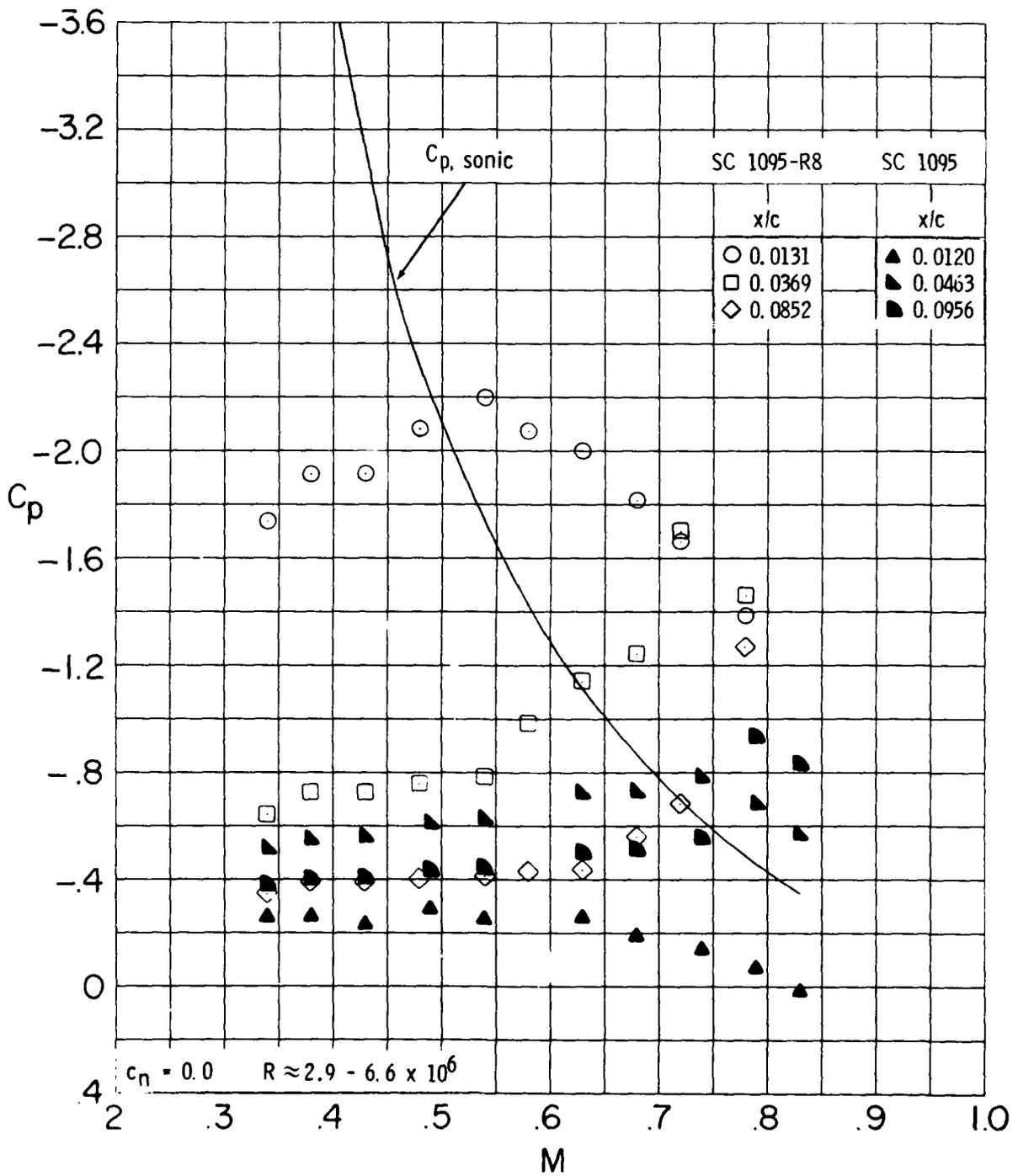
Effect of Mach number on some lower-surface pressure coefficients near the 10-percent-chord station of SC 1095-R8 and SC 1095 airfoils.
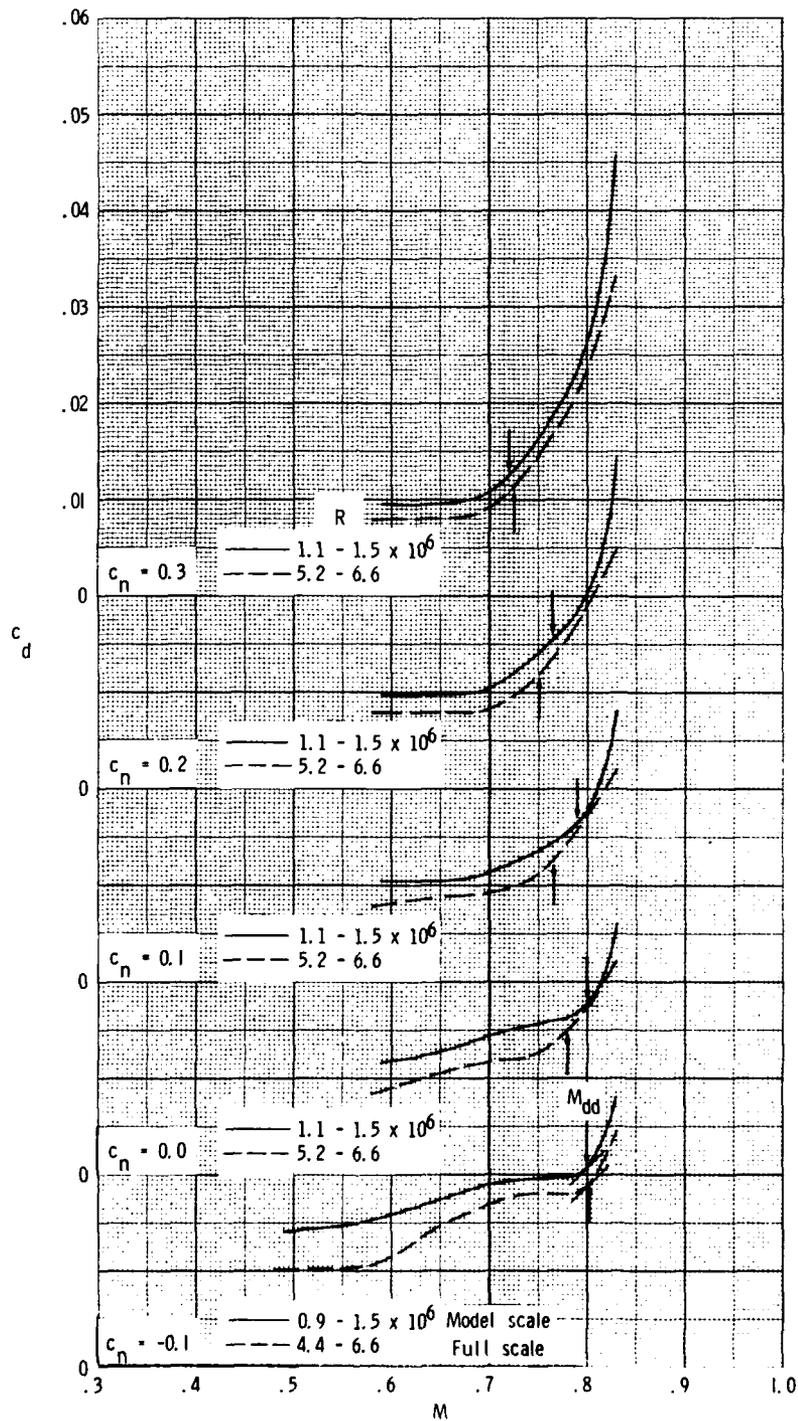
Figure 22.- Effect of Reynolds number on variation of section drag coefficient with Mach number of SC 1095-R8 airfoil.

1. Report No. NASA TP-1701 AVRADCOM TR 80-B-5	2. Government Accession No. AD-A089766	3. Recipient's Catalog No.		
4. Title and Subtitle AERODYNAMIC CHARACTERISTICS OF THREE HELICOPTER ROTOR AIRFOIL SECTIONS AT REYNOLDS NUMBERS FROM MODEL SCALE TO FULL SCALE AT MACH NUMBERS FROM 0.35 to 0.90		5. Report Date September 1980		
		6. Performing Organization Code		
7. Author(s) Kevin W. Noonan and Gene J. Bingham		8. Performing Organization Report No. L-13139		
		10. Work Unit No. 505-31-33-02		
9. Performing Organization Name and Address NASA Langley Research Center and Structures Laboratory AVRADCOM Research and Technology Laboratories Hampton, VA 23665				
		11. Contract or Grant No.		
		13. Type of Report and Period Covered Technical Paper		
12. Sponsoring Agency Name and Address National Aeronautics and Space Administration Washington, DC 20546 and U.S. Army Aviation Research and Development Command St. Louis, MO 63166				
		14. Army Project No. 1L161102AH45		

15. Supplementary Notes

Kevin W. Noonan and Gene J. Bingham: Structures Laboratory, AVRADCOM Research and Technology Laboratories.

16. Abstract

An investigation has been conducted in the Langley 6- by 28-Inch Transonic Tunnel to determine the two-dimensional aerodynamic characteristics of three helicopter rotor airfoils at Reynolds numbers from typical model scale to full scale at Mach numbers from about 0.35 to 0.90. The model-scale Reynolds numbers ranged from about 0.7×10^6 to 1.5×10^6 and the full-scale Reynolds numbers ranged from about 3.0×10^6 to 6.6×10^6. The airfoils tested were the NACA 0012 (0° Tab), the SC 1095-R8, and the SC 1095. Both the SC 1095 and the SC 1095-R8 airfoils had trailing-edge tabs. The results of this investigation indicate that Reynolds number effects can be significant on the maximum normal-force coefficient and all drag-related parameters; namely, drag at zero normal force, maximum normal-force—drag ratio, and drag-divergence Mach number. In general, the increments in these parameters at a given Mach number owing to the model-scale to full-scale Reynolds number change are different for each of the airfoils.

17. Key Words (Suggested by Author(s)) Airfoils Helicopters Rotors Reynolds number effects	18. Distribution Statement Unclassified - Unlimited Subject Category 02		
19. Security Classif. (of this report) Unclassified	20. Security Classif. (of this page) Unclassified	21. No. of Pages 82	22. Price* A05